Max-Planck-Institut
für Meteorologie

MAX-PLANCK-GESELLSCHAFT

International Max Planck Research School
on Earth System Modelling

Vegetation - albedo - precipitation interactions in North Africa during the Holocene

Freja S.E. Vamborg

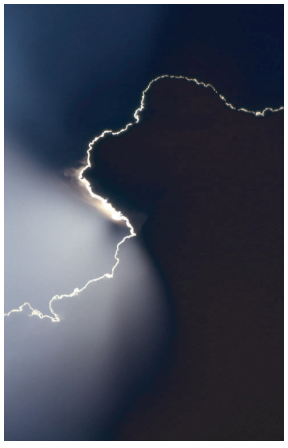

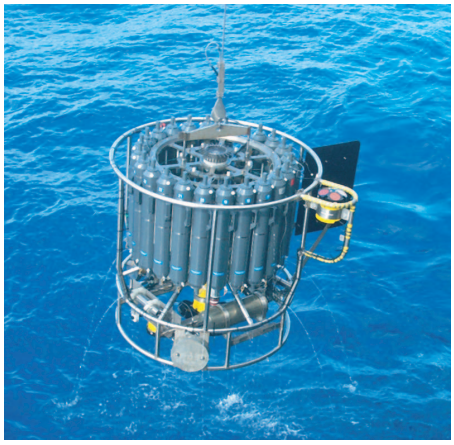

Berichte zur Erdsystemforschung 94
2011

Reports on Earth System Science

Hinweis

Die Berichte zur Erdsystemforschung werden vom Max-Planck-Institut für Meteorologie in Hamburg in unregelmäßiger Abfolge herausgegeben.

Sie enthalten wissenschaftliche und technische Beiträge, inklusive Dissertationen.

Die Beiträge geben nicht notwendigerweise die Auffassung des Instituts wieder.

Die "Berichte zur Erdsystemforschung" führen die vorherigen Reihen "Reports" und "Examensarbeiten" weiter.

Notice

The Reports on Earth System Science are published by the Max Planck Institute for Meteorology in Hamburg. They appear in irregular intervals.

They contain scientific and technical contributions, including Ph. D. theses.

The Reports do not necessarily reflect the opinion of the Institute.

The "Reports on Earth System Science" continue the former "Reports" and "Examensarbeiten" of the Max Planck Institute.

Anschrift / Address

Max-Planck-Institut für Meteorologie
Bundesstrasse 53
20146 Hamburg
Deutschland

Tel.: +49-(0)40-4 11 73-0
Fax: +49-(0)40-4 11 73-298
Web: www.mpimet.mpg.de

Layout:

Bettina Diallo, PR & Grafik

Titelfotos:
vorne:
Christian Klepp - Jochem Marotzke - Christian Klepp
hinten:
Clotilde Dubois - Christian Klepp - Katsumasa Tanaka

Berichte zur Erdsystemforschung 94/2011

Vegetation - albedo - precipitation interactions in North Africa during the Holocene

Freja S.E. Vamborg

aus Lund, Schweden

Hamburg 2011

Reports on Earth System Science 94/2011

ISSN 1614-1199

Freja S.E. Vamborg
Max-Planck-Institut für Meteorologie
Bundesstrasse 53
20146 Hamburg
Germany

Als Dissertation angenommen
vom Department Geowissenschaften der Universität Hamburg

auf Grund der Gutachten von
Prof. Dr. Martin Claussen
und
Dr. Victor Brovkin

Hamburg, den 17. Mai 2011
Prof. Dr. Jürgen Oßenbrügge
Leiter des Departments für Geowissenschaften

ISSN 1614-1199

Vegetation - albedo - precipitation interactions in North Africa during the Holocene

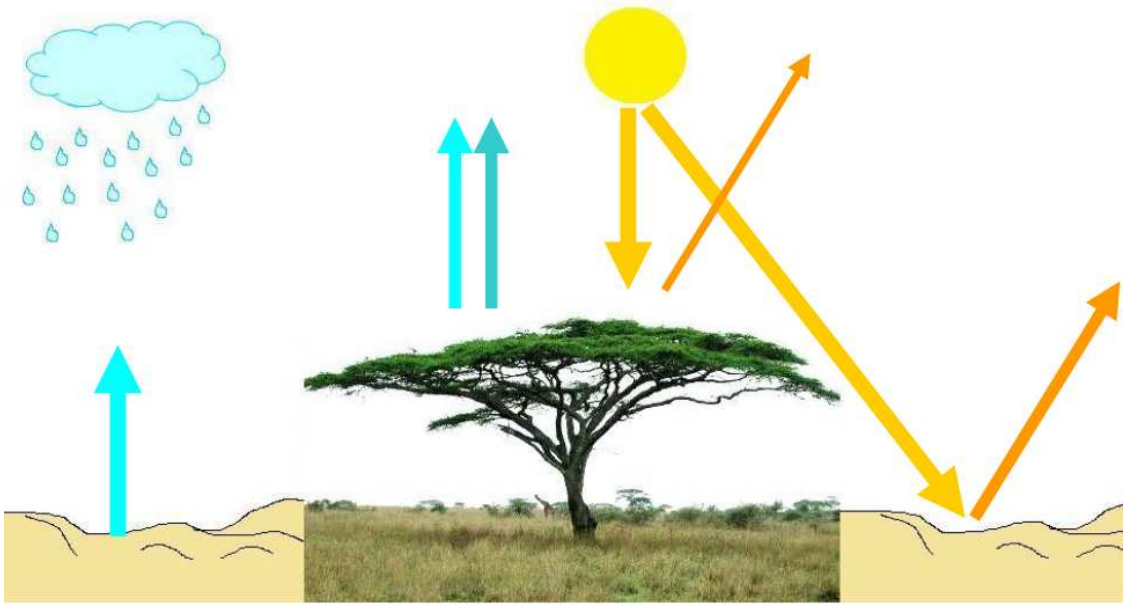

Freja S.E. Vamborg

Hamburg 2011

Overleaf
Sketch of main differences between desert-atmosphere and vegetation-atmosphere interactions.

Blue arrows for hydrological processes
Yellow arrows for radiative processes

Left and Right: Conceptual deserts
Middle: Acacia Tortilis – a tree species native to the Sahel and the Sahara, and other semi-dry and desert regions in Africa and on the Arabian Peninsula

Source for middle picture: Wikipedia

Abstract

A new land surface albedo scheme that takes the dynamic behaviour of the surface below the canopy into account, has been implemented into the land surface scheme of the Earth system model of the Max Planck Institute for Meteorology (MPI-ESM). The standard scheme calculates the seasonal canopy albedo as a function of leaf area index, whereas the background albedo is a gridbox constant derived from satellite measurements. The new scheme additionally models the background albedo as a slowly changing function of organic matter in the ground, and of litter and standing dead biomass covering the ground.

The new albedo scheme was developed to investigate the large climatic change between the present-day and the mid-Holocene, during which the Sahara was substantially wetter than today. Using different model setups of the MPI-ESM: a land surface with and without dynamic vegetation, and with and without the new albedo scheme, the interactions between vegetation, albedo and precipitation in the Sahel/Sahara on multiple timescales from multi-millennia to interannual are investigated.

The correspondence between annual mean albedo and vegetation seen in observations is well-captured with both albedo schemes in the pre-industrial simulations, but it is only captured with the dynamic scheme for the mid-Holocene. The dynamic scheme thus gives a better estimate of albedo change than the static scheme. With the introduction of the new scheme, precipitation in the Sahel/Sahara and the Arabian Peninsula is increased by 30 mm/year for the pre-industrial simulation and by about 80 mm/year for the mid-Holocene simulation. The sensitivity of regional precipitation to external forcing is thus increased by about one third.

The simulated desert border is shifted by at least 300 km in the mid-Holocene. The new scheme leads to increased vegetation variability in the remaining desert region during the mid-Holocene, indicating a higher frequency of green spells. The suitability of the simulated mean climate as the measure to compare with mid-Holocene palaeo-records is discussed. Due to spatial sparsity and low time resolution of vegetation proxies it might be more appropriate to consider vegetation variability or desert stability rather than the mean.

The interactions between vegetation, albedo and precipitation at sub-centennial timescales are also examined. It is found that by introducing dynamic vegetation,

the amplitude of rainfall anomalies is increased, due to an amplification at short timescales. The new albedo scheme acts as filter on precipitation variability, which reduces interannual variability and increases long-term persistence.

The results presented in this thesis highlight the importance of both dynamic vegetation and albedo schemes for the simulation of plausible precipitation dynamics at all timescales in the Sahel/Sahara region.

Contents

List of Figures

List of Tables

List of Abbreviations

0K	pre-industrial
6K	mid-Holocene
AEJ	African Easterly Jet
AP	Arabian Peninsula
BIOME 6000	Palaeovegetation Mapping Project
BP	before present
ENSO	El Niño-Southern Oscillation
ES	east Sahara
FAO	Food and Agriculture Organization
GCM	general circulation model
GIMMS	Global Inventory of Modeling and Mapping Studies
IPCC	Intergovernmental Panel on Climate Change
ITCZ	intertropical convergence zone
JAS	July–August–September
LAI	leaf area index
MODIS	Moderate Resolution Imaging Spectroradiometer
MPI-ESM	Earth system model of the Max Planck Institute for Meteorology
NDVI	normalised difference vegetation index
NIR	near infrared
NPP	net primary productivity
PFT	plant functional type
PMIP2	Paleoclimate Modelling Intercomparison Project Phase II
SIC	sea ice cover
SOC	soil organic carbon
SOM	soil organic matter
SST	sea surface temperatures
USGS	U.S. Geological Survey
UV	ultraviolet
VIS	visible
WAM	West African Monsoon
WS	west Sahara

Chapter 1

Introduction

1.1 Characteristics of the Sahara and the Sahel

Two major climatic regions characterise the northernmost part of Africa: the Sahel and the Sahara. The Sahel spans the African continent from west to east, roughly between 10 and 18° N. The Sahel is a semi-desert area that annually receives between 150 and 500 mm of rainfall (Lezine 1989). The vegetation cover mainly consists of open to sparse grassland and shrubland, in some places with savanna characteristics. The Sahel is the transition zone from the savannas and the tropical forests to the south and the Sahara to the north. The Sahara is the largest desert on earth. It receives minimal amounts of rainfall and vegetation cover is mainly constrained to groundwater-fed oases or to the mountainous regions, where rainfall is less scarce. Due to the low amounts of rainfall that fall on average in these two regions, they are extremely vulnerable to climatic change (IPCC 2007b) and to project reasonable climate change scenarios in this region is important.

In terms of future precipitation change, the Sahel and the Sahara is one of the regions in which global climate models disagree the most (IPCC 2007a). Some of the large disagreement is due to two extreme outliers, however these outliers simulate the present-day climate relatively well (Patricola and Cook 2010). Knowing

that the model simulates the present Sahelian climate well, is an indication, but not a guarantee that it will project future climate in a consistent way (Biasutti and Giannini 2006; Cook and Vizy 2006). It is thus necessary to consider methods that allow us to investigate the sensitivity of the models to external forcing.

The climate of the Sahel and the Sahara is highly variable on timescales from years to millennia. Investigating the mechanisms responsible for these variations will allow us to quantify the relative importance of various processes for the climate of the region. The atmosphere and the ocean play important roles for interannual, interdecadal (e.g. Lamb 1978) as well as millennial timescales (e.g. Liu et al. 2004). It has however been shown that for all these timescales vegetation might have an important role as an amplifier of the signals of the atmosphere and the ocean, such as increasing the long-term persistence for decadal variations (e.g. Zeng et al. 1999) and enhancing externally forced signals, such as orbitally induced signals (e.g. Claussen and Gayler 1997; de Noblet-Ducoudre et al. 2000; Claussen et al. 2006).

1.2 Sahelian and Saharan precipitation variability on multi-millennial timescales

During several intervals in the past the Sahel and the Sahara were considerably wetter than today. The occurrence of these wetter periods corresponds well with the precessional forcing of the Milankovitch cycles (Tjallingii et al. 2008) and represents variability on multi-millennial timescales. The most recent such period occurred during the early- to mid-Holocene, some 9500 to 6000 years before present (BP). During this period the monsoonal rainfall reached further north and the total amount of rainfall was larger, which was evidenced through increased vegetation cover and an increased abundance of lakes and wetlands. These large-scale climatic changes have been inferred from numerous sources of marine proxy records (e.g. Adkins et al. 2006) and terrestrial proxy records, such as archaeo-

logical records (Hoelzmann et al. 2001), pollen records (Lezine 1989; Jolly et al. 1998b; Lezine 2009), sediment records (Ritchie et al. 1985) and lake level reconstructions (e.g. Pachur and Rottinger 1997; Hoelzmann et al. 2000, 2001; Drake and Bristow 2006).

During the early-to mid Holocene the orbital configuration of the sun was different from the one of today (Berger 1978). Eccentricity was slightly larger but close to that of today. The largest difference arises from an increased obliquity and a perihelion that occurred close to summer solstice. These two factors lead to increased summer insolation and decreased winter insolation in the northern hemisphere, as well as decreased summer insolation and increased winter insolation in the southern hemisphere. This in turn leads to increased seasonality in the northern hemisphere and decreased seasonality in the southern hemisphere. It is now generally accepted that the main reason for the changes in the palaeo-monsoon during the mid-Holocene was the increased seasonal cycle of insolation in the northern hemisphere (de Noblet-Ducoudre et al. 2000). The insolation difference, compared to today, was at its extremum at around 9000 years BP. However at that time the climate of the Earth was still not in a proper interglacial state, since large ice sheets, such as the Laurentide ice sheet, covered large part of the northern continents. Sea level was also below the one of today. At the time of the mid-Holocene these ice sheets had disappeared and greenhouse gases levels were close to pre-industrial values. Being free of these two effects the mid-Holocene provides a more appropriate testing ground for Sahelian climate change than the insolation optimum (Jolly et al. 1998b).

The role of vegetation as an amplifier of the mid-Holocene palaeo-monsoon is under discussion. Many studies show that it plays an important role (e.g. Claussen and Gayler 1997; de Noblet-Ducoudre et al. 2000), others, such as the models with dynamic vegetation in the Paleoclimate Modelling Intercomparison Project Phase II (PMIP2) project show a rather weak amplification by vegetation (Braconnot et al. 2007b). Vegetation affects the energy exchange between

the land surface and the atmosphere in many ways, through the surface radiation budget (via the land surface albedo), the hydrological cycle (via transpiration) and the momentum flux (via roughness length). Several studies based on general circulation models (GCMs) have shown that land surface albedo is the key variable for obtaining a positive feedback between land surface and precipitation in the Sahel/Sahara region (e.g. Claussen 1997; Levis et al. 2004; Schurgers et al. 2007), rather than other processes. In order to properly estimate the strength of the amplification of the signal by vegetation, the land surface albedo change between the present and the mid-Holocene thus has to be simulated in an appropriate manner. The variations in land surface albedo in most current GCMs only depend on short-term changes such as soil moisture and canopy cover. When one considers longer timescales, changes to the vegetation structure below the canopy and the soil may affect the albedo. When ignoring the effects of these on land surface albedo, the simulated difference in albedo between today and the mid-Holocene might be inaccurate. This leads to the following questions:

- Can the land surface albedo change between today and the mid-Holocene be simulated in a more consistent way than in previous studies?
- What is the sensitivity of the mid-Holocene climate to the plausibly simulated land surface albedo change?

To evaluate the performance of the models, the model output needs to be compared to proxy data, such as pollen data and lake levels. Terrestrial palaeorecords from the Sahara suffer from a lack of coverage (Lezine 1989), which makes it difficult to properly assess the extent of the greening during the mid-Holocene. The scarcity of locations is mainly due to the poor preservation potential of Saharan sediments (Ritchie et al. 1985). Another challenge is the scarcity of high-resolution cores from which the pollen are taken (Lezine 2009). This makes dating and also the assessment of the continuity of the wet period difficult. Marine records provide continuous and high-resolution data, but one cannot be sure of

the extent to which these reflect conditions on land (Kröpelin and Petit-Maire 2000). In an attempt to overcome these problems, a major effort was made during the Palaeovegetation Mapping Project (BIOME 6000) (Prentice and Webb 1998) to collect all available pollen records for the mid-Holocene Sahara for a synthesis (Jolly et al. 1998b). This solves the problem of the spatial element, but not the time-resolution. It is well known that the extreme position of vegetation cover occurred relatively early in the Holocene, around 8500 years BP (Lezine 1989). Estimates for the location of the mid-Holocene desert border range between a northward displacement by some 400 to 500 km (e.g. Ritchie et al. 1985; Pachur and Kröpelin 1987; Ritchie and Haynes 1987) or up to 23° N (Jolly et al. 1998b). It is unclear to what extent and at what frequency the region north of 23° N was covered by vegetation during the mid-Holocene. In some recent modelling studies (e.g. Braconnot et al. 2007a), it has been assumed that a mean increase in precipitation of at least 200 mm per year is needed across the Sahara for a match with the data. This corresponds to the assumption that there was a change in mean climate. Due to the coarse resolution of the geological data, it is not possible to say if there was continuous or intermittent climate change north of 23° N. It has thus to be investigated if:

- the match between model and data in the Sahara can be improved by considering a change in variability, rather than considering a change in mean climate.

1.3 Sahelian and Saharan precipitation variability on sub-centennial timescales

The Sahel/Sahara is not only characterised by long-term fluctuations on orbital timescales. Variability at shorter timescales also plays an important role in this area. On the interannual timescale, fluctuations as large as the long-term mean are common and it has also been shown that decadal and multi-decadal dry or

wet periods have been an inherent part of the Sahel at least during the last centuries (Nicholson 1981, 1989). Climate variability is important for vegetation variability in semi-arid areas. There the vegetation response does not only depend on changes in the mean climate, but also on changes in patterns of variability, such as extreme events and the temporal structure of the change (Ni et al. 2006). Even though a lot of research has been devoted to the mid-Holocene palaeo-monsoon and the Sahara, only a few (e.g. Ni et al. 2006; Zhao et al. 2007) have considered variability on shorter timescales in the region during the mid-Holocene. The following questions arise:

- Does the coupled model ECHAM5-JSBACH/MPIOM represent precipitation variability in the Sahel in a plausible way for present day orbital forcing?
- Does simulated precipitation variability differ between the mid-Holocene and today?
- How do the response timescales that are inherent to vegetation dynamics and the dynamic background albedo, affect the precipitation variability of the pre-industrial and mid-Holocene simulations?

Ocean forcing and ocean variability play an important role for Sahelian precipitation variability (Giannini et al. 2003). It is possible that the role of vegetation in affecting precipitation variability at sub-centennial timescales is strongly controlled by the imposed ocean state. Using a different set of sea surface temperatures (SST), enables us to investigate the sensitivity of the relationship between vegetation and precipitation variability to ocean forcing. Using observed SSTs from the last century, one can test the robustness of and validate the results obtained with model-derived SSTs.

- Is ECHAM5-JSBACH able to reproduce the variability in the Sahel for the last century using reconstructed SSTs?

- How do the response timescales that are inherent to vegetation dynamics and the dynamic background albedo, affect the precipitation variability of the last century?

1.4 Thesis outline

The remaining chapters of this thesis are structured as follows.

- **Chapter 2**

  In the second chapter of this thesis a new albedo scheme is presented, which represents the correspondence between vegetation and albedo in a more consistent way for the mid-Holocene than the standard scheme used in ECHAM5-JSBACH. The simulated North African precipitation in the mid-Holocene and the pre-industrial climate with and without the new scheme is compared, focusing on the mean climate and changes in the spatial distribution of rainfall, as well as on changes in the seasonal cycle. The relevance of comparing mean state climate variables to the various palaeo-data sources is discussed and other measures that might be better for comparative purposes are suggested. This chapter has been published in *Climate of the Past*[1], and is reproduced here with editorial adjustments.

- **Chapter 3**

  In the third chapter the variability of Sahelian precipitation is investigated. The chapter is divided into two parts.

  In the first part, simulations for the pre-industrial and the mid-Holocene climates, where the atmosphere model ECHAM5 is forced with coupled-model SSTs, are used. Tropical SSTs are shown to excessively dominate the pre-industrial variability signal. In the mid-Holocene the tropical SST signal

[1] Vamborg, F. S. E., Brovkin, V., and Claussen, M.: The effect of a dynamic background albedo scheme on Sahel/Sahara precipitation during the mid-Holocene, Clim. Past, 7, 117-131, doi:10.5194/cp-7-117-2011, 2011.

is slightly reduced, however the low confidence in simulated pre-industrial variability indicate that these simulations are inappropriate for investigating variability in further detail.

In the second part, ECHAM5-JSBACH simulations forced with observed SSTs for the last century are used. Here the focus is on the effect of vegetation on precipitation variability and vice versa. Special attention is payed to how the persistence and strength of the different signals is affected by dynamic vegetation and the dynamic land surface albedo scheme.

- **Chapter 4**

  The fourth chapter contains a summary of the major findings and the conclusions one can draw from those, as well as a discussion on perspectives for future research in this area.

Chapter 2

The effect of a dynamic background albedo scheme on Sahel/Sahara precipitation during the mid-Holocene

2.1 Introduction

Investigating climates of the past offers an opportunity to improve our understanding of future Earth system dynamics. During the mid-Holocene, around six thousand years ago, the West African monsoon reached much further north than it does today. The area that today is covered by the Sahara was largely vegetated, as established using e.g. pollen reconstructions (e.g. Jolly et al. 1998b). The vegetation cover extended at least up to 23° N (Jolly et al. 1998a), if not across the whole of North Africa (Hoelzmann et al. 1998), compared to about 12° N today (de Noblet-Ducoudre et al. 2000). Lake abundance and lake levels also increased throughout North Africa and on the Arabian Peninsula (Hoelzmann et al. 1998).

The mechanisms responsible for the northward shift and intensification of the palaeo-monsoon and subsequent greening have been studied extensively using

models, including general circulation models (GCMs). The largest differences in external forcing between the mid-Holocene and today are radiative forcing anomalies arising from changes in the Earth's orbital parameters (Berger 1978). It is now largely accepted that the main reason for changes in the palaeo-monsoon was an increased seasonal cycle of insolation in the Northern Hemisphere due to a change in these parameters (de Noblet-Ducoudre et al. 2000). However, as demonstrated by several modelling experiments, a change in just the orbital parameters is not sufficient to induce strong enough changes in the monsoon to agree with reconstructed vegetation and precipitation (Joussaume et al. 1999). In order to obtain the correct signal, several feedback mechanisms have been suggested, such as ocean amplification (e.g. Kutzbach and Liu 1997) and vegetation-atmosphere feedbacks (e.g. Claussen and Gayler 1997; de Noblet-Ducoudre et al. 2000). The combined effect of orbital change, ocean feedbacks and vegetation feedbacks corresponds best to palaeo-reconstructions (Braconnot et al. 2007a).

A positive vegetation feedback in the Sahel/Sahara transition region was first proposed by Charney (1975). He suggested that areas with an elevated albedo (e.g. deserts) have a more stable air column than surrounding areas and thus precipitation is suppressed above the desert. With aridification this mechanism is extended and a positive feedback loop occurs, leading to self-stabilisation of the desert. If, reversely, vegetation growth is extended into a desert area, albedo is reduced and the mechanism works the opposite way. During the mid-Holocene, rainfall in the Sahel was increased by the insolation anomaly and this feedback could have taken place. The main driver behind Charney's theory is a change in surface albedo, but the theory ignores other vegetation-related moisture feedbacks, such as increased transpiration, which could also affect rainfall (Xue and Shukla 1993; Brovkin et al. 1998). Nevertheless, several GCM studies have shown that surface albedo is the key variable for obtaining a positive feedback between land surface and precipitation in the Sahel/Sahara region (e.g. Claussen 1997; Levis et al. 2004; Schurgers et al. 2007), rather than other processes. Thus, to

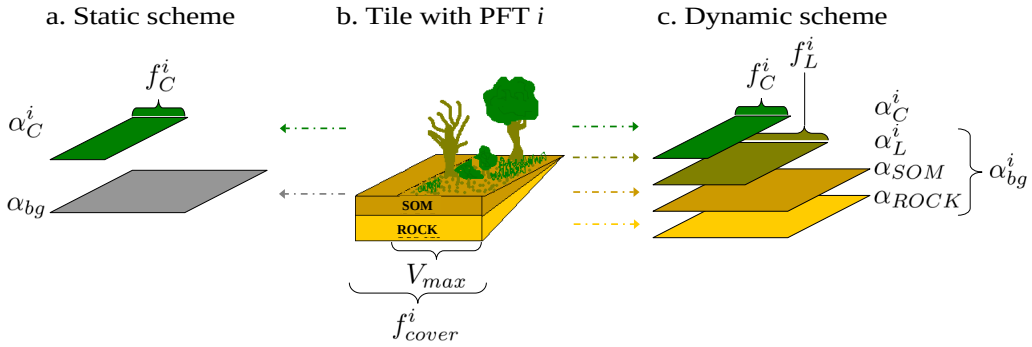

Figure 2.1: Sketch illustrating the components needed to calculate α^i, the land surface albedo of the tile containing PFT i according to the static **(a)** and dynamic **(c)** background albedo schemes. Arrows and colours indicate the correspondence between albedo and a modelled tile **(b)**. Several PFTs are depicted in this tile to illustrate the origin of the different albedo layers.
Notations are as follows:
(a) α_{C}^i – canopy-albedo for PFT i, α_{bg} – background albedo defined per gridbox, f_{C}^i – the fraction of α^i that is calculated from α_{C}^i
(b) SOM – organic soil layer, ROCK - mineral soil layer, V_{max} – vegetated fraction of tile, f_{cover}^i – fraction of gridbox covered by PFT i.
(c) α_{C}^i, f_{C}^i as in (a), α_{L}^i – litter and phytomass albedo for PFT i, f_{L}^i – the fraction of α_{bg}^i that is calculated from α_{L}^i, α_{SOM} – albedo of the gridbox bare ground, α_{ROCK} – albedo of SOM-free bare ground, α_{bg}^i – background albedo for PFT i.

correctly quantify the magnitude of this feedback, the land surface albedo of both deserts and vegetated areas has to be modelled realistically.

Land surface albedo schemes in the current generation of GCMs are usually based on the following considerations (Wang et al. 2007): land surface albedo, α_{S}, is calculated as the sum of the albedo of all plant functional types (PFTs), α^i, weighted by their cover fractions, f_{cover}^i. The albedo of PFT i, α^i, is calculated as the weighted average of the canopy albedo of PFT i, α_{C}^i, and the albedo of the surface below the canopy, the background albedo α_{bg} (see Fig. 2.1). The canopy fraction of PFT i, f_{C}^i, is based on the presence of green leaves, which is defined through the leaf area index (LAI). The background albedo is based on a time-invariant map, either derived from satellite data or from soil type data. In some cases the background albedo varies with soil moisture (e.g. Oleson et al. 2004;

Wang 2005), but in many schemes, e.g. in JSBACH, the land surface scheme of the Earth system model of the Max Planck Institute for Meteorology (MPI-ESM), it is constant. For the present-day situation the background albedo can be captured well by satellite observations and the method described above is appropriate. However, if the vegetation cover differs substantially from the one of today, for instance in the past or in possible future scenarios, this approach may be inadequate, since background albedo as well as canopy cover could change significantly within those time frames.

In arid to semi-arid regions, the land surface albedo varies seasonally, with changes in LAI being one of the main modulators of these changes. During the dry season, when LAI is close to zero, the albedo is controlled partly by the albedo of bare ground and partly by the amount of litter and standing dead phytomass masking the ground (Samain et al. 2008). To capture albedo changes in the Sahel/Sahara one should thus consider, not just the LAI-cycle, but also the albedo of bare ground and the albedo of litter. The background albedo values in the Sahara are very inhomogeneous, with some areas (hot desert) having extremely high albedo values. Albedo in these areas is linked to soil formation processes such as lake desiccation and salt crusting. High albedo areas in the present day act to suppress precipitation (Knorr et al. 2001; Knorr and Schnitzler 2006). In many models these inhomogeneities are ignored, leading to inter-model biases in the strength and extent of the present-day West African Monsoon (WAM) (Bonfils et al. 2001). Levis et al. (2004) showed that altering the soil composition and soil colour to represent different amounts of soil organic matter (SOM), in the Sahara during the mid-Holocene also leads to a further increase in precipitation, compared to using present-day values. This increase mainly arises from a reduction in albedo. These studies highlight the importance of considering all these components dynamically to fully capture the albedo differences between the mid-Holocene and today and thus to better quantify the vegetation-precipitation feedback.

In this chapter, we present a land surface albedo scheme, in which the α_{bg} changes in time as well as in space. We compare the effect on precipitation of two albedo schemes, the static and dynamic schemes, for the present day (pre-industrial setup) and for the mid-Holocene, focusing on North Africa and the Arabian Peninsula.

2.2 Dynamic background albedo scheme

For the experiments in this chapter we use the spectral atmosphere model ECHAM5 (Roeckner et al. 2003) in T31 resolution with 19 levels in the vertical coupled to the land surface scheme JSBACH extended with a dynamic vegetation module (Raddatz et al. 2007; Brovkin et al. 2009). A tiling approach is used to represent sub-gridbox vegetation dynamics. Tile i is the gridbox space that is occupied by PFT i.

All albedo values in JSBACH are calculated separately, but according to the same equation, for the two spectral bands; visible (VIS) and near infrared (NIR). Throughout the chapter, we only refer to albedo values as α_X^i or α_X, where i indicates PFT-specific values and X is the type of albedo referred to (such as S for surface, C for canopy etc.). The dependence on the spectral bands is thus implicit in the equations and only explicitly shown for parameterisation in Table 2.1. The radiation scheme in ECHAM5 used in these simulations represents six bands for incoming short-wave radiation in the range 0.25–4.00 μm; three ultraviolet (UV) and VIS bands, and three NIR bands. The VIS and NIR albedo values calculated in JSBACH are used by ECHAM5 accordingly (the VIS albedo for the UV + VIS bands and the NIR albedo for the NIR bands). The albedo discussed in the results section is the combined mean land surface albedo calculated by ECHAM5, at each output time-step, from the VIS and NIR albedo values calculated by JSBACH.

2.2.1 Standard albedo scheme in JSBACH

For snow-free land in JSBACH the albedo of each PFT i, α^i, is calculated according to:

$$\alpha^i \;=\; f_{\mathrm{C}}^i \; \alpha_{\mathrm{C}}^i \;+\; \left(1 \;-\; f_{\mathrm{C}}^i\right) \; \alpha_{\mathrm{bg}}. \tag{2.1}$$

The albedo of the canopy (green leaves), α_{C}^i, is PFT-specific (see Table 2.1), whereas the background albedo α_{bg} is defined per gridbox independent of PFTs. α_{bg} is constant in time and read in as two maps, one for each of the spectral bands, at the beginning of each experiment. These maps have been derived from MODIS (The Moderate Resolution Imaging Spectroradiometer) reflectance data in a manner similar to Rechid et al. (2009). The fraction of the tile for PFT i that is covered by the canopy, f_{C}^i (Eq. 2.2), varies with the fraction of the gridbox that is vegetated ($V_{\max}$) and with the leaf area index (LAI^i) of PFT i:

$$f_{\mathrm{C}}^i \;=\; V_{\max} \; \left(1 \;-\; e^{-\mathrm{LAI}^i/2}\right). \tag{2.2}$$

It can thus vary in space and time. Note that the stem area effect on albedo is only taken into account in snow-covered areas, and is thus not reflected here. Finally the albedo values of all PFTs are weighted by their vegetation cover fraction f_{cover}^i and summed to a gridbox-averaged surface albedo, α_{S}:

$$\alpha_{\mathrm{S}} \;=\; \sum_{\mathrm{PFT}} f_{\mathrm{cover}}^i \; \alpha^i. \tag{2.3}$$

2.2.2 Dynamic background albedo

In the above version of the scheme, α_{bg} is constant in time and defined per gridbox. We introduce a time-varying and PFT-specific background albedo α_{bg}^i, which replaces the α_{bg} in Eq. (2.1). The standard (static) and the dynamic approach are illustrated in Fig. 2.1. All other albedo calculations remain the same.

Table 2.1: Albedo values used in the dynamic albedo scheme.

Plant functional type	$\alpha^i_{\mathrm{C,vis}}$	$\alpha^i_{\mathrm{C,nir}}$	$\alpha^i_{\mathrm{L,vis}}$	$\alpha^i_{\mathrm{L,nir}}$
tropical broadleaf evergreen trees	0.03	0.22	0.09	0.07
tropical broadleaf deciduous trees	0.04	0.23	0.10	0.08
extra-tropical evergreen trees	0.04	0.22	0.07	0.07
extra-tropical deciduous trees	0.05	0.25	0.08	0.10
raingreen shrubs	0.05	0.25	0.11	0.20
deciduous shrubs	0.05	0.28	0.11	0.23
C3 grass	0.08	0.34	0.14	0.29
C4 grass	0.08	0.34	0.14	0.29

There are two main factors that affect the background albedo; bare ground and the standing non-green phytomass and litter. We will discuss the dynamic scheme around these two factors. The albedos corresponding to these factors are α_{SOM} and α^i_{L}. The new albedo of the background is then calculated per PFT as the weighted sum of these factors, where the weighting factor f^i_{L} represents the area of the tile covered by litter:

$$\alpha^i_{\mathrm{bg}} \;=\; f^i_{\mathrm{L}}\,\alpha^i_{\mathrm{L}} \;+\; \left(1 \;-\; f^i_{\mathrm{L}}\right)\,\alpha_{\mathrm{SOM}}. \tag{2.4}$$

As for the surface albedo, this albedo is calculated separately for the two spectral bands VIS and NIR.

2.2.2.1 Albedo of bare ground: α_{SOM}

The main properties modulating the reflectance of bare ground are the different mineral components (the underlying parent material) and soil organic matter (SOM) (Ladoni et al. 2010). The relationship between SOM and reflectance is often assumed to be linear, with SOM being negatively correlated to reflectance up to a saturation limit of around 5% SOM in the top soil layer (Curran 1985; Ladoni et al. 2010). The maximum change in VIS and NIR reflectance due to SOM ($a \cdot C_{\mathrm{lim}}$, in Eq. 2.5) is between 0.1 and 0.3 (e.g. Stoner and Baumgardner

1981; Curran 1985; Bartholomeus et al. 2008). Here we use a conservative estimate of 0.15. The relationship may vary spatially, mainly due to different parent materials (Henderson et al. 1992). To capture this, we define a variable representing the albedo of the bare ground that does not contain any SOM, α_{ROCK}. We assume, for the purpose of our study, that the timescales are too short for major changes in soil mineral composition and α_{ROCK} is thus constant in time in our simulations. We use the gridbox average of the modelled slow soil carbon pool C_{ss} ($\mathrm{mol(C)\,m^{-2}_{gridbox}}$) as a proxy for SOM. The slow soil carbon pool represents the carbon in the soil that mineralizes at a slow rate and it has a turnover time of 150 years. We introduce a saturation limit C_{lim} beyond which increasing SOM does not affect the albedo. The value of C_{lim} was chosen on one hand to correspond to the geographical transition from low to medium amounts of soil organic carbon (SOC) in the top-soils of tropical Africa (FAO 2007) and on the other hand to obtain reasonable estimates for α_{ROCK} (see below). The albedo of a bare ground surface containing SOM, α_{SOM}, is thus derived as a linear function of SOM up to the saturation limit C_{lim}, with α_{ROCK} as intercept:

$$\alpha_{\mathrm{SOM}} \;=\; \alpha_{\mathrm{ROCK}} \;-\; a \;\cdot\; \min\,(C_{\mathrm{ss}},\; C_{\mathrm{lim}}) \tag{2.5}$$

where $a = 3 \times 10^{-4}\,\mathrm{m^2_{gridbox}\,mol^{-1}(C)}$ and $C_{\mathrm{lim}} = 500\,\mathrm{mol(C)\ m^{-2}_{gridbox}}$. This calculation is done per gridbox and is not PFT specific.

Rock albedo, α_{ROCK}, should ideally be derived from bedrock or sediment properties. The standard α_{bg} is derived from satellite data, by considering the times of the year with the lowest LAI. For the variable α_{ROCK} it is not possible to derive the information directly from satellite data, except for desert regions. There have been attempts to correlate MODIS albedo with FAO soil maps and USGS geological maps (Tsvetsinskaya et al. 2002, 2006). These correlations are region-specific and only give data for present-day desert areas. Since we are interested in global data, this approach does not provide additional information for extracting α_{ROCK} compared to the MODIS-derived maps for α_{bg} currently used in JSBACH. We

derive α_{ROCK} by assuming that for the present-day simulation $\alpha_{\mathrm{SOM}} = \alpha_{\mathrm{bg}}$ and using the inverse calculation of Eq. (2.5). This of course does not hold for areas where litter and phytomass cover the bare ground.

We did not include the dependence of bare ground albedo on soil moisture in this relationship, even though it is well documented that background albedo generally decreases with increasing soil moisture (e.g. Domingo et al. 2000; Lobell and Asner 2002; Gascoin et al. 2009). This limitation is justified for two reasons: First, soil hydrology is represented by a rather crude bucket model in JSBACH of 1 m depth, while albedo is only affected by soil water if the upper few millimetres to centimetres of the soil are wet (Gascoin et al. 2009). This effect can thus not be included in the current version of JSBACH in an appropriate way. Second, the map used to derive the rock albedo is an annual mean and therefore neither represents completely dry nor completely wet soils, an appropriate dry albedo could thus not be derived. However, in principle, the soil moisture effect could easily be included.

2.2.2.2 Albedo of non-green phytomass: α_{L}

Litter storage is represented for each PFT i in JSBACH by two carbon pools: woody litter W^i and leaf litter L^i ($\mathrm{mol(C)\,m^{-2}_{vegetated\ area}}$). The turnover time of the leaf litter pool depends on soil moisture and temperature and is about one and a half years. We use L^i as a proxy for the combined amount of litter and aboveground dead phytomass in a tile. We assume that L^i is spread equally across the vegetated part of the tile ($V_{\max}$). Further we assume that the fraction of the tile covered by litter can be derived in a similar way to the derivation of the fraction of the tile covered by green leaves (see Eq. 2.2). The LAI^i ($\mathrm{m^2_{leaf}\,m^{-2}_{canopy}}$) in Eq. 2.2 is derived by multiplying the specific leaf area SLA^i (leaf area per unit mass, $\mathrm{m^2_{leaf}\,mol^{-1}(C)}$) with the mass of green leaves M^i ($\mathrm{mol(C)\,m^{-2}_{canopy}}$). Here we introduce a leaf area index for litter, $\mathrm{LAI}^i_{\mathrm{L}}$ ($\mathrm{m^2_{leaf}\,m^{-2}_{vegetated\ area}}$), derived by

multiplying L^i with SLA^i:

$$\mathrm{LAI}_{\mathrm{L}}^i \;=\; \mathrm{SLA}^i \; L^i. \tag{2.6}$$

For the canopy, the factor of 0.5 in the exponent represents the non-ordering of leaves, i.e. that leaves hang at different angles and thus do not cover the ground with maximum area. For litter it would be possible that all leaves align, in which case this factor underestimates the actual coverage by litter. Litter is however freer to move than leaves in the canopy, which means that it could be subjected to clumping, in which case this factor would over-estimate the area covered by litter. Since we lack data on which of these effects is stronger, we keep this factor at 0.5 for the litter equation. The fraction of the tile that is covered by litter is thus calculated as follows:

$$f_{\mathrm{L}}^i \;=\; V_{\max} \left(1 \;-\; e^{-\mathrm{LAI}_{\mathrm{L}}^i/2}\right) \tag{2.7}$$

To derive the albedo values for litter, α_L^i, we grouped the PFTs into two larger groups, the first representing trees and the second shrubs and grasses, and assumed that the change from canopy to litter albedo was the same within the groups. We used the values for live and dead leaves in Sellers et al. (1996) as guidance for the direction of change. The general pattern is that dead leaves have a higher reflectivity in the visible spectrum than green leaves, in the near infrared the tendency is rather the opposite, although this is not always the case (Asner et al. 1998). The MODIS maps for α_{bg} are the best approximation that we have for the background albedo. We calculated a new gridbox average albedo, $\alpha_{\mathrm{bg}}^{\mathrm{dyn}}$, using the new scheme:

$$\alpha_{\mathrm{bg}}^{\mathrm{dyn}} \;=\; \sum_{\mathrm{PFT}} f_{\mathrm{cover}}^i \; \alpha_{\mathrm{bg}}^i. \tag{2.8}$$

The carbon pools needed for this calculation were taken from a pre-industrial control simulation with fixed vegetation and static background albedo scheme

(exp. 0K in Table 2.2). By assuming that $\alpha_{\mathrm{dyn}}^{\mathrm{bg}}$ should fit α_{bg} as closely as possible, we adjusted the litter albedo values to arrive at the final parameterisation (see Table 2.1). In the VIS we subdivided the tree group into extra-tropical and tropical trees to obtain a better fit.

2.3 Experimental design

The main purpose of the dynamic background albedo scheme is to investigate the interaction between the land surface and precipitation in the mid-Holocene Sahara. We thus focus on the interactions between the land and the atmosphere, which means that it is sufficient to run the model with only atmospheric components, forced with sea surface temperatures (SSTs) and sea ice cover (SIC). To capture interannual variability in the SSTs, we use 100 years of monthly mean SSTs and SIC from two coupled atmosphere-ocean simulations with the MPI-ESM that only differ in the orbital forcing, one for pre-industrial and one for the mid-Holocene, as described in Fischer and Jungclaus (2010). Since the dynamic background albedo scheme depends on the carbon pools, the carbon model has to be run into equilibrium. The simulations with dynamic background albedo were first integrated for 100 years to produce a preliminary climatology. This climatology was used as forcing for the JSBACH carbon model until equilibrium was reached. The carbon pools thus obtained were used to re-initialise the ECHAM5-JSBACH simulations, which were run until a reasonable equilibrium in the vegetation distribution and the carbon pools was reached.

The experiments were performed with either: (1) Orbital- and SST-forcing for pre-industrial or mid-Holocene and (2) static or dynamic background albedo (see Table 2.2). We focus our analysis on four of these simulations: 0K_st (pre-industrial, static), 6K_st (mid-Holocene, static), 0K_dyn (pre-industrial, dynamic), 6K_dyn (mid-Holocene, dynamic). Dynamic vegetation was used in all simulations. We use the last 100 years of each multi-century simulation (see

Table 2.2: Experimental setup. Experiment: analysed (bold), Component: AV = echam5-jsbach (T31L19), −O = coupled to MPIOM, Veg: prescribed (−) or dynamic (dyn) vegetation, Albedo: static (−) or dynamic (dyn) background albedo scheme, Init veg: run from which initial or prescribed vegetation was taken, Cpool: run from which forcing for carbon offline model (used to initialise carbon pools) was derived, SST: run from which SST and SIC were derived, Orbit: 0K or 6K orbital forcing, Years: length of run in years.

Experiment	Component	Veg	Albedo	Init veg	Cpool	SST	Orbit	Years
0K_ctrl	AV-O	dyn	–	–	–	–	0K	>4500
0K	AV	–	–	0K_ctrl	–	0K_ctrl	0K	200
0K_st	AV	dyn	–	0K_ctrl	0K	0K_ctrl	0K	300
0K_dyn	AV	dyn	dyn	0K_ctrl	0K,0K_dyn	0K_ctrl	0K	100 + 300
6K_ctrl	AV-O	dyn	–	–	–	–	6K	>4500
6K	AV	–	–	6K_ctrl	–	6K_ctrl	6K	200
6K_st	AV	dyn	–	6K_ctrl	6K	6K_ctrl	6K	300
6K_dyn	AV	dyn	dyn	6K_ctrl	6K, 6K_dyn	6K_ctrl	6K	100 + 300

"Years" in Table 2.2) as analysis period. We focus on the region 10° W–50° E, 10° N–32° N, subdivided zonally in: WS - Western Sahara, 10° W–10° E, ES – Eastern Sahara, 10° E–30° E, and AP – the Red Sea and the Arabian Peninsula, 30° E–50° E. We refer to the scheme presented in this chapter as the dynamic scheme and the static scheme for the standard version in JSBACH. The terms pre-industrial and mid-Holocene simulations refer to the two sets of simulations for each time-slice (0K_st and 0K_dyn resp. 6K_st and 6K_dyn).

2.4 Results

2.4.1 Mean changes in albedo, precipitation and desert fraction

The observed annual mean land surface albedo in north Africa has a distinct meridional geographical pattern, with an abrupt transition from low albedo values in the south (ca. 0.2), progressively increasing through the Sahel, culminating in high to very high albedo values (0.35–0.5) in the Sahara within some four degrees

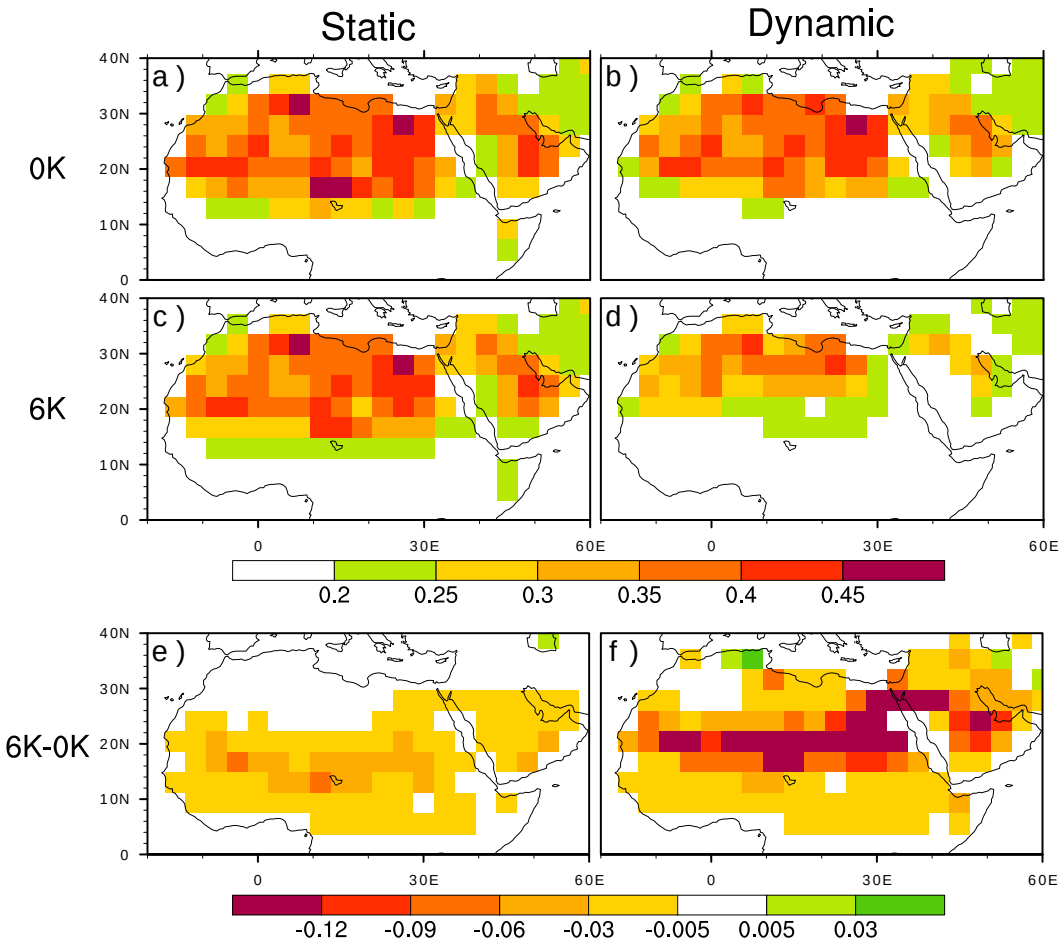

Figure 2.2: Land surface albedo α_S averaged over 100 years for **(a)** 0K_st, **(b)** 0K_dyn, **(c)** 6K_st, **(d)** 6K_dyn. 100-year mean land surface albedo differences between **(e)** 6K_st and 0K_st, **(f)** 6K_dyn and 0K_dyn.

latitude (e.g. Rechid et al. 2009). This pattern is closely linked to the vegetation cover, from fully covered in the south to sparse and no cover in the north (Tucker and Nicholson 1999). The transition in albedo is also clearly seen in the dry-season albedo and thus does not only arise from varying amounts of canopy cover (Samain et al. 2008).

We use the model-simulated variable desert fraction as a measure for vegetation in the simulations. The desert fraction is the fraction of a gridbox that has been completely non-vegetated for 50 years. The remaining part of the gridbox may display intermittent bare ground behaviour. In 0K_st, the desert border (the

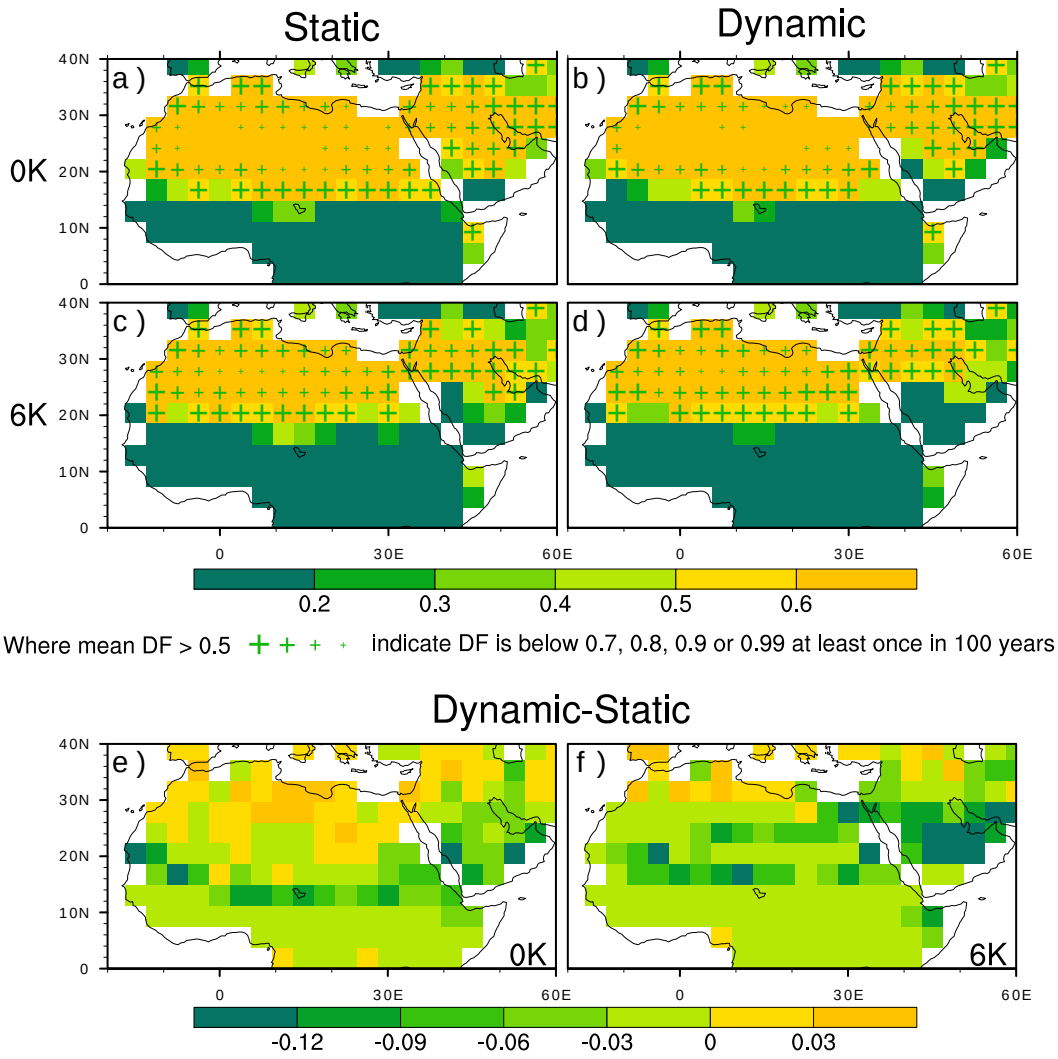

Figure 2.3: Desert fraction (DF) averaged over 100 years for **(a)** 0K_st, **(b)** 0K_dyn, **(c)** 6K_st, **(d)** 6K_dyn. 100-year mean desert fraction differences between **(e)** 0K_dyn and 0K_st, **(f)** 6K_dyn and 6K_st.

border of 0.5 desert fraction) is at around 14° N (Fig. 2.3a), which corresponds well to the present-day Sahel/Sahara border (Tucker and Nicholson 1999). As in observations, the fast transition from low to high albedo values coincides with the desert border and the gridboxes with very high albedo values (above 0.35) all lie north of the desert border (Fig. 2.2a). The general correspondence between vegetation cover and albedo seen in the annual mean observations is thus well represented in 0K_st.

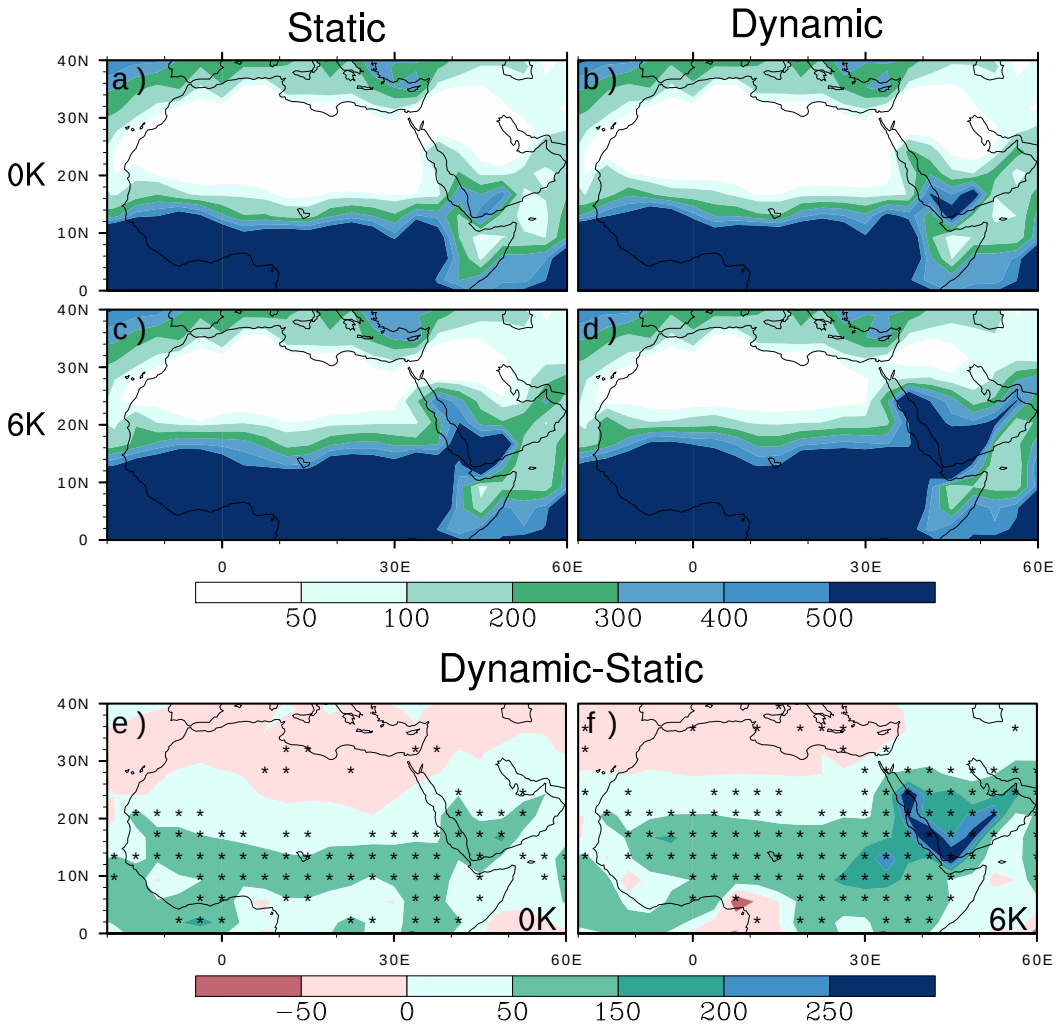

Figure 2.4: Precipitation (mm/year) averaged over 100 years for **(a)** 0K_st, **(b)** 0K_dyn, **(c)** 6K_st, **(d)** 6K_dyn. Differences in annual mean precipitation between **(e)** 0K_dyn and 0K_st, **(f)** 6K_dyn and 6K_st, gridbox differences significant (Student's T-test) at the 95% level are marked with an asterix.

In 0K_dyn, the albedo (Fig. 2.2b) remains close to that of 0K_st, except across the Sahel, from around 10° N to 18° N, where the albedo is reduced by around 0.06. The transition from low to high albedo values, though shifted sligthly northward, still agrees well with observations (e.g. Knorr et al. 2001) and as with the static scheme, the vegetation cover and albedo correspondence is captured well (Fig. 2.3b). The reduction in albedo in the Sahel leads to a local intensification of precipitation across the region of about 30 mm/year (Fig. 2.4e).

The observed regional annual mean precipitation is almost twice as large as the precipitation in 0K_st (1906–2006, CRU TS 3 0.5 (land); Mitchell and Jones 2005) and the modelled 200 mm/year isoline (Fig. 2.4a) is some degrees too far to the south (Fink et al. 2010). The introduction of the dynamic scheme thus reduces the dry bias in the Sahel that is apparent in 0K_st (standard ECHAM5).

It has previously been shown that the parameterisation of hot desert albedo controls the northward extent of the monsoon (Bonfils et al. 2001; Knorr et al. 2001; Knorr and Schnitzler 2006). With the dynamic scheme, most of the hot desert gridboxes persist and the albedo is reduced mainly in areas where the albedo values with the static scheme are relatively low as well. This indicates that it is not just the extent of rainfall that is controlled by the albedo, but that the annual mean albedo in the Sahel controls the intensity of the annual mean precipitation for timescales above decadal.

In 6K_st, the desert border is shifted northward by some four degrees, both in the Sahel/Sahara and on the Arabian Peninsula (Fig. 2.3c). The albedo differences are very small between 0K_st and 6K_st (Fig. 2.2e). Since gridboxes in the newly vegetated areas have desert-like albedo values, the correspondence between vegetation cover and albedo, particularly at the desert border, is not apparent in this simulation (6K_st). This geographical correspondence between modelled vegetation and albedo is captured much better in the dynamic simulation 6K_dyn (Figs. 2.3d, 2.2d). Since the correspondence between vegetation cover and albedo is captured well with the dynamic scheme for both the pre-industrial and the mid-Holocene, we expect the albedo change between the two times-slices to be more realistic with the dynamic scheme than with the static scheme (Fig. 2.2f vs. e).

The lower albedo in the mid-Holocene simulation 6K_dyn leads to an increase in precipitation of 80 mm/year in the studied region compared to 6K_st (Table 2.3). The sensitivity of precipitation to mid-Holocene orbital and SST forcings is thus increased by over a third through the introduction of the dynamic scheme.

Table 2.3: 100-year mean albedo, precipitation (mm/year) and desert fraction for the three areas WS, ES and AP.

Experiment	WS	ES	AP	Total
		Albedo		
0K_st	0.34	0.36	0.26	0.32
6K_st	0.32	0.34	0.24	0.30
0K_dyn	0.31	0.33	0.23	0.29
6K_dyn	0.26	0.25	0.17	0.23
6K_st–0K_st[1]	−0.02	−0.02	−0.01	−0.02
6K_dyn–0K_dyn[2]	−0.05	−0.08	−0.06	−0.06
		Precipitation (mm/year)		
0K_st	86 (±37)*	58 (±36)	114 (±83)	90 (±55)
6K_st	195 (±39)	167 (±47)	261 (±99)	217 (±62)
0K_dyn	115 (±40)	77 (±39)	152 (±87)	119 (±57)
6K_dyn	247 (±40)	214 (±44)	382 (±102)	295 (±57)
6K_st–0K_st[1]	109	109	147	128
6K_dyn–0K_dyn[2]	131	137	230	175
		Desert fraction		
0K_st	0.70	0.75	0.62	0.69
6K_st	0.53	0.53	0.41	0.49
0K_dyn	0.69	0.74	0.57	0.67
6K_dyn	0.49	0.50	0.33	0.45
6K_st–0K_st[1]	−0.17	−0.21	−0.21	−0.20
6K_dyn–0K_dyn[2]	−0.19	−0.24	−0.24	−0.23

[1,2] Differences in mean between 6K_st and 0K_st resp. between 6K_dyn and 0K_dyn.

* Standard deviations in precipitation calculated from 100-year climatology for each area.

2.4.2 Spatial variability of albedo and precipitation

To investigate spatial variability in more detail we consider zonal means over land for WS, ES and AP (Fig. 2.5a–c respectively and Table 2.3). As discussed in the previous section, the dynamic scheme increases precipitation in the pre-industrial simulation. However, the desert borders in WS and ES are barely affected and the largest changes in precipitation occur around or south of this border, showing that the dynamic scheme does not shift the rainfall substantially northwards into the Sahara. In AP the change in precipitation is smoother and stretched over a

larger latitudinal band, which results in a northward shift of the desert border. The albedo change introduced by the dynamic scheme peaks south of or around the desert border in all the regions.

In the mid-Holocene static simulation (6K_st), the desert border is shifted northwards by some four degrees in WS and ES, and by almost six degrees in AP. This leads to a slight reduction in albedo compared to the pre-industrial simulation (6K_st–0K_st). This reduction is at most as large as the reduction seen between the pre-industrial simulations (0K_dyn–0K_st). Even so, the difference in precipitation between the static simulations is at many latitudes more than twice as large as the one between the pre-industrial simulations. It is thus clear that the orbital and SST forcings play an important role in the northward extent and the intensification of precipitation during the mid-Holocene. This is in line with many other studies (e.g. Braconnot et al. 2007b), but not in line with a previous study using ECHAM, where albedo forcing was a stronger driver for a northward migration of the intertropical convergence zone (ITCZ) than orbital and SST forcings (Knorr and Schnitzler 2006).

The different response of the regions is most apparent when comparing the differences between pre-industrial and mid-Holocene simulations for both schemes (red resp. yellow lines in Fig. 2.5). In WS the precipitation difference between the two static simulations is negative south of 8° N, and positive between 8° N and 25° N. We can thus infer that precipitation is simultaneously increased and shifted northward. The dynamic scheme intensifies both the positive and the negative anomalies seen in the static case, showing that, in the zonal mean, the rain belt is shifted even further north by the dynamic scheme. This shift is relatively small and negligibly affects the desert border. A reason for this might be the inhibiting mechanism proposed by Knorr et al. (2001) for the present-day, since many high-albedo gridboxes persist north of the desert border even with the introduction of the dynamic scheme.

In ES, both the static and dynamic differences show a precipitation increase

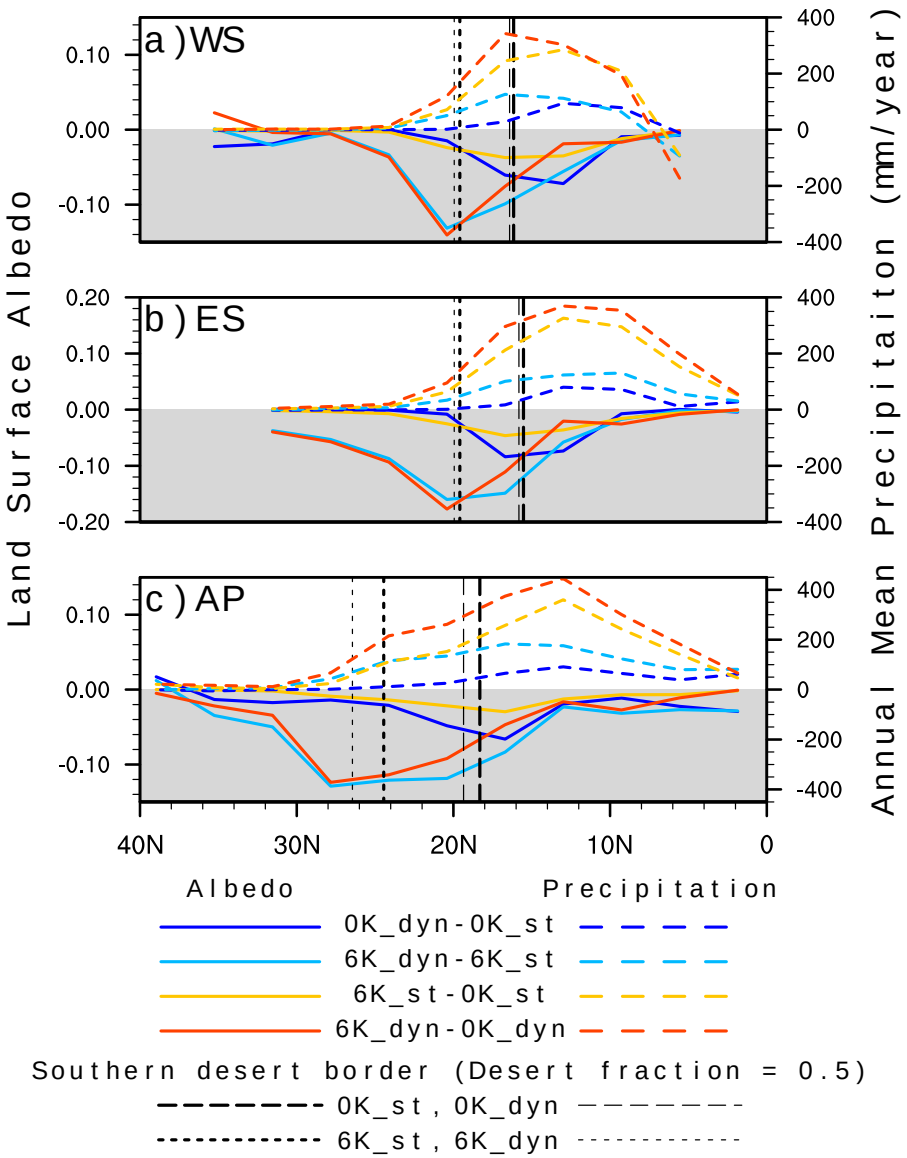

Figure 2.5: Change in precipitation (mm /year) and albedo averaged zonally over land and over 100 years for the regions **(a)** WS, **(b)** ES and **(c)** AP.

that is spread evenly across all latitudes. There is no reduction in rainfall to the south as seen in WS, neither for the static nor for the dynamic scheme. The dynamic scheme introduces large albedo differences across the whole desert region, even though the desert border barely shifts northwards. High albedo values can thus not be the reason for the lack of northward shift of rainfall, as they may be in WS.

The mid-Holocene response to the increased albedo forcing due to the dynamic scheme is strongest in AP. South of 20° N, the response is similar to that of the other regions, with the dynamic scheme additionally increasing the response by one third or below. North of 20° N, the dynamic scheme increases the precipitation by almost 100% and this occurs even though the absolute albedo anomalies are smaller in this region than they are in the other two.

The dynamic scheme thus shifts the most sensitive region eastward compared to the static scheme. A large response across the Red Sea and the Arabian Peninsula was also found by Levis et al. (2004) when prescribing the albedo of loam-like soil in the Sahara. Here we show that this response is not just the result of imposing an uncertain but plausible boundary condition, but that it is possible to dynamically simulate this response.

2.4.3 Seasonal changes in precipitation and albedo

Precipitation in North Africa is seasonal and mainly occurs during the summer months, approximately between June and September. For a forcing mechanism to have a large impact on precipitation it would thus need to occur within or closely before the rainy season (Braconnot et al. 2008). We therefore analyse the rainfall anomalies in more detail by considering the daily means of an average year. We use running means of 15 days to reduce noise in the differences between the static and dynamic simulations and of 30 days to reduce calendar-related problems (Joussaume and Braconnot 1997) in the differences between the pre-industrial and mid-Holocene simulations.

For the pre-industrial simulations the introduction of the dynamic scheme leads to anomalies of around 0.25 to 0.75 mm/day (Fig. 2.6a–c) that are evenly spread across the rainy season (indicated by the overlaid contours) for all three regions. Since the rainy season is longer in WS than in ES, the absolute change is larger. The difference between the seasonal cycles of albedo for the two schemes (not shown) is almost constant throughout the year. The dynamic scheme thus does

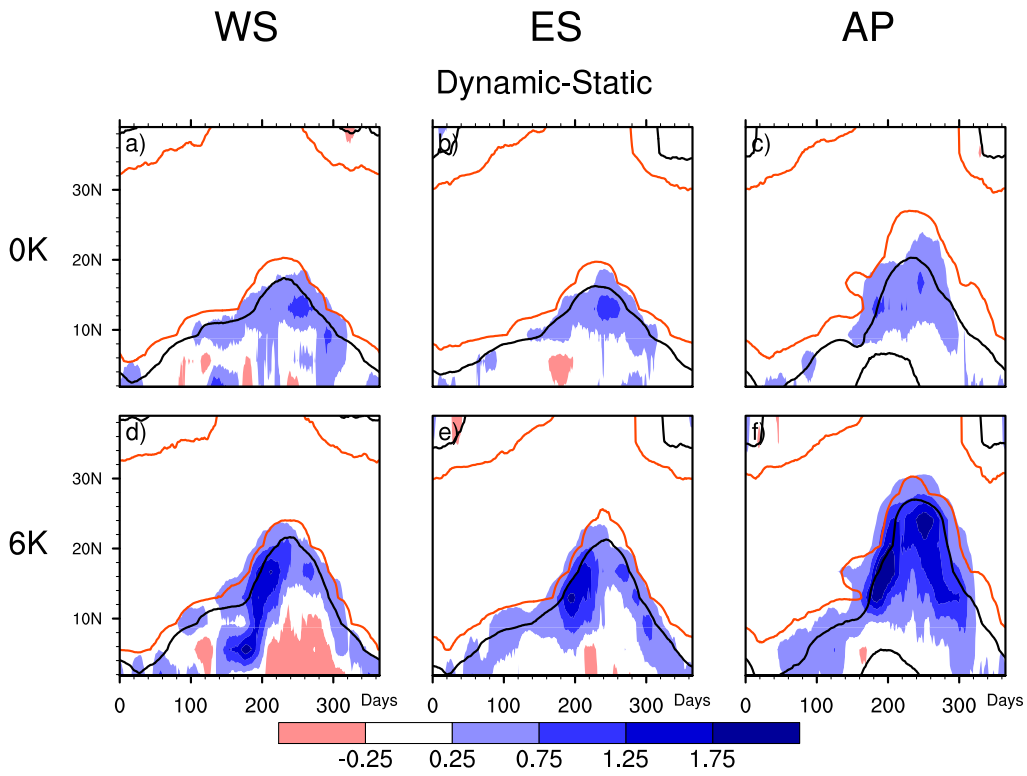

Figure 2.6: Shown are differences in the annual cycle of precipitation in mm/day derived from 100 simulation years (further filtered by 15-day running means) for the regions WS, ES and AP between 0K_dyn and 0K_st – **(a)** to **(c)** and between 6K_dyn and 6K_st – **(d)** to **(f)**. Overlaid are red and black contours representing the 0.25 and 1.25 mm/day isolines for 0K_st – **(a)** to **(c)** and 6K_st – **(d)** to **(f)**.

not affect the seasonality of neither albedo nor precipitation.

During the mid-Holocene (Fig. 2.6d–f) the positive precipitation anomalies are not limited to the 0.25 contour of the static simulation, indicating that the dynamic scheme prolongs the rainy season in all regions. In WS there is a large increase in precipitation at the beginning of the rainy season, whereas in the later part of the rainy season the anomalies are of the same order of magnitude as for the pre-industrial simulations. A drying south of 10° N occurs mid-season, and cancels out the increase at the beginning, which explains the northward shift of the rain belt noted in Sect. 4.2. In WS the dynamic scheme also mainly affects the beginning of the rainy season, but there is no accompanying drying to the south.

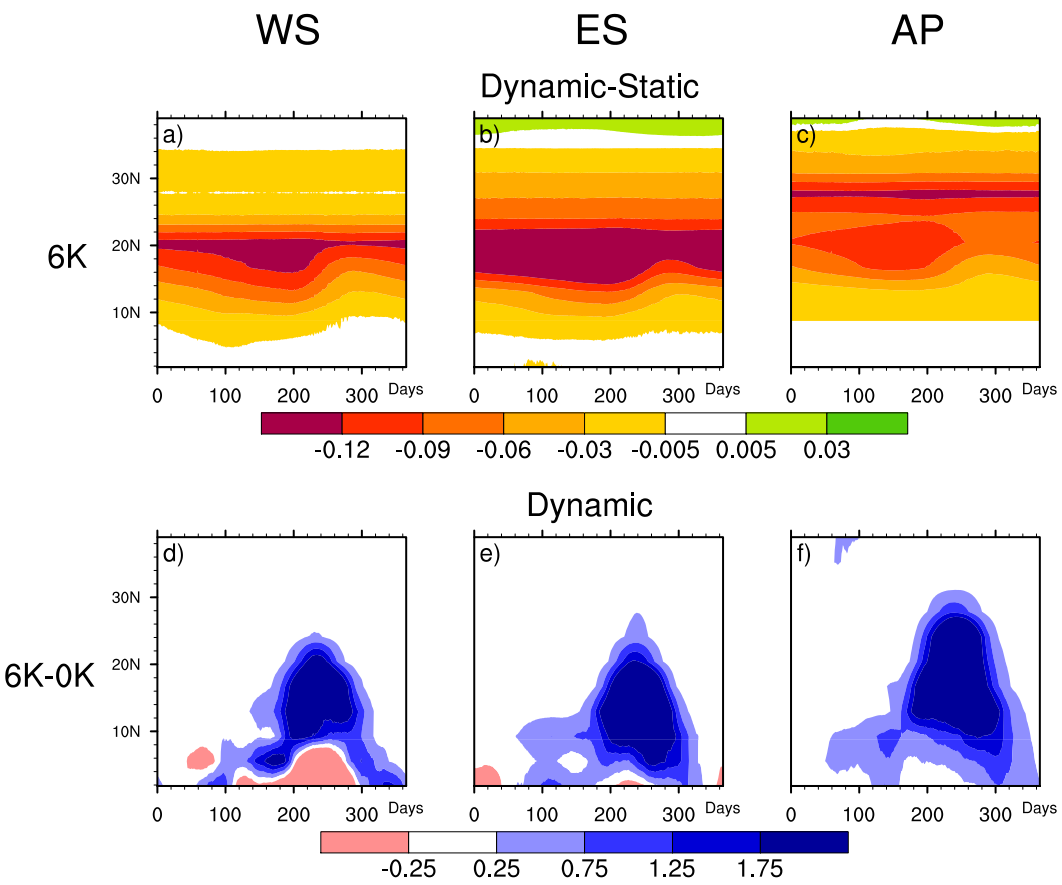

Figure 2.7: Shown are differences in the annual cycle of precipitation and albedo derived from 100 simulation years. **(a)** to **(c)** show albedo differences between 6K_dyn and 6K_st, for regions WS, ES and AP. **(d)** to **(f)** show precipitation differences in mm/day (further filtered by 30-day running means) between 6K_dyn and 0K_dyn, for regions WS, ES and AP.

In AP there is a clear intensification of rainfall throughout the rainy season.

These differences are also reflected in the albedo differences for the three regions (Fig. 2.7a–c). In WS and ES the seasonal cycle of albedo clearly changes, whereas the albedo change in AP is constant across the year. The change in albedo seasonality thus clearly matches the changed seasonality in precipitation (Fig. 2.6d–f), however one would need additional simulations to establish any lead-lag relationships.

Due to the extremely high background albedo values in 6K_st, the amplitude of the seasonal cycle is overestimated compared to similarly vegetated gridboxes

in 0K_st (not shown). With the introduction of the dynamic scheme the seasonal cycle in albedo becomes more consistent, since comparably vegetated gridboxes also display similar albedo seasonal cycles. We thus expect the dynamic scheme to represent the seasonal distribution of rainfall in the mid-Holocene in a more consistent way than the static scheme.

When considering the combined effect of orbital, SST and dynamic albedo forcings (Fig. 2.7d–f), the differences between the pre-industrial and mid-Holocene simulations are most marked between WS and the two other regions. In the WS the northward shift of the monsoon rain belt can be seen, so that the area that has a bipolar structure in seasonal rainfall is extending further north in the mid-Holocene than in the pre-industrial simulations. In ES and AP there is a tendency towards larger increases at the end of the season. We have shown above, that the dynamic albedo scheme mainly affects rainfall at the beginning of or throughout the rainy season. The large increase at the end of the season that we see here, must thus mainly be due to the orbital and SST forcings.

2.5 Discussion

In this section we will focus on the agreement between palaeo-records and our modelling results for the mid-Holocene and discuss possible ways of reducing discrepancies. According to reconstructions by Hoelzmann et al. (1998) the location of the largest increase in lake abundance was south of 20° N in the Sahara and along the East Coast of the Arabian Peninsula. The mid-Holocene lakes in eastern Sahara would have needed between 350–500 mm of precipitation a year, sometimes up to 700 mm/year, to be sustained (Hoelzmann et al. 2000). Assuming this to hold for the entire region analysed, the amount of rainfall is underestimated in both mid-Holocene simulations. However, the simulated mid-Holocene desert border is far enough north to match the 20° N estimate. Annual P-E values in 6K_dyn are on average 50% larger compared to 6K_st, showing an

increased potential for the existence of lakes. Note that the two pre-industrial simulations have similar annual P-E values, indicating that a P-E bias that could be transferred from the pre-industrial dynamic simulation to the mid-Holocene simulation is unlikely.

The Sahara was clearly reduced in the mid-Holocene compared to today (Jolly et al. 1998b). However, it is not clear if the increase in vegetation cover was restricted to favourable locations or was wide-spread as suggested by Hoelzmann et al. (1998). If there was a long-term continuous cover, one would need a very low modelled desert fraction for a close agreement between modelled values and the palaeo-record. If the pollen stem from less long-lived or patchy vegetation cover, the variability of the desert and thus its stability should be considered. As already shown, mean vegetation cover only reaches four degrees further north in the mid-Holocene simulations compared to the pre-industrial simulations. Our model results are thus clearly not consistent with a long-term continuously vegetated Sahara. However, we did consider the stability of the desert by studying the minimum annual mean values obtained during the 100-year analysis period (+ signs in Fig. 2.3a–d). One can interpret the size of these + signs as indicators of the frequency of growth events or green spells. In the pre-industrial simulations there is a large number of gridboxes where the desert fraction stays above 99% for all years, 16 boxes for 0K_dyn vs. nine for 0K_st. The desert state is thus a very stable one. In the mid-Holocene simulations these very dry conditions completely disappear. 6K_dyn shows a higher frequency of green spells than its static counterpart 6K_st, indicating a mid-Holocene Saharan climate that is more compatible with finding pollen remnants.

To match the precipitation estimates needed to sustain lakes, the increase in rainfall in our simulations seems to reach far enough north, but precipitation would need to be increased locally. There are some factors that affect the land surface albedo in the Sahel/Sahara that we have not included that may influence our results. The most important are soil moisture, fire effects (Govaerts

et al. 2002; Myhre et al. 2005) and lakes and wetlands that all have the effect of reducing albedo. Fires disturbing the biosphere contributes largely to albedo variability over Africa, however the vast majority of these fires can be attributed to anthropogenic influence (see Govaerts et al. 2002, for instance) and might have been of lesser importance during the mid-Holocene. Fires affect the albedo by burnt scars on the surface, but also through their aerosol radiative effect (Govaerts et al. 2002; Myhre et al. 2005). Broström et al. (1998) found that including effects of wetlands and lakes increases the magnitude of the monsoon precipitation in the area around the prescribed lakes, but does not contribute to extending the monsoon further northward. Introducing lakes or wetlands does not only reduce the albedo, but it could also have the effect of enhancing local recycling by increasing evaporation, resulting in an increase in precipitation. This latter effect may have been important to help maintain the reconstructed palaeo lakes and wetlands (Carrington et al. 2001). One should keep in mind that our scheme produces a low albedo in the pre-industrial simulation that may bias the mid-Holocene simulation. Introducing further albedo-reducing mechanisms may thus push the scheme towards unrealistically low albedo values for the mid-Holocene. Thus, in order to obtain a closer agreement with lake estimates, it may be more important to introduce lakes and wetlands and their evaporative effect, rather than to further extend the albedo scheme.

We find that the vegetation effect on precipitation is almost non-existent without the dynamic scheme, which is similar to the results of e.g. PMIP2 (Braconnot et al. 2007b). However, we would argue that the albedo change is underestimated with the static scheme. Since other GCMs use schemes very similar to the static scheme, we would assume that the albedo change, and thus the vegetation-precipitation feedback, is underestimated there as well. On the other hand, other studies that find a very strong effect of vegetation on precipitation may have overestimated the change in albedo. This overestimation could for instance arise from a bias introduced by the changed boundary conditions, such

as prescribing low albedo values to the background even though the simulated precipitation increase would theoretically not lead to lower albedo values (e.g. Knorr and Schnitzler 2006) or from over-estimating the effect of the vegetation on albedo, by e.g. using a too high fixed annual mean LAI as a basis for the albedo calculation (e.g. Claussen 1997).

Bonfils et al. (2001) found that most of the increased rainfall in the mid-Holocene was due to an increased number of extreme events. We have not gone into the details of extreme events in the analysis of our simulations. However, we find that the already low temporal variability of land surface albedo in the area is reduced by the introduction of the dynamic scheme, going from a standard deviation of around 0.004 to 0.002 (Table 2.3). This is also mirrored by a reduced temporal variability in rainfall. This may indicate that the occurrence of extreme events is reduced. It has been hypothesised that squall lines, today playing an important role in heavy precipitation events in the Sahel (Peters and Tetzlaff 1988), might also have played an important role in the wetter state of the Sahara during the mid-Holocene (Pachur and Altmann 1997). Squall lines can become very long, but their width is typically in the order of tens of kilometres, well below the scales resolved in our model simulations of T31 resolution (about 300 km). Increasing resolution would be a step towards better representing heavy rainfall events in the Sahel. The combination of the dynamic scheme and higher resolution might then result in a higher mean precipitation with a large variability, which would also give rise to a higher frequency of green spells in the Sahara during the mid-Holocene.

2.6 Summary of Chapter 2

In this chapter we introduce a new albedo scheme that takes the dynamic behaviour of the surface below the green canopy into account, into the land surface scheme of the atmosphere GCM ECHAM5. The scheme dynamically models the

dependence of albedo on both the canopy and the surface below it, the "background". The dependence of albedo on the canopy is modelled in the way common for most GCMs, using an exponential function of LAI to define the area covered by green leaves (Beer's law; Monsi and Saeki 1953). Background albedo is modelled as a function of the amount of soil organic matter in the bare ground and the amount of litter and standing dead biomass covering the ground, using the leaf litter and slow soil carbon pools in JSBACH as proxies for these factors. We compare the dynamic scheme with the static one for two time-slices; pre-industrial and mid-Holocene.

The dynamic scheme introduces a lower albedo in the Sahel of the pre-industrial simulation and an increase in precipitation of around 30 mm/year across the studied region, reducing the existing low precipitation bias of ECHAM5 within this region. The correspondence between annual mean albedo and the vegetation seen in observations is well-captured in the pre-industrial for both schemes, but it is only captured with the dynamic scheme for the mid-Holocene. The dynamic scheme thus gives a better estimate of albedo change than the static scheme. In the mid-Holocene, the dynamic scheme leads to an enhanced increase in precipitation of 80 mm/year compared to the static scheme. The sensitivity of regional precipitation to external forcing is thus increased by about one third. Albedo alone is not responsible for the northward shift and intensification of precipitation in the mid-Holocene, the orbital and SST forcings used play a major role as well. The desert albedo calculated by the dynamic scheme may inhibit the northward movement of rainfall in mid-Holocene western Sahara, since it also remains high for this time period. In the two other regions considered, albedo does not seem to be a driver of the northward shift in rainfall, rather of intensifying rainfall south of the desert border. The dynamic scheme does not just affect the sensitivity of precipitation of the whole region, it also shifts the region of large sensitivity further eastward. In western Sahara the dynamic scheme shows a lower sensitivity than the static scheme, whereas over the Red Sea and the

Arabian Peninsula its sensitivity is higher. The dynamic scheme also leads to a more consistent representation of the seasonal cycle in albedo, which results in a prolongation of the rainy season in the mid-Holocene and a marked increase compared to the static scheme, especially at the beginning of the rainy season.

For both mid-Holocene simulations, the desert border is compatible with the estimated geographical extent of mid-Holocene lakes. However, the magnitude of rainfall is too low to sustain large lakes, although the dynamic scheme produces precipitation that is closer to the estimates. The results are also in disagreement with the assumption of a continuously vegetated Sahara. With the dynamic scheme, the variability in vegetation indicates the possibility of green spells. The introduction of the dynamic scheme thus results in a mid-Holocene climate that is closer to palaeo-records than the static (standard JSBACH) scheme. It also reduces the need to impose mid-Holocene boundary conditions for the albedo, allowing a more realistic representation of albedo change and the vegetation-precipitation feedback.

In this chapter we mainly focus on the mean climate response, both to orbital forcing and to the dynamic albedo scheme. In the second part of the thesis, we focus on climate variability within each time period. We investigate how precipitation variability is affected on the one hand by the dynamic modelling of vegetation patterns and on the other hand by the slow response timescales that are inherent to the dynamic albedo scheme, because of the slower response timescales of the litter pool and the slow soil pool.

Chapter 3

Variability of Sahelian rainfall as simulated for the mid-Holocene, the pre-industrial and the last century.

3.1 Introduction

Climate variability is important for vegetation distribution and vegetation variability especially in semi-arid areas, where the vegetation response does not only depend on changes in the mean climate, but also on changes in patterns of variability, such as extreme events and the temporal structure of the change (Ni et al. 2006). In the Sahel, vegetation is mainly water limited and thus controlled by rainfall (Brovkin et al. 1998). Rainfall variability may in turn be influenced by vegetation variability through slow changes in the vegetation cover (Delire et al. 2004). In Chapter 2 the mean state of precipitation and vegetation, and the interactions between them are discussed. In this chapter we focus on the processes controlling precipitation variability in the Sahel in simulations of the pre-industrial, mid-Holocene and the last century.

The processes controlling rainfall variability in the Sahel have been in the spotlight for the last few decades, mainly because of the persisting drought which

began at the end of the 1960ies, which caused a lot of distress to an already fragile system. The cause of this drought has been widely discussed, with hypothesis ranging from man-made desertification (e.g. Otterman 1974; Charney 1975) to SST patterns favouring drier conditions in the Sahel (Lamb 1978; Lamb and Peppler 1992). Evidence for multi-decadal variations in Sahelian climate have been found for several intervals during the past few centuries (Nicholson 1981, 1989), which indicates that slow variations in the climate have been an inherent part of the Sahelian climate at least for the last few hundred years. It is now generally accepted that SST patterns provide the background variability for decadal variability in Sahelian precipitation (Giannini et al. 2003; IPCC 2007a), though there is still some debate regarding which SST pattern is the dominant one. The main modes of SST variability arise from natural variability, though some authors argue that the drought-inducing SST patterns can be attributed to some extent to anthropogenic forcing (e.g. Biasutti and Giannini 2006). The full persistence and intensity of these low-frequency variations cannot be fully explained by forcing atmospheric models with observed SSTs (Zeng et al. 1999). Many studies suggest that the strength and especially the persistence of these longer wet or dry periods, can only be explained by other factors, that either enhance the natural SST signal or act to increase the signal seen in the precipitation (e.g. Biasutti and Giannini 2006). Using models of varying degrees of complexity, Zeng et al. (1999); Wang and Eltahir (2000); Schnitzler et al. (2001) and Wang et al. (2004) showed that, by including dynamic vegetation, the persistence of the dry period is better captured than with static vegetation as a boundary condition.

It is likely that a change in the mean climate also introduces a change in precipitation variability and a change in the strength of interaction between precipitation and vegetation variability. During the mid-Holocene there was, as discussed in Chapter 2, a substantial change in the mean climate state of the Sahel/Sahara region. Even so, only few studies (Ni et al. 2006) have focused on mid-Holocene orbital forcing and the effect on climate and vegetation variability,

and the relationship between these two factors in the Sahel.

Here precipitation variability, as simulated by ECHAM5-JSBACH for the pre-industrial and the mid-Holocene, forced by model-derived SSTs, is analysed and compared. The interactions between precipitation variability and vegetation variability are investigated by using simulations with and without dynamic vegetation, and with and without the dynamic background albedo scheme, which was introduced in Chapter 2. The sensitivity of the results, on the interactions between precipitation and vegetation variability, to the choice of SSTs, is tested by imposing another set of SSTs to the system. Observed SSTs for the last century are used, since this provides an opportunity to compare the results against observations and thus test their robustness.

This chapter is structured as follows: The experimental setups, the region and time periods analysed, and the main difference between the setups are explained in the methods section. The third section is split into two parts. In the first part, precipitation variability for simulations forced with SSTs, derived from coupled atmosphere-ocean runs with the MPI-ESM, is analysed and the plausibility of the results is evaluated. In the second part, precipitation variability for simulations forced with observed SSTs for the last century is analysed and discussed. The chapter ends with a discussion of the results and a summary of the chapter findings.

3.2 Methods

3.2.1 Experimental setup

For the experiments described in the first part of this chapter (Section 3.3) we use the same experimental setup as in the previous chapter. However, we extend our analysis to include also one simulation with static vegetation for both the pre-industrial and the mid-Holocene (Table 3.1). For completeness, we also include the coupled model simulation with pre-industrial orbital forcing, 0K_ctrl,

in our analysis. Additionally, we use precipitation output from a transient experiment, where the orbital forcing was varied to represent the orbital changes from the mid-Holocene to the present-day. This experiment is described in Fischer and Jungclaus (2011) and apart from the varying orbital forcing, the setup is the same as for the 0K_st and 6K_st experiments. It should be noted that the SSTs, which were used for uncoupled simulations, are derived from coupled simulations that were run with the appropriate orbital forcing. We refer to these SSTs as "MPIOM SSTs", MPIOM (Marsland et al. 2003) being the ocean model of the MPI-ESM.

For the second part of this chapter (Section 3.4), the same configuration of ECHAM5-JSBACH as in the first part is used. We also use the same setup; with and without dynamic vegetation, and with and without dynamic background albedo scheme. However, instead of forcing the atmosphere with coupled-model (MPIOM) SSTs, we use the observed SSTs for the years 1871-2008. These SSTs are from the merged HadISST and NOAA SST dataset as described in Hurrell et al. (2008). For these simulations, "A" is used to indicate that vegetation and background albedo is static, "V" that vegetation is dynamic and background albedo is static, and "D" indicate that both vegetation and background albedo are dynamic. To assess model uncertainty arising from model internal variability, initial value ensembles are performed by minimally perturbing the top of the atmosphere. This is done by altering the value of the factor by which stratospheric horizontal diffusion is increased from one level to the next level above, for the first year of each experiment. All in all, we perform three simulations for each vegetation/albedo setup (Table 3.1). For technical reasons, one simulation was started in 1871, run for two years and then interrupted. The atmosphere end-state of this run was used to initialise ECHAM5 in all nine simulations in the year 1873. The land surface of all nine simulations was initialised in 1873 from the JSBACH end-state of the 0K_dyn simulation. Greenhouse gases are kept constant at pre-industrial values in all the simulations analysed in this chapter.

Table 3.1: Experiments analysed in this chapter. Component: AV = echam5-jsbach (T31L19), −O = coupled to MPIOM, Veg: prescribed (−) or dynamic (dyn) vegetation, Albedo: static (−) or dynamic (dyn) background albedo scheme, SST: run from which SST and SIC were derived, Orbit: 0K or 6K orbital forcing, Years: length of run in years, entsdif: parameter used for initialisation of ensemble members.

a. MPIOM SSTs						
Experiments	Component	Veg	Albedo	SST	Orbit	Years
0K_ctrl	AV-O	dyn	–	–	0K	>4500
0K	AV	–	–	0K_ctrl	0K	200
0K_st	AV	dyn	–	0K_ctrl	0K	300
0K_dyn	AV	dyn	dyn	0K_ctrl	0K	400
6K_ctrl	AV-O	dyn	–	–	6K	>4500
6K	AV	–	–	6K_ctrl	6K	200
6K_st	AV	dyn	–	6K_ctrl	6K	300
6K_dyn	AV	dyn	dyn	6K_ctrl	6K	400
transient	AV-O	dyn	–	–	6K to 0K	6000
b. Observed SSTs (Hurrell et al. 2008)						
Experiment	Component	Veg	Albedo	enstdif		
$A_{0/1/2}$	AV	–	–	1.0000 / 1.0001 / 0.9999		
$V_{0/1/2}$	AV	dyn	–	1.0000 / 1.0001 / 0.9999		
$D_{0/1/2}$	AV	dyn	dyn	1.0000 / 1.0001 / 0.9999		

3.2.2 Dynamic versus static vegetation in JSBACH

In Chapter 2, we compared simulations with and without dynamic background albedo scheme, and the difference between the two setups was explained in detail. The vegetation was dynamic in all simulations that were analysed. In this chapter, we additionally discuss simulations in which the vegetation distribution is prescribed. Vegetation patterns are defined by the fraction of the gridbox that is vegetated and the distribution of plant functional types (PFTs) within that fraction. For simulations with prescribed vegetation these two are constants. In simulations with dynamic vegetation, these variables are updated on an annual basis and vegetation patterns can shift in accordance with climatic change. The equations governing these dynamics are described in detail in Brovkin et al.

(2009). It should be noted that the phenological cycle is calculated in all simulations, whether the vegetation is dynamic or not. The phenological cycle is driven solely by temperature, soil moisture and net primary productivity (NPP) and does not depend on the calendar date (Raddatz et al. 2007).

3.2.3 Analysed region and time period

In this chapter we restrict our analysis to the Sahel region. We define the Sahel as the 16 gridboxes from 11.25° W–33.75° E and 11.125° N–18.55° N (Fig. 3.1). The results are robust to small changes in the choice of the area. For the simulations in the first part (Section 3.3), we use the last 100 simulation years for our analysis. The simulations of the second part (Section 3.4) are compared to observed precipitation from the land precipitation dataset CRU TS 3 0.5° for the years 1901-2006 (Mitchell and Jones 2005). We therefore also base our statistical analysis on the simulated years 1901-2006.

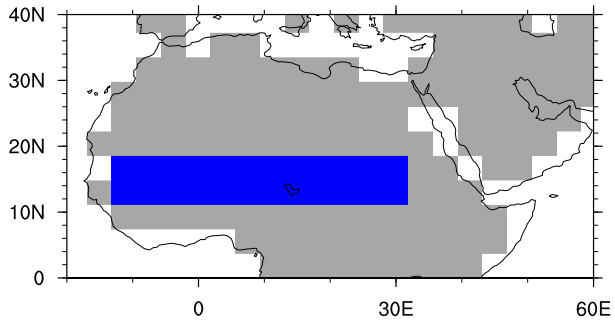

Figure 3.1: Region of analysis. The blue gridboxes are those defined as the Sahel in this chapter. Grey indicates land and white indicates ocean.

3.3 Simulations with MPIOM SSTs

In this section, we concentrate on Sahelian precipitation variability in the preindustrial and the mid-Holocene, as simulated by ECHAM5-JSBACH, either coupled to the ocean model MPIOM or forced by SSTs derived from coupled model

simulations of the appropriate time-slice. The main processes controlling Sahelian variability during the pre-industrial and the mid-Holocene are investigated. The plausibility of these results is discussed in detail.

3.3.1 Results

3.3.1.1 Variability in the pre-industrial simulations

To investigate the major timescales of variability of Sahelian precipitation in the six simulations with MPIOM SSTs, we calculate the power spectra of normalised area-mean time series for the Sahel region (Fig. 3.2). Here, we focus on the pre-industrial simulations (Fig. 3.2a–c). All three simulations show a highly significant band (when compared to the appropriate background spectra based on a red noise time series) between approximately three and four years. There are no obvious differences between the three setups, indicating that the land surface does not affect the timescale of variability in any significant way.

The time series used to calculate these spectra are short and it could be that the 100 years of coupled model SSTs that we chose, are not representative of the equilibrium ocean state from which these SSTs were derived. In order to test the robustness of the signal, both against the length of the time series used and also if the uncoupled setup might influence the spectrum, we perform the same analysis for the 0K_ctrl simulation (Table 3.1). This is a coupled atmosphere-ocean simulation that was run for close to 5000 years and the ocean shows no important trends. The last 100 years of this simulation, were used to create the SST forcing for the uncoupled pre-industrial simulations. For the spectral analysis, we use the last thousand years of 0K_ctrl (Fig. 3.3a). The highly significant peak remains, though it is slightly flatter than for the shorter simulations. With the long time series, it is also possible to investigate the properties of low-frequency variability in detail. The tail of the spectrum is below the 5% confidence interval of the appropriate red noise time series for periods above 7 years. Precipitation

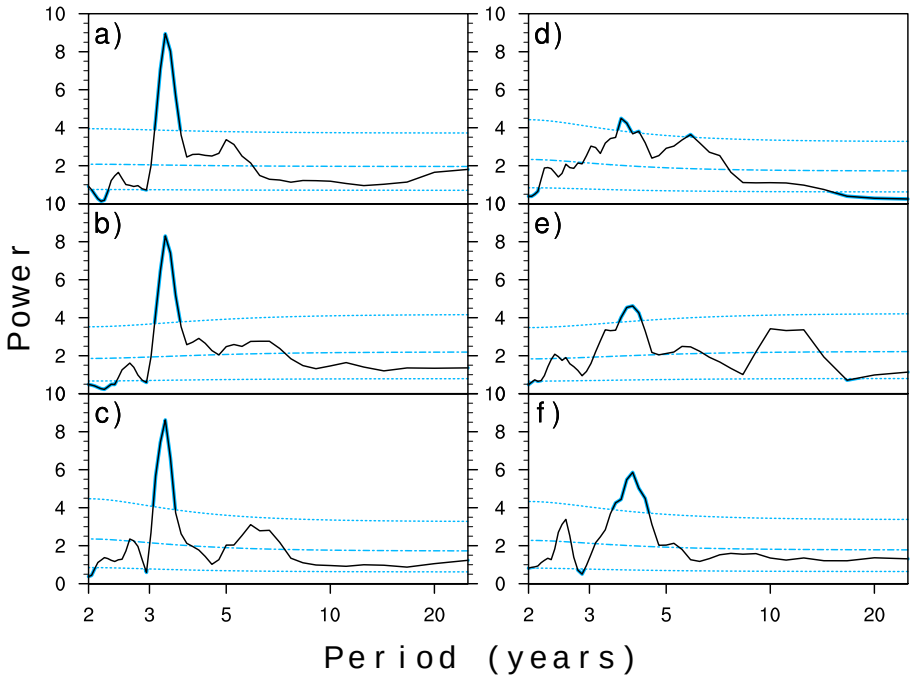

Figure 3.2: Power spectrum for 100 years of normalised precipitation for the Sahel region of simulation **(a)** 0K, **(b)** 0K_st, **(c)** 0K_dyn, **(d)** 6K, **(e)** 6K_st, **(f)** 6K_dyn. Dotted lines indicate the 5% and 95% confidence bounds of the appropriate red noise spectra and dashed lines indicate the estimated red noise spectra.

in the pre-industrial setup is thus clearly lacking any long-term memory. The lag-1 autocorrelation, which is a measure for persistence in a time series, is also very low (not shown) for all the pre-industrial simulations. It is thus clear that both the high peak in high-frequency variability and the lack of low-frequency variability is a robust feature of the pre-industrial simulations.

Both the pre-industrial and the mid-Holocene SSTs are representative of equilibrium ocean states. It may thus be, that the consistency of these peaks is an artifact of the equilibrium state. To investigate this, we calculate the spectrum of the transient simulation (Table 3.1), using the same method as before, and additionally detrending the time series (Fig. 3.3b). In shape it looks very similar to the 0K_ctrl spectra, showing that this is a very robust signal of the coupled model.

Since there is no large difference in the spectra between the three setups, the

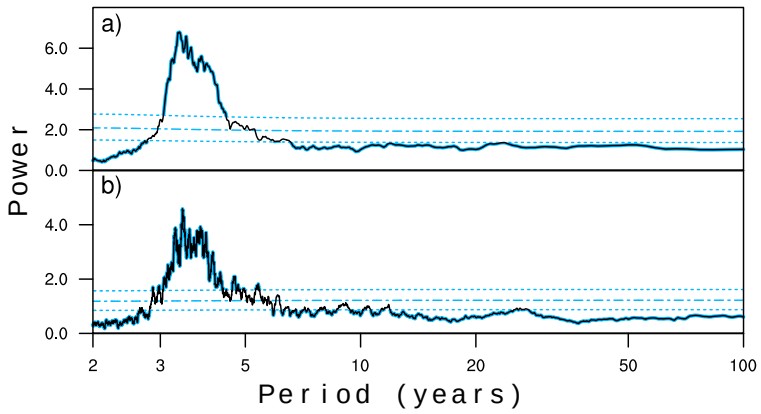

Figure 3.3: Power spectrum for normalised precipitation for the Sahel region calculated using **(a)** 1000 years of 0K_ctrl, **(b)** 6000 years of the transient experiment. Dotted lines indicate the 5% and 95% confidence bounds of the appropriate red noise spectra and dashed lines indicate the estimated red noise spectra.

high-frequency peak arises either from internal variability of the atmosphere or from the ocean. Since it is a very strong signal of a longer than annual timescale, it is unlikely to arise from atmospheric variability. We therefore correlate the area-averaged anomalies from the annual mean of Sahelian precipitation with global SSTs to investigate the influence from different ocean basins. In all pre-industrial simulations there is a significant negative correlation between Sahelian precipitation and the SSTs in all tropical ocean basins, both in the annual mean (Fig. 3.4a–c) and in the July–August–September (JAS) mean (not shown). The correlation is strongest in the Pacific basin and especially so for the western part of this basin.

The time-interval of the highly significant spectral peak is close to the observed period of El Niño-Southern Oscillation (ENSO) variability (3-7 year) (Fig. 3.5c). To test a possible connection between the Sahel and ENSO we analyse the SSTs of the so-called Nino3.4 region (5° N–5° S, 170° W–220° W), which is often used for investigating ENSO variability on a global scale (e.g. Liu et al. 2000). The power spectrum of the sea surface temperatures for the pre-industrial simulations is shown in Figure 3.5a. There is a striking resemblance between the Nino3.4 SST spectrum and the Sahel rainfall spectra seen in Figure 3.2. The co-spectra

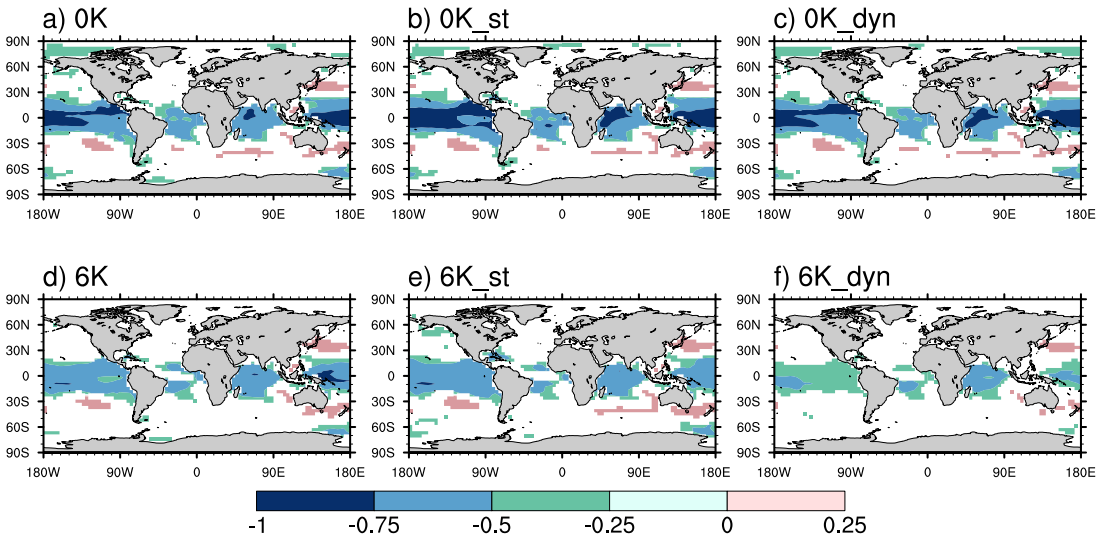

Figure 3.4: Correlation between Sahel annual mean precipitation anomalies and global annual sea surface temperature anomalies calculated using 100 years of **(a)** 0K, **(b)** 0K_st, **(c)** 0K_dyn, **(d)** 6K, **(e)** 6K_st, **(f)** 6K_dyn. Only significant correlations at the 99% confidence level are shown in colour.

between Nino3.4 SSTs and Sahelian rainfall confirm that the Nino3.4. SSTs are responsible for the timing, as well as a large portion of the power of the peak (Fig. 3.5d). The coefficient of determination (R^2) between Sahelian rainfall anomalies and the annual Nino3.4 SST anomalies is above 0.55 for all three pre-industrial simulations (Fig. 3.6), thus confirming the close connection between ENSO and Sahelian rainfall in the model.

The correlation between Sahelian precipitation and annual Nino3.4 SSTs is higher for the 0K_st simulation compared to the other two pre-industrial simulations. The R^2 is also above 0.6 in the 0K_ctrl simulation, which, as 0K_st, has dynamic vegetation and static background albedo, which may be an indication that the higher correlation is due to the dynamic vegetation.

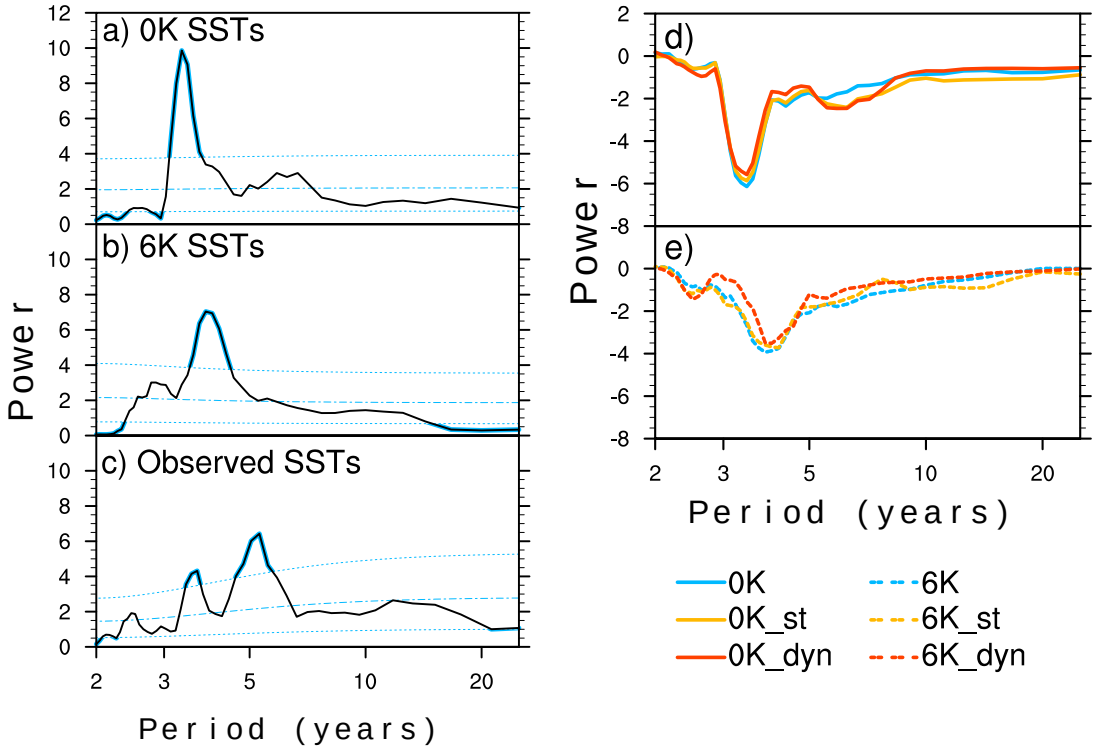

Figure 3.5: **(a)**–**(c)** Power spectrum for the Nino3.4 SSTs calculated from 100 years of **(a)** the pre-industrial (0K) and **(b)** the mid-Holocene (6K) simulations, and **(c)** for the years 1901-2006 of the observed SSTs (Hurrell et al. 2008). Dotted lines indicate the 5% and 95% confidence bounds of the appropriate red noise spectra and dashed lines indicate the estimated red noise spectra. **(d)**–**(e)** Co-spectra (real part of the cross-spectrum) for Nino3.4 SSTs and Sahel precipitation calculate from 100 years of the **(d)** pre-industrial (0K , 0K_st , 0K_dyn) and **(e)** mid-Holocene (6K , 6K_st , 6K_dyn) simulations.

3.3.1.2 Variability in the mid-Holocene compared to the pre-industrial simulations

In the mid-Holocene simulations, the spectral peak that was seen for the pre-industrial simulations, though it still exists, is flattened and widened, as well as slightly shifted to peaking at longer periods (Fig. 3.2d–f). There is also less consistency between the three setups. The pre-industrial simulations have almost identical spectra, both in shape and in power. The two mid-Holocene simulations with dynamic vegetation (6K_st and 6K_dyn) show increased spectral power between two and three years. However, when using a larger smoothing parameter

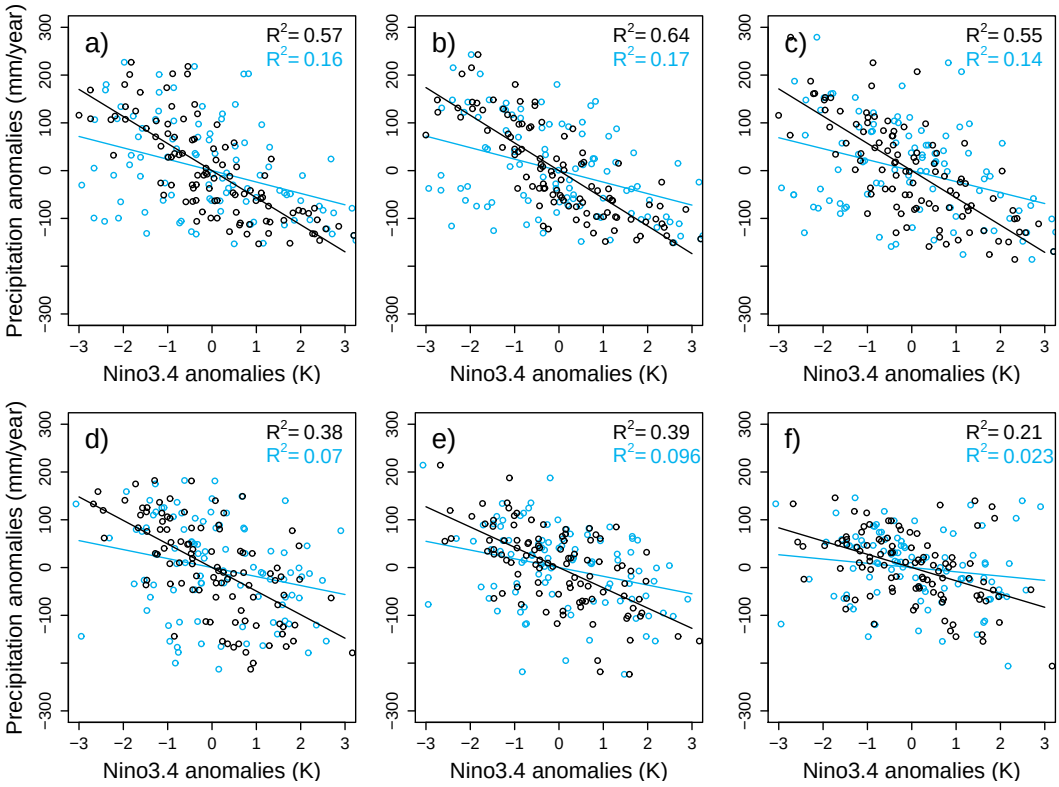

Figure 3.6: Scatter plot and linear least squares fit of annual Sahel precipitation anomalies and Nino3.4 annual (black) or JAS (blue) SST anomalies calculated using 100 years of **(a)** 0K, **(b)** 0K_st, **(c)** 0K_dyn, **(d)** 6K, **(e)** 6K_st, **(f)** 6K_dyn. The coefficient of determination (R^2) of each fit is indicated in the corner, with black for annual SSTs and blue for JAS SSTs.

for the spectra, these differences disappear and only the peak between three and five years remains. As for the pre-industrial simulations there is a correlation between Sahelian rainfall anomalies and tropical SSTs both for annual (Fig. 3.4d–f) and JAS SSTs (not shown), but it is clearly reduced for all three setups.

In the mid-Holocene, ENSO variability is reduced by around 6% (Table 3.2) compared to the pre-industrial. The period is also increased to around four years (Fig. 3.5b), which as in the pre-industrial matches the timing of the peak of the Sahel rainfall spectra (Fig. 3.2d–f). As for the pre-industrial simulations, the co-spectra between Nino3.4 SSTs and Sahelian rainfall confirm that the Nino3.4. SSTs are responsible for the timing, as well as a large part of Sahelian rainfall variability (Fig. 3.5e). ENSO is thus still the phenomenon controlling Sahelian

rainfall variability in the mid-Holocene, but the reduced ENSO variability leads to a connection that is weaker than in the pre-industrial, which indicates an increased influence of other factors or increased internal variability. In line with previous studies, the mid-Holocene simulations show reduced ENSO variability (e.g. Otto-Bliesner et al. 2003; Brown et al. 2008) and increased periodicity (e.g. Zheng et al. 2008), as well as the reduced teleconnection between ENSO and the Sahel (Zhao et al. 2007). However, several studies based on analysis of oxygen isotopes in fossil corals indicate that ENSO amplitude was between 15 to 60 % smaller in the mid-Holocene than today (e.g. Tudhope et al. 2001; McGregor and Gagan 2004). The 6 % reduction seen here is thus on the lower side of estimates.

The most striking difference between the 0K and the 6K simulations is the difference in Sahelian precipitation/Pacific SSTs correlation strength between the simulations 6K and 6K_st, and the 6K_dyn simulation. The inclusion of the dynamic albedo scheme reduces the strength of the correlation between the Sahel and the Pacific SSTs (Fig. 3.4d–e. and Fig. 3.6d–e). We also investigate if the albedo scheme impacts the occurrence of extreme events (not shown), but we do not find an increased or decreased occurrence of extreme events. Neither is there an important increase in year-to-year variability. Since the period of main variability and the distribution of rainfall remains the same, this indicates that the dynamic albedo scheme just slightly delays or dampens the response to the ENSO influence, rather than significantly increasing variability at other periodicities.

3.3.1.3 Differences between vegetation and albedo setups with a filtered ENSO signal

ENSO forcing clearly dominates both pre-industrial and mid-Holocene precipitation variability in these simulations. Therefore, it is not possible to make any firm conclusions about the influence of vegetation dynamics or the dynamic background albedo scheme on rainfall variability in these simulations, when analysing the complete time series. The plausibility of such a strong ENSO signal is dis-

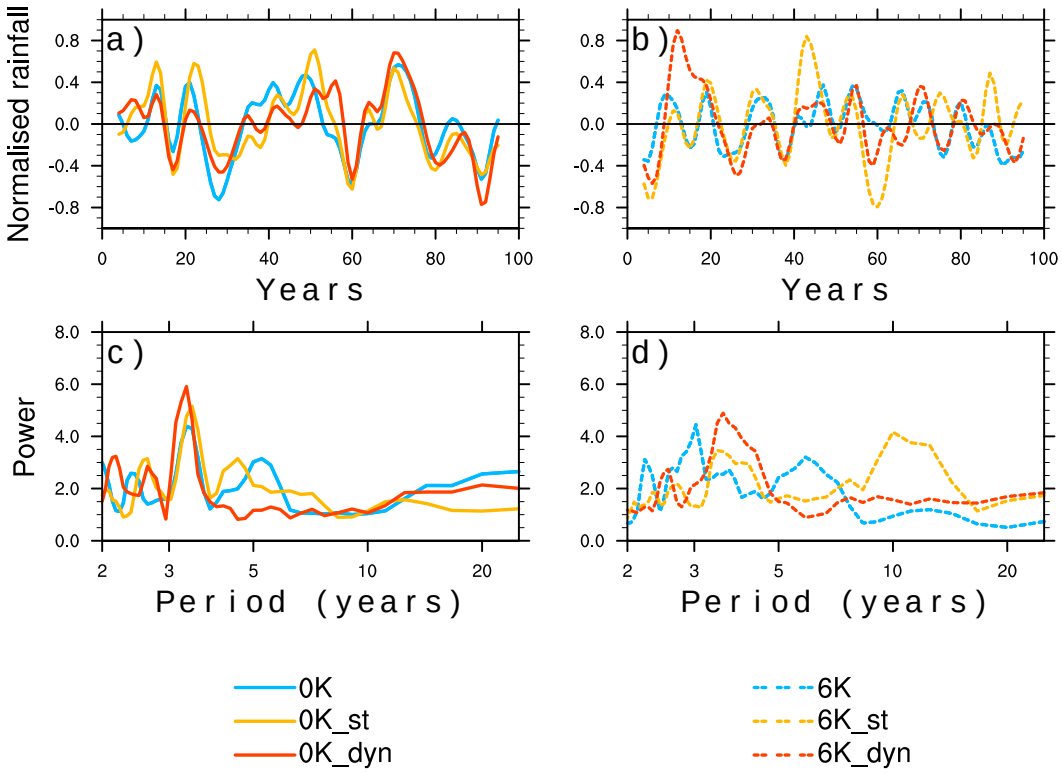

Figure 3.7: Sahel precipitation time series with a reduced ENSO signal. Normalised time series of low-pass filtered (10 years) Sahelian precipitation for the **(a)** pre-industrial and **(b)** mid-Holocene simulations. Power spectra of the normalised time series of the residuals of the linear least square fit between Sahelian precipitation and the Nino3.4 region for the **(c)** pre-industrial and **(d)** mid-Holocene simulations.

cussed in the following section. To investigate the influence of dynamic vegetation or the dynamic background albedo scheme on rainfall variability the ENSO signal needs to be removed or reduced. There are two main ways of doing so; either use a low-pass filter or analyse the residuals of the linear least squares fit between Sahelian precipitation and the Nino3.4 SSTs (See Fig. 3.6). A low-pass filter is appropriate, since the co-spectra both for the pre-industrial and the mid-Holocene show low or no power at low-frequencies, here we use 10 years as the cut-off point (Fig. 3.7a–b). Analysing the residuals of the linear least squares fit is a way of filtering out exactly the Nino3.4 signal and keeping other forcings that may act in the same frequency range. The spectra of the residuals can be seen in Figure 3.7c–d. For the pre-industrial simulations, these spectra show that even

though the ENSO signal is removed, the high spectral peak remains, though it is reduced. This peak is caused by the tropical SSTs of the Atlantic and Indian basins (not shown), which suggests that this strong signal propagates along the equator. As for the complete time series, there are no large differences between the setups neither in the spectra of the residuals nor in the low-pass filtered time series. In the mid-Holocene simulations the removal of the ENSO signal via regression is more successful and the three setups show increased peaks at different periodicities. The low-pass filtered time series reveal larger fluctuations in the two mid-Holocene setups with dynamic vegetation (6K_st and 6K_dyn).

3.3.2 Discussion of the pre-industrial ENSO-Sahel connection

Using MPIOM SSTs, the ENSO signal in Sahelian rainfall is very strong both in the pre-industrial and the mid-Holocene simulations. Dynamic vegetation and dynamic albedo only play minor roles in affecting the variability of the region. In this section, the plausibility of these results is discussed, by looking both at previous modelling results and also at ENSO-Sahel relationships as seen from observations.

Table 3.2: Mean and standard deviation (SD) of the SSTs in the Nino3.4 region.

SSTs	Mean (°C)	SD (°C)	Years used
0K SSTs	23.9	1.35	100
6K SSTs	23.8	1.27	100
Observed SSTs*	26.7	0.60	1901-1996 (135)

* (Hurrell et al. 2008)

Rainfall variability in the Sahel is strongly influenced by SSTs (Giannini et al. 2003; IPCC 2007a; Mohino et al. 2010), and even though there are a lot of different theories regarding which ocean basin has the largest influence, a relatively consistent picture emerges. A large part of the research regarding the Sahel-SST connection has been dedicated to long-term fluctuations in SSTs, which are

thought to influence the long wet and dry periods seen in the last century in the Sahel. There are two main arguments that have been used to explain these fluctuations (Giannini et al. 2008), one related to Atlantic SSTs and one to Indo-Pacific SSTs.

The Atlantic argument is of a north/south gradient in low-latitude Atlantic SSTs (e.g. Lamb 1978; Folland et al. 1986; Lamb and Peppler 1992), where a positive anomaly in the north and a negative anomaly in the south leads to a southward displacement of the Atlantic ITCZ and a weaker monsoon flow in the North Atlantic basin and thus a drier Sahel. The sustained drought might then be explained by multi-decadal fluctuations in the Atlantic, such as the Atlantic Meridional Oscillation (AMO) (Zhang and Delworth 2007). The Indo-Pacific argument is explained by a warming of Indo-Pacific SSTs, which in turn warms the troposphere. This stabilises the atmosphere from above over the Sahel, which leads to drier conditions there (e.g. Bader and Latif 2003). Both of these arguments have been suggested from modelling as well as observational studies. The extent to which a warming in e.g. the Indian Ocean or an increase of drought-favourable SSTs in the Atlantic can be attributed to anthropogenic influence is still unclear (Bader and Latif 2003). However, Biasutti and Giannini (2006) attribute up to 30% of the enhancement of the Atlantic SST gradient in favour of a drier Sahel to anthropogenic influence, mainly through the increased release of reflective aerosols. If it is the case that the frequency of these drought-inducing modes have increased with global warming of the oceans, it may explain why for instance the low-latitude dipole in the Atlantic does not correlate with Sahelian rainfall in the pre-industrial simulations (where greenhouse gases and aerosol forcing are constant). However, since it has been shown that multi-decadal variability has existed in the Sahel for some centuries it is unlikely that these patterns are completely human-induced and thus they are underestimated in the simulations.

The ENSO influence on Sahelian rainfall is less well understood (Janicot et al. 2001). The rainy period in the Sahel does not concur with the season when

the ENSO signal is strongest (Janicot et al. 2001), which may explain why we see stronger correlations for the annual SSTs than for the JAS SSTs (Fig. 3.4a–c. and Fig. 3.6a–c). Additionally, ENSO is a driver of interannual variability and can thus not explain the long-term changes that we have discussed above. Janicot et al. (1996, 2001) suggest that there are periods of weak and periods of strong teleconnections between the Pacific and the Sahel, modulated by the background SST patterns responsible for decadal and multi-decadal trends in Sahelian rainfall. Several authors have shown, that if one breaks down Sahelian rainfall in its low-frequency and high-frequency components, then the variability of the low-frequency component can be attributed to one of the above explanations for decadal variability (Ward 1998; Janicot et al. 2001; Giannini et al. 2003). The high-frequency component is either related to ENSO or to the Atlantic dipole (e.g. Janicot et al. 2001; Giannini et al. 2008), where the Pacific connection occurs during years when the Sahel and the Guinea Coast have same sign anomalies (Ward 1998), and the Atlantic connection is dominant during years with a Sahel/Guinea Coast dipole (years with opposite sign anomalies in the two regions, see e.g. Nicholson (1980); Nicholson and Webster (2007)).

In order to confirm that the analysis is not biased by the choice of the region of study, we repeat the analysis for a reduced Sahel region (just the western half of the gridboxes), for the Guinea Coast and for the southernmost part of the Sahara. The results change slightly, quantatively, mainly because the distribution of the rainfall looks slightly different in the different areas, but the qualitative picture remains; that of a very strong Pacific influence on Sahelian rainfall. The consistency between these regions is not found in analyses of observed data. The east Sahel and the west Sahel rainfall variability tend to correlate with slightly different strengths with the different ocean basins (Bader and Latif 2003). Another striking phenomenon is that the simulated Guinea Coast precipitation always correlate with the SSTs with the same sign as the Sahelian precipitation. This is consistent with interannual variability arising from ENSO, but is inconsistent

with observations, in the sense that the dipole between the Guinea Coast and the Sahel is at least as likely to occur as a same-sign anomaly between these two regions (Nicholson and Grist 2001). This model discrepancy might be due to a lack of variability in the position of the ITCZ, probably due to too infrequent or too weak Atlantic dipole anomalies.

The simulated SSTs are three degrees colder than the observed mean (Table 3.2, mean). The main explanation for this is probably the well known "equatorial cold bias" that can be found in many GCMs (e.g. Jungclaus et al. 2005). In addition to the cold bias, the variability in Pacific SSTs is almost twice as large as the observed (Table 3.2, SD). This may be due to a too strong eastward propagation of SST anomalies into the eastern Pacific warm pool, as has been described for another version of ECHAM5/MPIOM by Jungclaus et al. (2005). The excessively large anomalies may explain why the ENSO signal is so strong in the model. An overestimation of the correlation between the Pacific and the Sahel is also noted by Zhao et al. (2007) for a previous version of ECHAM5/MPIOM. They did not study the details of the overestimated correlation strength, thus a direct comparison is not possible.

To conclude this section, the MPI-ESM does simulate a realistic coupling between ENSO and Sahelian rainfall, however the coupling is far too dominant. The excessive signal could be due to a too strong ENSO combined with a too stable ITZC or to other factors that we have not investigated here. When filtering out the ENSO signal, either via regression or with a low-pass filter, there are no large differences between the three different setups for the land surface for the pre-industrial simulations. In the mid-Holocene, the inclusion of dynamic vegetation increases the amplitude of precipitation fluctuations. Because of the strong ENSO signal, it may well be that the differences between the setups is misrepresented. Therefore to test the sensitivity of these results to a different set of SSTs, that do not contain such a strong ENSO signal, we use observed SSTs to force ECHAM5-JSBACH in the following section of this chapter.

3.4 Simulations with observed SSTs

By coupling ECHAM5 to MPIOM or using SSTs from coupled runs, we find a very strong influence of the tropical oceans on Sahelian rainfall variability, which may mask a land surface signal in the precipitation variability. A weak land surface signal may be realistic. However, to test the sensitivity of ECHAM5 to different SSTs we perform another set of experiments, where we use the same setup of ECHAM5-JSBACH as discussed in section 3.3, but with observed SSTs instead of SSTs derived from a coupled model. We thus expect to have a rather different background variability when we use these SSTs, compared to the coupled model SSTs from equilibrium simulations that we used in the previous part of this chapter.

3.4.1 Results

3.4.1.1 Observed rainfall variability

Observed rainfall in the Sahel for the last century reveals two main characteristics: long-term persistence and severity. By long-term persistence, we mean to describe the large number of years with rainfall anomalies consequently being above or below the long-term mean and by severity, the large amplitudes of these anomalies. During the 20th century there were two periods in particular that are typical for persistence; a long period of above-mean anomalies between the 1930ies and the end of the 1960ies, "the wet period", which was followed by an equally long period of below mean anomalies, "the dry period" (Fig. 3.8a). Since the mid-nineties, there has been an increasing trend in rainfall (Fontaine et al. 2011), leading to a return towards the long-term mean. The tendency towards low-frequency (above-decadal) variability is also to be seen in the power spectrum of the observed rainfall time series (Fig. 3.9a).

3.4.1.2 Simulated rainfall variability

All nine simulations (Table 3.1), capture the general characteristics of the observed rainfall by simulating a long wet and a long dry period, as well as the timing of the transition between the two periods (Fig. 3.8). There are however differences between the simulated rainfall of the setups. To analyse the differences between the setups and to compare the simulated rainfall with observed rainfall, we use four measures: the anomalies from the long-term mean, the power spectra, the auto-correlation function and the difference in mean between the wet and the dry period. Spectra and anomalies are calculated from normalised time series (mean is zero and standard deviation is one) for the years 1901 to 2006, so that all time series are directly comparable. The wet period mean is calculated as the mean of the annual precipitation for the years 1938 to 1967, and the dry period mean is for the years 1969 to 1998.

The scatter between ensemble member long-term mean is low for all three setups (Fig. 3.10a). Also when calculating the scatter for each year and then averaging over the whole analysis periods, all three setups have a value of 70±2 mm/year, which shows that none of the included schemes cause a drift in the simulated precipitation.

In the control setups (A–simulations) that have both static vegetation cover and static albedo, the long-term mean rainfall is consistently underestimated by ca. 50 mm/year, for all ensemble members (Fig. 3.10a). The A time series have high spectral power in the same low-frequency interval as the observed values, the long-term persistence is thus well captured (Fig. 3.9a,b). During the wet period, the amplitude of the anomalies are close to those observed (Fig. 3.8b). In the dry period, the amplitude of anomalies are smaller than those observed. The severity of the drought is thus underestimated. The too small dry-period anomalies, explain why the difference in mean between the wet and the dry periods is underestimated in all A–simulations (Fig. 3.10b).

The V–simulations differ, in their setup, from the control simulations ("A")

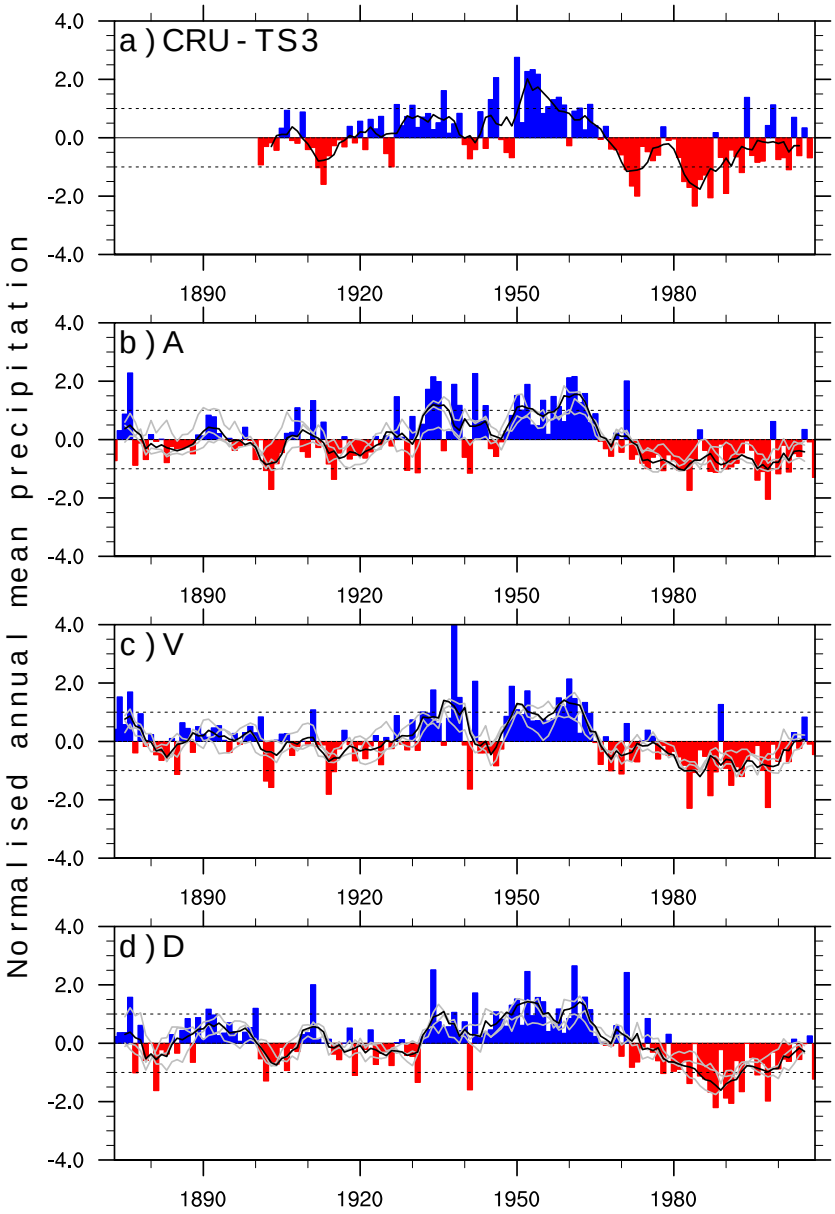

Figure 3.8: Normalised annual mean precipitation w.r.t. mean rainfall for the years 1901-2006 in the Sahel. **(a)** Observed precipitation from the CRU-TS3 land data set (Mitchell and Jones 2005), bars show yearly values, lines show five-year running averages. Simulated precipitation for the **(b)** static (A) simulations, **(c)** dynamic vegetation (V) simulations, **(d)** dynamic vegetation and dynamic albedo (D) simulations. Bars show annual values of the ensemble mean. Lines show five-year running averages for the individual ensemble members (grey) and the ensemble mean (black). The dotted lines indicate one standard deviation from the mean.

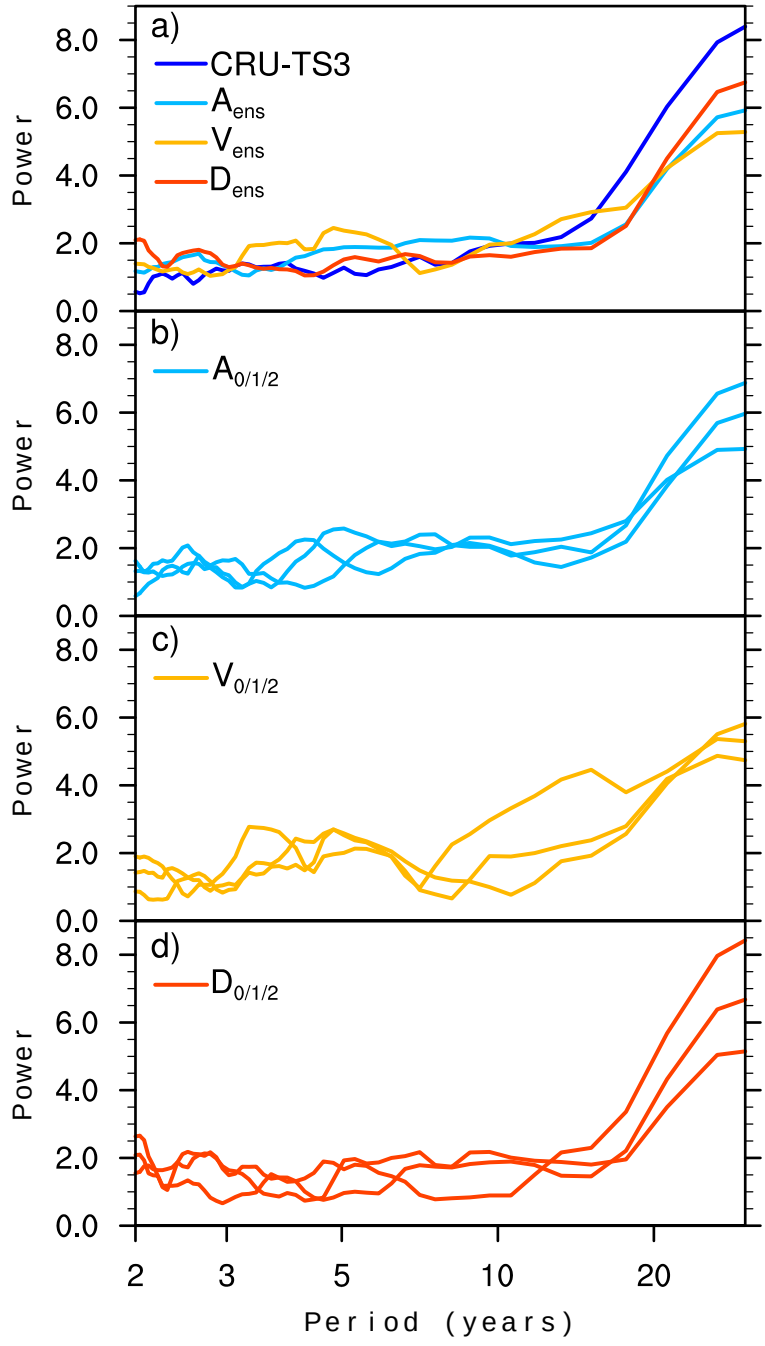

Figure 3.9: Power spectra of normalised precipitation for the years 1901-2006. **(a)** Observed precipitation, CRU-TS3 (Mitchell and Jones 2005), (black) and the mean spectra of the ensemble member spectra of each setup (A_{ens} , V_{ens} , D_{ens}). Power spectra of individual ensemble members for the **(b)** $A_{0,1,2}$, **(c)** $V_{0,1,2}$ and **(d)** $D_{0,1,2}$ simulations.

only through the dynamic vegetation. The long-term mean of the V–simulations are close to those of the A–simulations, thus also underestimating the mean by around 50 mm/year compared to the observed values (Fig. 3.10a). Considering the anomalies (Fig. 3.8c), the wet and the dry periods are clearly captured and the inter-period standard deviation is higher in the V–simulations than in the A–simulations. During the dry period the number of high-amplitude events is also larger. The time series show reduced power at low-frequencies in favour of higher frequencies, leading to a flattening of the spectra compared to the spectra of both the observed time series and the A–simulations (Fig. 3.9a–c). The V–simulations also underestimate the difference in mean between the wet and the dry periods. However, in this case, it can be attributed to a lack of persistence rather than to too low amplitudes.

The long-term mean of the simulations with dynamic vegetation and the dynamic background albedo scheme (the D–simulations) matches the observed long-term mean well, by increasing mean rainfall by up to 15% compared to the A– and the V–simulations (Fig. 3.10a). The reason for this increase in mean rainfall is related to a decrease in mean albedo by around 0.06, much as we see for the pre-industrial simulations in section 2.4.1 of Chapter 2. These simulations show both high spectral power at low-frequencies (strong persistence) and high amplitude anomalies for both the wet and the dry periods (Fig. 3.9a,d and Fig. 3.8d). The difference in mean between the wet and the dry period is thus increased compared to the A– and the V–simulations, and matches the observed difference better (Fig. 3.10b). Another feature that is better captured by the D–simulations is the successive increase and decrease in anomalies, that leads to a pyramidal shape of the anomalies in both the wet and in the dry periods of the observed time series. The timing of the start and the end of the periods simulated in these simulations are lagging those of the observed time series, whereas the timing is well captured in the A– and the V–simulations.

Some caution should be taken in interpreting the results of the spectral analysis

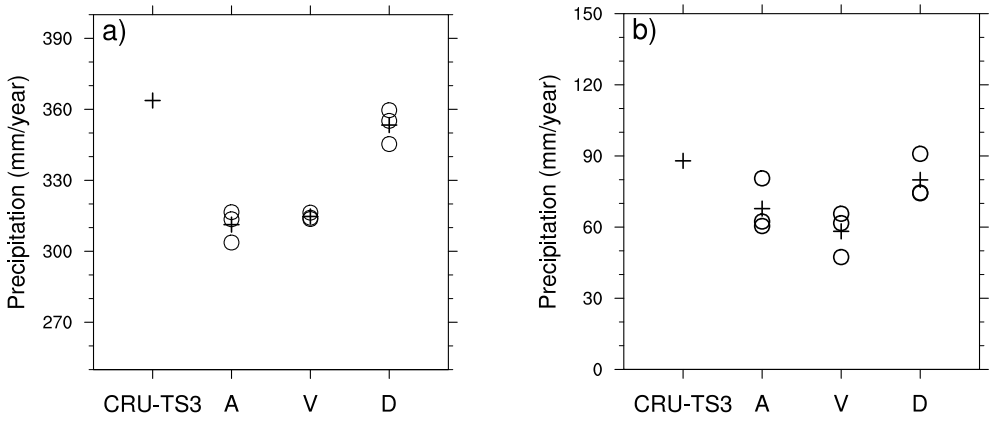

Figure 3.10: (a) Mean annual precipitation over the years 1901–2006, **(b)** Difference between the annual mean precipitation of the wet years (1938–1967) and the mean of the dry years (1969–1998). Crosses: observed precipitation or ensemble mean precipitation, open circles: individual ensemble members

in Figure 3.9, since the spread between the ensemble members is sometimes larger than the differences between the mean spectra of each setup. Another measure to use for persistence of the anomalies are autocorrelations at various lags. At lag 1, which is a sign of short-term persistence, there is no difference between the setups, neither in the value-range of the correlation nor in the ensemble spread. At larger lags (longer-term persistence), the D–simulations lie above the range of the V–simulations, and the A–simulations lie between the other two setups. This increases our confidence that the differences between the setups seen in the spectra are robust and not due to internal variability.

We cannot expect a direct correspondence between simulated and observed annual values, since the internal variability of the atmosphere model adds random noise to the time series. However, comparing five-year running means, we can expect some correlation. Comparing the five-year running mean observed time series to the five-year running mean simulated time series, we do find a good correlation between all nine simulations and the observed data, with correlation coefficients lying in the range of 0.55 to 0.77. However, it is not possible to say which setup fits better, since the scatter in the fit between ensemble members is larger than the inter-setup differences.

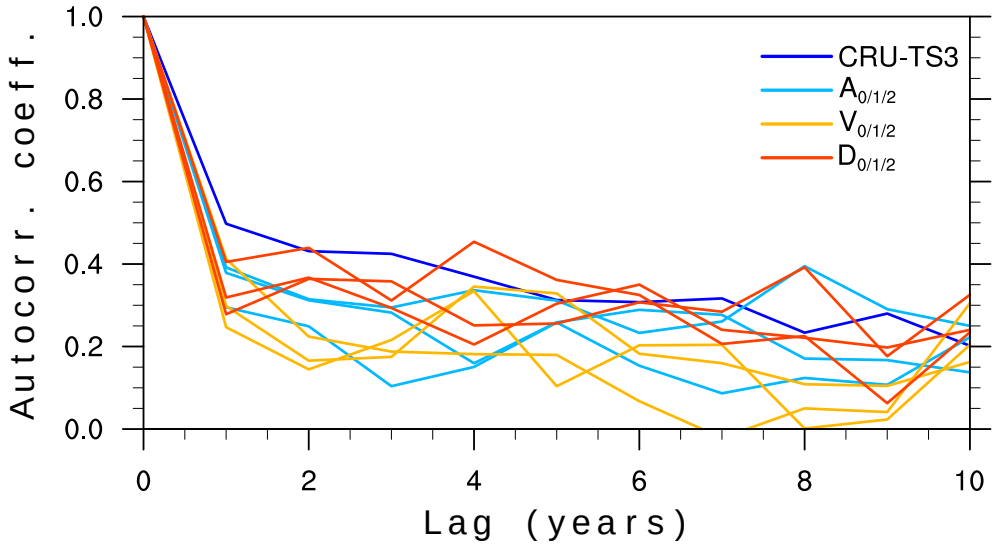

Figure 3.11: Autocorrelation function calculated for the years 1901-2006 for observed precipitation (CRU–TS3) and for simulated precipitation of the ensemble members $A_{0,1,2}$, $V_{0,1,2}$ and $D_{0,1,2}$ simulations.

3.4.1.3 Sources of rainfall variability

Since all nine simulations are able to reproduce the observed precipitation with some skill, it is clear that SSTs and synergies between SSTs and the atmosphere and/or the land surface play a major role in shaping the rainfall variability. To go into the details of the influence of observed SSTs on Sahelian rainfall is beyond the scope of this study, and it is a topic that has been widely researched in the past (see Section 3.3.2). Here we highlight the clear difference between the simulated Sahelian rainfall/MPIOM SSTs correlation patterns seen in section 3.3 (Fig. 3.4a–c) and the correlation patterns between observed rainfall and observed SSTs (Fig. 3.12a), and the correlation patterns between the simulated rainfall for the last century and observed SSTs (Fig. 3.12b–d). The tropical SSTs signal that was dominating the pre-industrial simulations, is not to be seen in either of the correlation patterns in Figure 3.12.

It is not possible to completely exclude an influence of the land surface on precipitation variability in the A–simulations. Even though the vegetation fraction and the distribution of PFTs is prescribed, the phenological cycle is seasonally

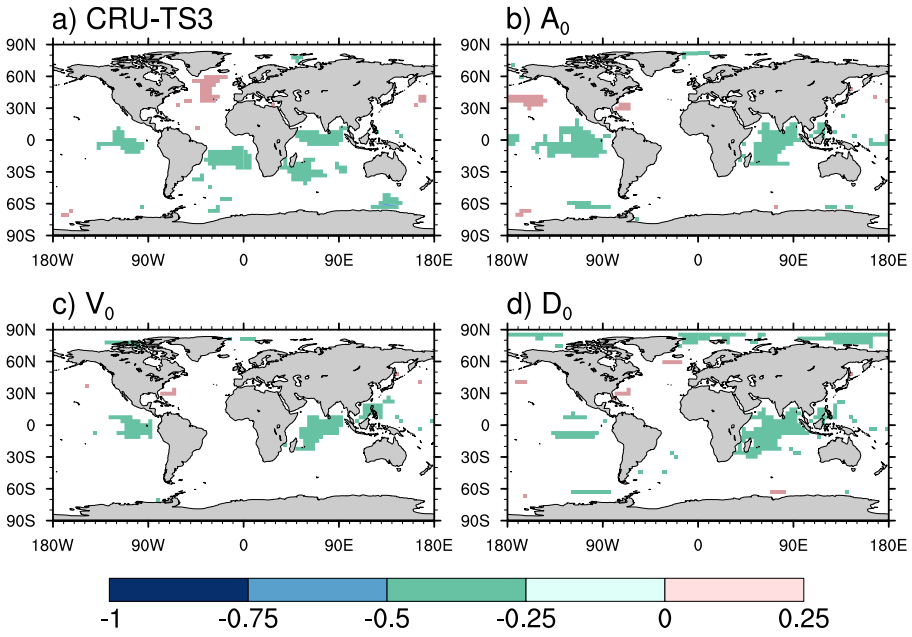

Figure 3.12: Correlation between global annual SSTs and annual mean precipitation in the Sahel from **(a)** observed data (CRU-TS3), one ensemble member of the **(b)** A, **(c)** V, **(d)** D setups for the years 1901–2006.

and interannually varying which affects the exchange of energy between the atmosphere and the land surface. With the setup of the simulations here, we are not interested in detangling the SST influence from that of the land surface influence in general, rather we are interested in the effect that dynamic vegetation and the dynamic background albedo scheme have on precipitation variability. We will therefore focus on explaining the differences between the setups that we found in the last section. In order to highlight these dissimilarities, we focus on the parameters of the model that lead to the main differences between the setups.

The energy exchange between the atmosphere and the land surface is mainly modulated via albedo and stomatal conductance. The albedo affects the shortwave radiation budget and the stomatal conductance affects the transpiration of the plants, and thus, the relative importance of transpirative, evaporative and, latent and sensible heat fluxes. The main parameter controlling canopy albedo and transpiration is the LAI, mostly in the form of the projective cover, PC (the

area of a gridcell covered by the green canopy):

$$PC \;=\; V_{\max} \sum_{\mathrm{PFT}} f^{i}_{\mathrm{cover}} \,(1 \;-\; e^{-\mathrm{LAI^i}/2}) \tag{3.1}$$

where $V_{\max}$ is the vegetated fraction of the gridbox, f^{i}_{cover} is the fractional cover of PFT i and LAI^i is the leaf area index (LAI) of PFT i. LAI is updated at every model time-step (subdaily) in all setups (with and without dynamic vegetation). $V_{\max}$ and f^{i}_{cover} are constant for static vegetation simulations and is updated on an annual basis for dynamic vegetation simulations. Due to imposing the same initial land surface conditions in all simulations, the initial vegetation cover V_0 may not be in equilibrium with the climate. In the V–simulations the vegetation shows no trend, however in the D–simulations there is a slight drift in the vegetation cover. We assume this trend to have had minor effects on the results, since the trend is neither seen in the albedo nor in the evapotranspiration time series (not shown).

In the Sahel, LAI variability is closely controlled by precipitation, which is reflected in the projective cover anomalies (Fig. 3.13). During the wet period the projective cover is above the long-term mean and vice versa for the dry period. The concurrent changes in NPP lead to an expansion of the vegetated area during the long wet period and a decline in vegetated area during the dry period in the two setups with dynamic vegetation (Fig. 3.13b,c).

Since $V_{\max}$ and f^{i}_{cover} are constant in the A–simulations, it is only variability in the annual LAI that can affect the variability in the annual mean projective cover, whereas in the V– and the D–simulations all three are varying. This leads to an amplification of the projective cover anomalies in both simulation setups with dynamic vegetation (Fig. 3.13b,c). The amplification of the projective cover anomalies is transferred to the anomalies of transpiration and the canopy albedo. In the V–simulations, albedo for the background is fixed, and changes in the albedo are only related to changes in the canopy albedo. This means that the

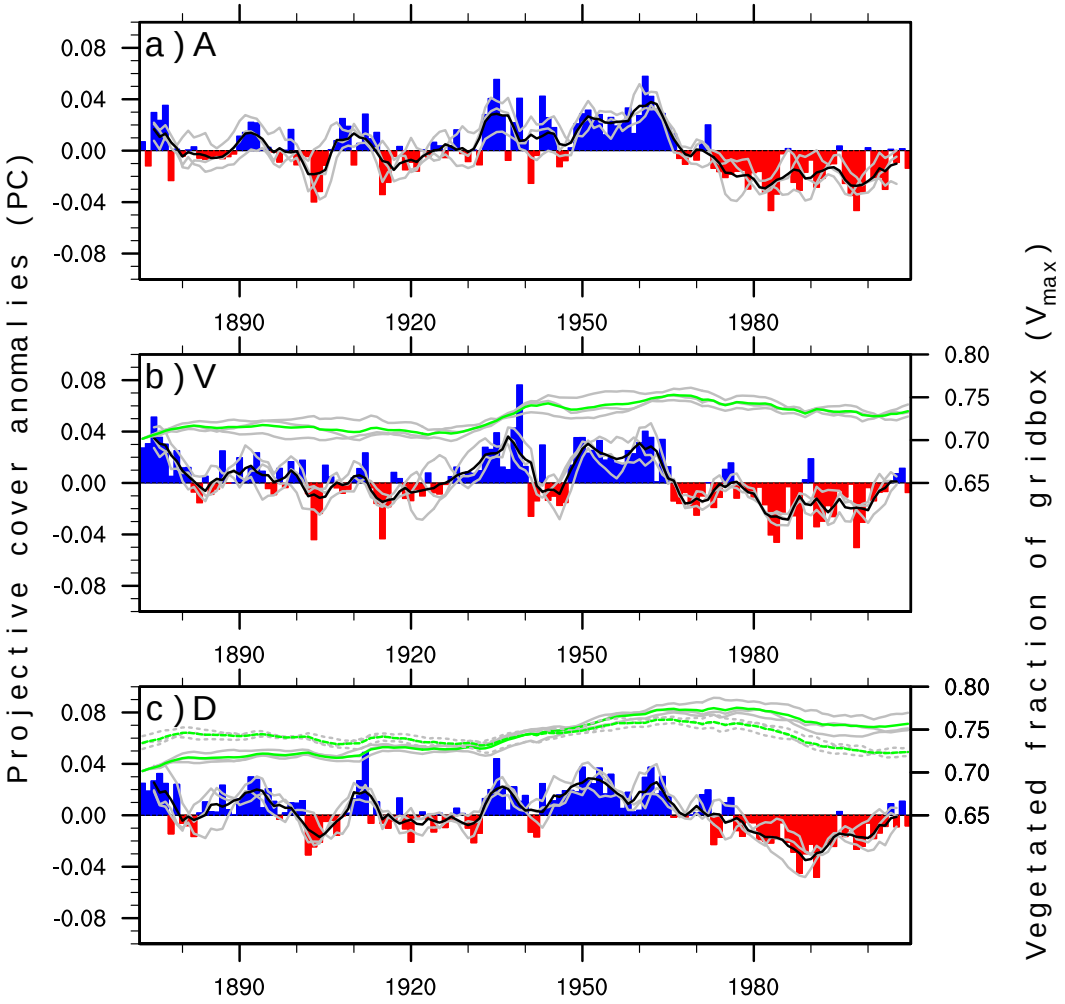

Figure 3.13: Projective cover anomalies w.r.t. mean projective cover for the years 1901-2006 in the Sahel for the **(a)** static (A) simulations, **(b)** dynamic vegetation (V) simulations, **(c)** dynamic vegetation and albedo (D) simulations. Bars show annual values of the ensemble mean. Lines over the bars show five-year running averages for the individual ensemble members (grey) and the ensemble mean (black). Annual mean values of V_{max} (right axis) for the individual ensemble members (grey) and for the ensemble mean (green). The dashed lines show the detrended series for the D–simulations.

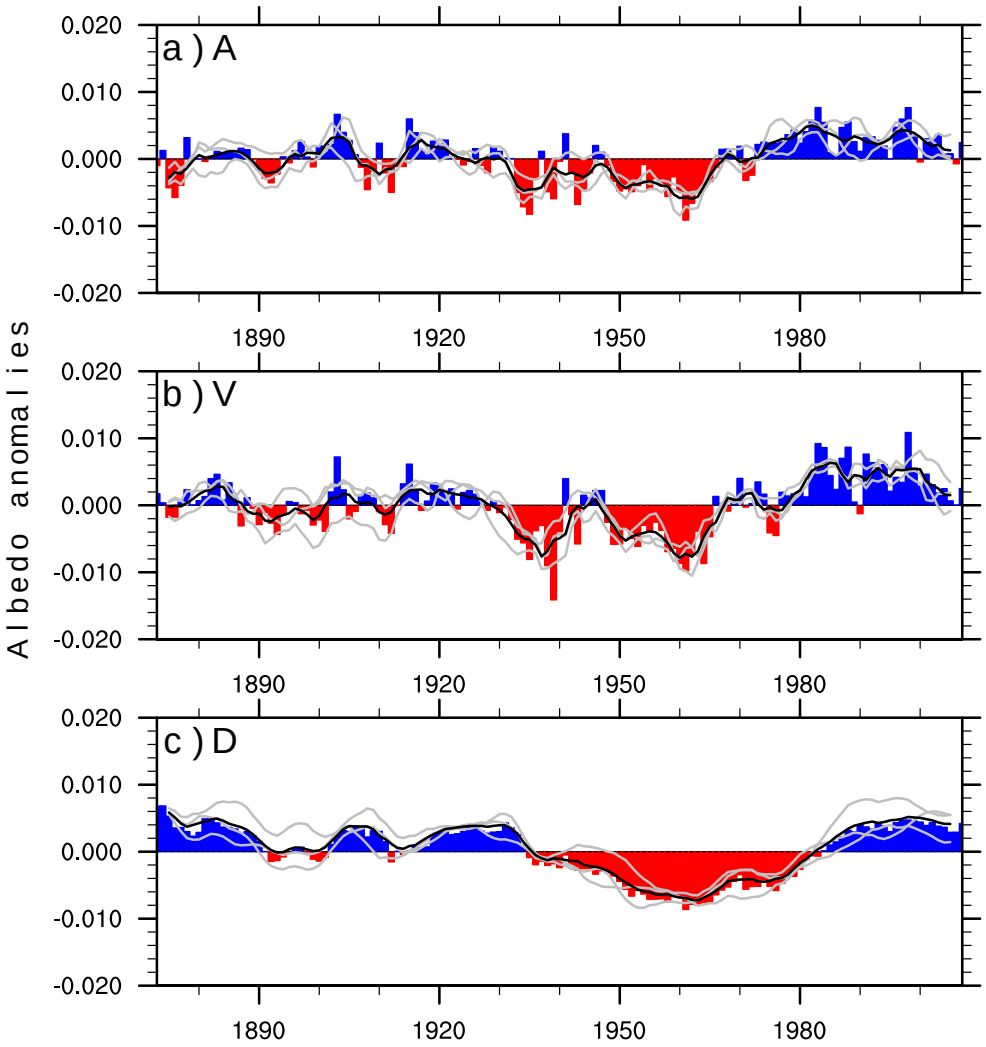

Figure 3.14: Albedo anomalies w.r.t. mean albedo for the years 1901-2006 in the Sahel for the **(a)** static (A) simulations, **(b)** dynamic vegetation (V) simulations, **(c)** dynamic vegetation and albedo (D) simulations. Bars show annual values of the ensemble mean. Lines show five-year running averages for the individual ensemble members (grey) and the ensemble mean (black).

amplification of the projective cover is directly affecting the energy exchange between the land surface and the atmosphere, both via evapotranspiration (not shown) and via the albedo in the V–simulations (Fig. 3.14b), explaining the amplification of rainfall anomalies seen in section 3.4.1.2.

For the D–simulations, the energy fluxes between the land surface and the atmosphere that are affected by changes in evapotranspiration are, similarly to the A and the V–simulations, modulated by the projective cover. The albedo, on the other hand, is modulated not only by changes in the canopy albedo, but also by changes in the background albedo, via changes in the slow soil carbon pool and the litter pool (see explanation of the dynamic albedo scheme in Chapter 2, section 2.2). These pools have a much longer response timescale than the LAI and they introduce a slowly varying filter to the albedo. This leads to albedo anomalies that slightly lag the precipitation anomalies (Fig. 3.14c), as well as reduced interannual variability of the albedo. The albedo thus leads to a dampening of the variability of the system, which is reflected through the increased persistence that was seen in section 3.4.1.2.

3.4.2 Discussion of simulated albedo and projective cover anomalies

The model behaviour can be explained by fluctuations in the projective cover and the albedo. It is not possible to obtain observational data for albedo or projective cover for the entire simulated period to validate these results. However, for albedo we can use the longest available albedo time series for North Africa: the Meteosat albedo product for the years 1982 to mid-2006 (Loew and Govaerts 2010). We use the bihemispherical reflectance (bhr) channel (white sky albedo) averaged over the region 10° W–30° E and 10° N–20° N. Due to a large number of missing pixels at the beginning of the time series and an absence of data for half of 2006, we only consider annual mean values for the years 1989-2005. The mean of the Meteosat time series is 0.249, which is clearly below the simulated values

for the same time period of the A– and the V–simulations (0.301 resp. 0.298) and slightly above those of the D–simulations (0.23). The standard deviation is on the other hand better captured by the A and the V–simulations than for the D–simulations (Meteosat: 0.0033, A: 0.003, V: 0.004, D: 0.013), which might be an indication that the slowly varying component introduced in the dynamic albedo scheme is too dominant. Precipitation does not only have a direct effect on albedo through soil moisture (an effect that we have omitted, see discussion in Chapter 2), and through the greening of the canopy, but also a lagged effect on albedo due to accumulation of litter and increased non-green biomass (Samain et al. 2008). However, due to the few years of albedo data and the sparsity of locations from which precipitation data is derived, it is not possible to investigate the plausibility of the slow response of albedo that is simulated by the dynamic albedo scheme. A clear annual effect of vegetation on albedo is not found in observational data (Fuller and Ottke 2002), which indicates that only including the effect of LAI fluctuations in the albedo calculations, might exaggerate the importance of year-to-year LAI variability for albedo variability.

The normalised difference vegetation index (NDVI), is a measure of the photosynthetically active vegetation and can thus be used as a proxy for the projective cover (e.g. Tucker and Nicholson 1999). The NDVI data we use here, comes from the Global Inventory of Modeling and Mapping Studies (GIMMS - Pinzon et al. (2005); Tucker et al. (2005)), and covers the same regional box that we used for the Meteosat albedo. The standard deviation of the annual mean observed NDVI for the years 1982 to 2006 is ca. 4% of the annual mean value. For the same period, the standard deviation from the mean for the simulated projective cover is between 5.6 and 6.7% for the A–simulations, 6.5 and 7.5% for the V–simulations and 4.5 and 6.6% for the D–simulations. This indicates that the projective cover is slightly too variable on an annual basis for the A– and the V–simulations. Here, we have focused on the annual variations in projective cover. For the interpretation of our results, this is an appropriate measure, since we know from Chapter

2, that the seasonal distribution of rainfall is not affected by the addition of the dynamic background albedo scheme. To properly judge the models capacity to correctly simulate LAI in general, one should consider sub-annual values.

3.5 Discussion

There have been a number of studies investigating the relationship between vegetation and precipitation variability in the Sahel (e.g. Zeng et al. 1999; Crucifix et al. 2005; Delire et al. 2004). Like Crucifix et al. (2005), we do not find a strong coupling between vegetation variability and precipitation variability in a coupled atmosphere-ocean setup. They did not attribute the weak coupling in their case, to the ocean forcing, but rather to low resolution. However, most of the studies that did find a strong coupling between vegetation variability and precipitation variability were using observed SSTs (e.g. Zeng et al. 1999; Wang and Eltahir 2000; Schnitzler et al. 2001; Giannini et al. 2003; Wang et al. 2004), similar to the simulations we presented in Section 3.4. This is an indication, that the strength of the coupling between the land surface and the atmosphere heavily depends on the oceanic forcing scenario and probably on the type of variability contained in the ocean signal (Zeng et al. 1999). Zeng et al. (1999); Wang and Eltahir (2000); Schnitzler et al. (2001); Wang et al. (2004) all find that vegetation dynamics increase persistence, whereas we find that vegetation dynamics increases the amplitude of the signal, but not necessarily the persistence of it. The discrepancy between our study and the other studies, can possibly be explained by differing complexity of models, both in the atmospheric (Zeng et al. 1999; Wang and Eltahir 2000) and the land surface models used (Zeng et al. 1999; Schnitzler et al. 2001). Wang et al. (2004) performed the study with a setup most similar to the ones presented here, in terms of the complexity of the models used. Two of the studies previously mentioned (Wang and Eltahir 2000; Wang et al. 2004) used different atmospheric models, but the same land surface

model, the Integrated BIosphere Simulator (IBIS Foley et al. 1996). This model was also used in a study with climatological SSTs (Delire et al. 2004), where a strong influence on year-to-year persistence of rainfall, due to dynamic vegetation, was found. It thus seems as if the IBIS model, show a strong coupling between vegetation dynamics and precipitation variability regardless of the ocean state. Therefore, it is likely, that the differences between the studies arise from model specific representations of processes and the choices of parameters within the land surface models. In the standard ECHAM5-JSBACH neither soil moisture nor land surface albedo exhibit a strong memory effect in the Sahel. Here we show, that indeed slow variations (super-annual) in albedo can play a role in enhancing the persistence of the precipitation variability. The longer memory is introduced here primarily via the background albedo scheme, whereas in the other models other processes might carry more memory. These inter-model discrepancies stress the importance of increased involvement of vegetation models in land surface model benchmarking, as well as coupled atmosphere-vegetation model intercomparison projects.

In this chapter we have not taken varying greenhouse gas concentrations into account. Greenhouse gas concentrations are kept at pre-industrial levels in all simulations. CO_2 levels do not only affect vegetation indirectly by changing the radiation budget and thus climate, but higher CO_2 levels may also lead to CO_2 fertilisation of plants. Under higher CO_2 concentrations, plants, especially C_3 plants, increase their productivity and reduce their stomatal conductance (Körner et al. 2007; Bonan 2008). The mid-Holocene and the pre-industrial CO_2 levels only differ by some 10 ppm, and the effect is negligible both for the physical climate and for the physiological effect on plants. Since the industrial revolution, CO_2 levels have increased by over 100 ppm (Etheridge et al. 1996; IPCC 2007a) and could thus have some effect on the plant distribution in the Sahel. We assume that the warming signal is carried in the SSTs and that neglecting greenhouse gas changes would not affect the physical climate to a large extent. CO_2 fertilisation

could, however, alter the competition between C_3 and C_4 plants, by increasing C_3 plant productivity without increasing water demand. This could either lead to an increased fraction of C_3 plants, because of increased productivity or an increased fraction of C_4 plants due to increased water availability. In the simulations, there is an equal distribution between C_3 and C_4 plants, with C_4 grasses being dominant compared to C_3 grasses (not shown). This distribution is not significantly affected by changed water availability during the wet and the dry periods. The additional effect due to CO_2 fertilisation would therefore be negligible, which is in line with a study investigating the contribution of the CO_2 fertilisation effect to the recent greening of the Sahel (Hickler et al. 2005). They show that most of the greening can be explained by the increase in precipitation in the region during the same time period.

3.6 Summary of Chapter 3

In this chapter, we investigate rainfall and vegetation variability and the way they interact in the Sahel region using the atmospheric GCM ECHAM5 including a comprehensive land surface scheme, JSBACH. In the first part of the chapter, we investigate simulations forced with model-derived SSTs. These SSTs were taken from two fully coupled atmosphere-ocean simulations of the MPI-ESM, one with pre-industrial orbital configuration and one with mid-Holocene orbital configuration. In the second part, we use observed SSTs for the last century to force ECHAM5-JSBACH.

In the pre-industrial simulations, precipitation variability is controlled by tropical SSTs, in particular by SSTs that are related to ENSO variability. The connection between ENSO and the Sahel is modelled in a plausible way, but the signal is excessively strong, leading to unrealistic patterns of variability in the Sahel. In the mid-Holocene, both ENSO variability and its connection with the Sahel is reduced. It is not possible to detect neither low-frequency variability nor

a strong effect of vegetation dynamics on variability in these simulations.

Using observed SSTs to force ECHAM5, we investigate the effect of various land surface processes on precipitation variability in more detail. We test the influence of changes in vegetation distribution (dynamic vegetation) and of a newly developed albedo scheme that accounts for slow dynamics of the land surface albedo. All setups are able to reproduce the general pattern of observed precipitation in the Sahel, such as the wet period during the middle of the last century and the dry period that followed. The standard setup tends to underestimate the severity of these periods and the amplitude of the dry or wet anomalies. The inclusion of dynamic vegetation increases the amplitudes, but reduces the persistence. Additionally using the dynamic background albedo scheme, both anomalies and the long-term persistence are well captured compared to observations. This highlights the importance of both dynamic vegetation and albedo schemes for the simulation of plausible precipitation dynamics in the Sahel region.

Chapter 4

Conclusions and Outlook

In this concluding chapter, we summarise the answers to the research questions we posed in the introduction. This is followed by an outlook for possible future directions of research. This chapter ends with a short résumée of the thesis.

4.1 Summary of findings

- **Can the land surface albedo change between today and the mid-Holocene be simulated in a more consistent way than in previous studies?**

We developed and implemented a new albedo scheme that takes the dynamic behaviour of the surface below the canopy into account, into the land surface scheme JSBACH of the MPI-ESM. The standard scheme that is used in JSBACH calculates the seasonal canopy albedo as a function of leaf area index, whereas the background albedo is a gridbox constant derived from satellite measurements. The new scheme additionally models the background albedo as a slowly changing function of organic matter in the ground, and of litter and standing dead biomass covering the ground. Both the standard and the new scheme simulate a good correspondence between vegetation and albedo for the present day. Using the new scheme the simulated mid-Holocene albedo is improved, since it corresponds

better to permanent and seasonally varying vegetation cover.

- **What is the sensitivity of the mid-Holocene climate to the plausibly simulated land surface albedo change?**

The new albedo scheme increases the sensitivity of precipitation to the orbital forcing by 30% in the whole of North Africa and the Arabian Peninsula. Though the new albedo scheme does increase rainfall during the whole rainy period, the increase in sensitivity can largely be attributed to an increase in precipitation at the beginning of the rainy period. The new albedo scheme also affects the spatial distribution of rainfall, by increasing sensitivity more in the east of the Sahara/Sahel and over the Arabian Peninsula.

- **Can the match between model and data in the Sahara be improved by considering a change in variability, rather than considering a change in mean climate?**

Using the mean desert fraction as a measure for the change in the position of the desert border between the present and the mid-Holocene, one would conclude that the simulated change in vegetation cover between the present and the mid-Holocene is presumably smaller than expected from palaeo-records, by moving only some three to four degrees northward. If however, the stability of the desert is considered, as measured by maximum departures from the mean, we find that the desert is much more stable in the pre-industrial simulations than in the mid-Holocene. The simulated mid-Holocene climate would thus be compatible with short-lived green spells in the desert, whereas the pre-industrial simulations would not. Due to the spatial sparsity and the low time-resolution of vegetation proxies it might be more appropriate to consider vegetation variability or desert stability rather than the mean.

- **Does the coupled model ECHAM5-JSBACH/MPIOM represent precipitation variability in the Sahel in a plausible way for present day orbital forcing?**

The coupled atmosphere-ocean model, and ECHAM5-JSBACH forced by SSTs derived from the coupled model, simulate a very strong connection between tropical SSTs in general and SSTs in the Nino3.4 region (representative for ENSO variability) in particular. The ENSO connection is realistic in the sense that it corresponds to years of same sign rainfall anomalies in the Sahel and on the Guinea Coast. It is however unrealistically dominant, since many of the other modes of SST variability, that influence observed Sahelian rainfall, are not found to influence the simulated precipitation in the pre-industrial simulations.

- **Does simulated precipitation variability differ between the mid-Holocene and today?**

During the mid-Holocene the amplitude of ENSO variability is reduced in the model, which is in line with palaeo-proxies. Thereby the ENSO influence on Sahelian rainfall variability is also reduced. However, even though it is reduced, it still remains a dominant forcing. The temporal structure of the variability thus does not change significantly. There is also no change in the occurrence of extreme events.

- **How do the response timescales that are inherent to vegetation dynamics and the dynamic background albedo, affect the precipitation variability of the pre-industrial and mid-Holocene simulations?**

In the pre-industrial, as well as in the mid-Holocene simulations, the precipitation variability is dominated by the ENSO signal and there are no large differences induced by the different setups of vegetation and albedo. The strong tropical

SST forcing remains in the pre-industrial simulations even when filtering out the ENSO signal. It is thus not possible to make any firm conclusions on the strength of the interactions between precipitation and vegetation variability in these simulations.

- **Is ECHAM5-JSBACH able to reproduce the variability in the Sahel for the last century using reconstructed SSTs?**

We performed nine ensemble simulations, based on three different setups with regards to the modelling of the land surface. All nine simulations reproduce observed precipitation variability with good skill. The persistent wet and dry periods are relatively well captured by all simulations. However, most simulations underestimate the mean rainfall and also its standard deviation.

- **How do the response timescales that are inherent to vegetation dynamics and the dynamic background albedo, affect the precipitation variability of the last century in simulations with observed SSTs as forcing?**

Using the standard setup of ECHAM5-JSBACH, with prescribed vegetation and the standard albedo scheme, the amplitude of the anomalies during the wet and the dry periods are underestimated, whereas persistence is well-captured. In the setup with dynamic vegetation, the number of years with high-amplitude anomalies is increased, but long-term persistence is reduced. In the third setup, with both dynamic vegetation and the dynamic background (new) albedo scheme, both anomalies and persistence are well-captured. The introduction of the dynamic vegetation leads to an amplification of the interannual variability in vegetation cover, which in turns leads to an amplification of the precipitation anomalies. The introduction of the dynamic background albedo scheme, with its slowly varying components, leads to a dampening of the variability of the system, which is reflected through increased persistence. The importance of the timescale of change of the land surface albedo is thus highlighted by this study.

4.2 Perspectives

The simulation of precipitation and precipitation variability in the Sahel and the Sahara necessitates the inclusion of many processes in the ocean, atmosphere and the land surface that all contribute to the complexity of the West African Monsoon. Using atmosphere-ocean GCMs to simulate precipitation in this area, it is crucial that both the modelling of SSTs and of convection is done in an appropriate way and in ECHAM5/MPIOM both these aspects need further improvement. The perspectives for further research on Sahelian/Saharan precipitation from a land surface point of view are also manifold.

Albedo and data assimilation

In this thesis we demonstrate that albedo affects precipitation on multiple timescales in the Sahel/Sahara region. Not only does the mean albedo affect the mean rainfall, changes in albedo variability can also affect precipitation variability. The response timescales in the dynamic background albedo scheme are inherent to the carbon model of JSBACH and the parameterisation of this scheme was aimed at capturing reasonable equilibrium values. The response timescales were thus not considered in detail. There is a large difference in the precipitation variability between modelling the albedo with just interannual variations (no memory) or with the lagged effect of precipitation on albedo on longer timescales (Chapter 3). With the existence of long satellite time series for both albedo (e.g. Meteosat, Loew and Govaerts 2010) and vegetation indices, such as NDVI (e.g. GIMMS, Pinzon et al. 2005; Tucker et al. 2005) one could envisage data assimilation methods (e.g. Quaife et al. 2008; Hill et al. 2011) to investigate both the rate and magnitude of change of albedo and its dependence on vegetation. However, doing this, care needs to be taken to account for non-linearities between the satellite measurements and the ecosystem properties that they represent (Chen 1999; Wijk and Williams 2005). Since satellite retrievals can only be obtained for about the last 30 years, one can only aim to distinguish between timescales from months to sev-

eral years. For the Community Land Model (CLM), such methods have already been applied for the soil moisture dependence of albedo (Lawrence and Chase 2007), though without considering the timescales of variability.

The rate of change of albedo becomes even more crucial, when one considers abrupt rather than slow climate change. This could for instance be when investigating future climate change or the transition from one climate state to another, such as the transition from the mid-Holocene green Sahara to the present day. It is still not clear at what rate of change this transition took place, and if precipitation and vegetation declines were strongly coupled via vegetation feedbacks or not. There are some modelling studies and proxy records that indicate a fast transition in both precipitation and vegetation (Claussen et al. 1999; deMenocal et al. 2000), and some that show a slower and/or a decoupled transition for both variables (e.g. Liu et al. 2007; Kröpelin et al. 2008; Lezine 2009). It has been suggested that the transition may be non-synchronous for different parts of North Africa (Brovkin and Claussen 2008), which would explain some of the discrepancies. Using a land surface albedo scheme, with well-constrained response timescales, could shed some further light on this question.

Model resolution

The simulations in this thesis are from one specific model running at one specific spatio-temporal resolution, which means that the results may be either model or resolution dependent. Under varying spatial resolution, both horizontal, but more importantly vertical, ECHAM5 has very different rainfall regimes (Hagemann et al. 2006; Dallmeyer 2008) and the land-atmosphere coupling may also be resolution dependent (Crucifix et al. 2005). It would be advisable to use an ensemble of resolutions and possibly also an updated version of the model, where the ENSO-Sahel connection is more realistic, to increase the robustness of the results presented here.

Soil moisture

The results may also be biased by the choice of processes that are included in the land surface model. One process, which might have an important role in the Sahara is the partitioning between bare soil evaporation and leaf transpiration, which depends on the available soil moisture. As mentioned in Chapter 2, we have not considered soil moisture effects in detail, because soil hydrology in the version of JSBACH that was used here, is represented by a simple bucket model and does not provide an appropriate basis to conduct sensitivity studies for this effect. A five-layer soil scheme has been developed, which would provide a better basis for investigating the role of soil hydrology, and a better platform for investigating the relative importance of vegetation-albedo-precipitation feedbacks versus vegetation-soil/canopy hydrology feedbacks.

Dust aerosols

Another important process, which was completely omitted in these simulations, is the effect of dust aerosols. Dust affects Sahelian rainfall through its role as an aerosol forcing in the atmosphere (Yoshioka et al. 2007), where increased amounts of dust can lead to a suppression of rainfall (Hui et al. 2008) or affect strength of the African Easterly Jet (AEJ) (Tompkins et al. 2005). For millennial-scale simulations, the modelling of dust would be interesting for its role as an inert tracer, that is affected by vegetation changes (Werner et al. 2002). This would allow a direct comparison with dust-records, such as the one of deMenocal et al. (2000) and thus increase the ways by which one can interpret the model results. For shorter timescales, or the transition between two climate states, the feedback between vegetation and precipitation may be strengthened or weakened by the inclusion of dust. A forcing that leads to decreased vegetation cover, could lead to an increased dust release and a possible reduction of rainfall (Yoshioka et al. 2007).

4.3 Concluding summary

We introduce a new land surface albedo scheme into ECHAM5-JSBACH, which takes both fast and slow vegetation processes into account. With this scheme we can simulate a plausible vegetation-dependent mean albedo change for the mid-Holocene Sahara, which increases the sensitivity of mean precipitation to orbital forcing. Using the same albedo scheme, we additionally underline the importance of albedo change on shorter timescales, which, dependent on the response timescales inherent to the albedo model, clearly affect precipitation variability, both in terms of amplitudes and persistence.

Bibliography

Adkins, J., deMenocal, P., and G., E.: The "African humid period" and the record of marine upwelling from excess ^{230}Th in Ocean Drilling Program Hole 658C, Paleoceanography, 21, PA4203, doi:10.1029/2005PA001200, 2006.

Asner, G., Wessman, C., and Bateson, C.: Sources of variability in plant canopy hyperspectral reflectance data in a savanna ecosystem., in: Proceedings of the 7th Annual Airborne Earth Science Workshop 1:23-32., 1998.

Bader, J. and Latif, M.: The impact of decadal-scale Indian Ocean sea surface temperature anomalies on Sahelian rainfall and the North Atlantic Oscillation, Geophysical Research Letters, 30, 2169, doi:10.1029/2003GL018426, 2003.

Bartholomeus, H. M., Schaepman, M. E., Kooistra, L., Stevens, A., Hoogmoed, W. B., and Spaargaren, O. S. P.: Spectral reflectance based indices for soil organic carbon quantification, Geoderma, 145, 28–36, 2008.

Berger, A. L.: Long-Term Variations Of Daily Insolation And Quaternary Climatic Changes, Journal Of The Atmospheric Sciences, 35, 2362–2367, 1978.

Biasutti, M. and Giannini, A.: Robust Sahel drying in response to late 20th century forcings, Geophysical Research Letters, 33, L11 706, doi: 10.1029/2006GL026067, 2006.

Bonan, G.: Ecological Climatology (2nd Edition), Cambridge University Press, 550 pp, 2008.

Bonfils, C., de Noblet-Ducoudre, N., Braconnot, P., and Joussaume, S.: Hot desert albedo and climate change: Mid-Holocene monsoon in North Africa, Journal Of Climate, 14, 3724–3737, 2001.

Braconnot, P., Otto-Bliesner, B., Harrison, S., Joussaume, S., Peterchmitt, J. Y., Abe-Ouchi, A., Crucifix, M., Driesschaert, E., Fichefet, T., Hewitt, C. D., Kageyama, M., Kitoh, A., Laine, A., Loutre, M. F., Marti, O., Merkel, U.,

Ramstein, G., Valdes, P., Weber, S. L., Yu, Y., and Zhao, Y.: Results of PMIP2 coupled simulations of the Mid-Holocene and Last Glacial Maximum - Part 1: experiments and large-scale features, Climate Of The Past, 3, 261–277, 2007a.

Braconnot, P., Otto-Bliesner, B., Harrison, S., Joussaume, S., Peterchmitt, J. Y., Abe-Ouchi, A., Crucifix, M., Driesschaert, E., Fichefet, T., Hewitt, C. D., Kageyama, M., Kitoh, A., Loutre, M. F., Marti, O., Merkel, U., Ramstein, G., Valdes, P., Weber, L., Yu, Y., and Zhao, Y.: Results of PMIP2 coupled simulations of the Mid-Holocene and Last Glacial Maximum - Part 2: feedbacks with emphasis on the location of the ITCZ and mid- and high latitudes heat budget, Climate Of The Past, 3, 279–296, 2007b.

Braconnot, P., Marzin, C., Gregoire, L., Mosquet, E., and Marti, O.: Monsoon response to changes in Earth's orbital parameters: comparisons between simulations of the Eemian and of the Holocene, Climate Of The Past, 4, 281–294, 2008.

Broström, A., Coe, M., Harrison, S. P., Gallimore, R., Kutzbach, J. E., Foley, J., Prentice, I. C., and Behling, P.: Land surface feedbacks and palaeomonsoons in northern Africa, Geophysical Research Letters, 25, 3615–3618, 1998.

Brovkin, V. and Claussen, M.: Comment on "Climate-Driven Ecosystem Succession in the Sahara: The Past 6000 Years", Science, 322, 1326b, doi: 10.1126/science.1163381, 2008.

Brovkin, V., Claussen, M., Petoukhov, V., and Ganopolski, A.: On the stability of the atmosphere-vegetation system in the Sahara/Sahel region, Journal Of Geophysical Research-Atmospheres, 103, 31 613–31 624, 1998.

Brovkin, V., Raddatz, T., Reick, C. H., Claussen, M., and Gayler, V.: Global biogeophysical interactions between forest and climate, Geophysical Research Letters, 36, L07 405, doi:10.1029/2009GL037543, 2009.

Brown, J., Collins, M., Tudhope, A. W., and Toniazzo, T.: Modelling mid-Holocene tropical climate and ENSO variability: towards constraining predictions of future change with palaeo-data, Climate Dynamics, 30, 19–36, 2008.

Carrington, D. P., Gallimore, R. G., and Kutzbach, J. E.: Climate sensitivity to wetlands and wetland vegetation in mid-Holocene North Africa, Climate Dynamics, 17, 151–157, 2001.

Charney, J. G.: Dynamics Of Deserts And Drought In Sahel, Quarterly Journal Of The Royal Meteorological Society, 101, 193–202, 1975.

Chen, J. M.: Spatial Scaling of a Remotely Sensed Surface Parameter by Contexture, Remote Sensing of Environment, 69, 30 – 42, doi:DOI: 10.1016/S0034-4257(99)00006-1, 1999.

Claussen, M.: Modeling bio-geophysical feedback in the African and Indian monsoon region, Climate Dynamics, 13, 247–257, 1997.

Claussen, M. and Gayler, V.: The greening of the Sahara during the mid-Holocene: results of an interactive atmosphere-biome model, Global Ecology And Biogeography Letters, 6, 369–377, 1997.

Claussen, M., Kubatzki, C., Brovkin, V., Ganopolski, A., Hoelzmann, P., and Pachur, H.: Simulation of an abrupt change in Saharan vegetation at the end of the mid-Holocene, Geophysical Research Letters, 24 (14), 2037–2040, 1999.

Claussen, M., Fohlmeister, J., Ganopolski, A., and Brovkin, V.: Vegetation dynamics amplifies precessional forcing, Geophysical Research Letters, 33, 2006.

Cook, K. and Vizy, E.: Coupled model simulations of the West African monsoon system: 20th century simulations and 21st century predictions, Journal of Climate, 19, 3681–3703, doi:10.1175/JCLI3814.1, 2006.

Crucifix, M., Betts, R. A., and Cox, P. M.: Vegetation and climate variability: a GCM modelling study, Climate Dynamics, 24, 457–467, doi:10.1007/s00382-004-0504-z, 2005.

Curran, P.: Principles of remote sensing, Longman, London and New York, 282 pp, 1985.

Dallmeyer, A.: Simulation des Nordafrikanischen Sommermonsuns in ECHAM5 Analyse der Modellempfindlichkeit, Diplomarbeit im Fach Meteorologie, Fachbereich Geowissenschaften, Universität Hamburg, 2008.

de Noblet-Ducoudre, N., Claussen, M., and Prentice, C.: Mid-Holocene greening of the Sahara: first results of the GAIM 6000 year BP Experiment with two asynchronously coupled atmosphere/biome models, Climate Dynamics, 16, 643–659, 2000.

Delire, C., Foley, J. A., and Thompson, S.: Long-term variability in a coupled atmosphere-biosphere model, Journal Of Climate, 17, 3947–3959, 2004.

deMenocal, P., Ortiz, J., Guilderson, T., Adkins, J., Sarnthein, M., Baker, L., and Yarusinsky, M.: Abrupt onset and termination of the African Humid Period: rapid climate responses to gradual insolation forcing, Quaternary Science Reviews, 19, 347–361, 2000.

Domingo, F., Villagarcia, L., Brenner, A. J., and Puigdefabregas, J.: Measuring and modelling the radiation balance of a heterogeneous shrubland, Plant Cell And Environment, 23, 27–38, 2000.

Drake, N. and Bristow, C.: Shorelines in the Sahara: geomorphological evidence for an enhanced monsoon from palaeolake Megachad, Holocene, 16, 901–911, 2006.

Etheridge, D. M., Steele, L., Langenfelds, R., Francey, R., Barnola, J.-M., and Morgan, V. I.: Natural and anthropogenic changes in atmospheric CO2 over the last 1000 years from air in Antarctic ice and firn, Journal of Geophysical Research, 101(D2), 4115–4128, doi:10.1029/95JD03410., 1996.

FAO: Digital Soil Map of the World. Version 3.6., vol. URL http://www.fao.org/geonetwork/srv/en/metadata.show?id=14116&currTab=simple [accessed on 11 January 2011]., 2007.

Fink, A., Christoph, M., Born, K., Brücher, T., Piecha, K., Pohle, S., Schulz, O., and Ermert, V.: Climate, in: Impacts of global change the hydrological cycle in West and Northwest Africa, edited by Speth, P., Christoph, M., and Diekkrüger, B., pp. 54–58, Springer, Heidelberg, Germany, 2010.

Fischer, N. and Jungclaus, J. H.: Effects of orbital forcing on atmosphere and ocean heat transports in Holocene and Eemian climate simulations with a comprehensive Earth system model, Climate Of The Past, 6, 155–168, 2010.

Fischer, N. and Jungclaus, J. H.: Evolution of the seasonal temperature cycle in a transient Holocene simulation: orbital forcing and sea-ice, Climate of the Past Discussions, 7, 463–483, doi:10.5194/cpd-7-463-2011, 2011.

Foley, J. A., Prentice, I. C., Ramankutty, N., Levis, S., Pollard, D., Sitch, S., and Haxeltine, A.: An integrated biosphere model of land surface processes,

terrestrial carbon balance, and vegetation dynamics, Global Biogeochemical Cycles, 10, 603–628, 1996.

Folland, C. K., Palmer, T. N., and Parker, D. E.: Sahel Rainfall And Worldwide Sea Temperatures, 1901-85, Nature, 320, 602–607, 1986.

Fontaine, B., Roucou, P., Gaetani, M., and Marteau, R.: Recent changes in precipitation, ITCZ convection and northern tropical circulation over North Africa (1979-2007), International Journal of Climatology, 31, 633–648, doi: 10.1002/joc.2108, 2011.

Fuller, D. O. and Ottke, C.: Land cover, rainfall and land-surface albedo in West Africa, Climatic Change, 54, 181–204, 2002.

Gascoin, S., Ducharne, A., Ribstein, P., Perroy, E., and Wagnon, P.: Sensitivity of bare soil albedo to surface soil moisture on the moraine of the Zongo glacier (Bolivia), Geophysical Research Letters, 36, L02 405, doi:10.1029/2008GL036377, 2009.

Giannini, A., Saravanan, R., and Chang, P.: Oceanic forcing of Sahel rainfall on interannual to interdecadal time scales, Science, 302, 1027–1030, 2003.

Giannini, A., Biasutti, M., Held, I. M., and Sobel, A. H.: A global perspective on African climate, Climatic Change, 90, 359–383, doi:10.1007/s10584-008-9396-y, 2008.

Govaerts, Y. M., Pereira, J. M., Pinty, B., and Mota, B.: Impact of fires on surface albedo dynamics over the African continent, Journal Of Geophysical Research-Atmospheres, 107, 4629, 2002.

Hagemann, S., Arpe, K., and Roeckner, E.: Evaluation of the Hydrological Cycle in the ECHAM5 Model, Journal of Climate, 19, 3810–3827, doi: 10.1175/JCLI3831.1, 2006.

Henderson, T. L., Baumgardner, M. F., Franzmeier, D. P., Stott, D. E., and Coster, D. C.: High Dimensional Reflectance Analysis Of Soil Organic-Matter, Soil Science Society Of America Journal, 56, 865–872, 1992.

Hickler, T., Eklundh, L., Seaquist, J. W., Smith, B., Ardo, J., Olsson, L., Sykes, M. T., and Sjöström, M.: Precipitation controls Sahel greening trend, Geophysical Research Letters, 32, L21 415, doi:10.1029/2005GL024370, 2005.

Hill, T., Quaife, T., and Williams, M.: A data assimilation method for using low-resolution Earth observation data in heterogeneous ecosystems, Journal of Geophysical Research, 116, D08 117, doi:10.1029/2010JD015268, 2011.

Hoelzmann, P., Jolly, D., Harrison, S. P., Laarif, F., Bonnefille, R., and Pachur, H. J.: Mid-Holocene land-surface conditions in northern Africa and the Arabian Peninsula: A data set for the analysis of biogeophysical feedbacks in the climate system, Global Biogeochemical Cycles, 12, 35–51, 1998.

Hoelzmann, P., Kruse, H. J., and Rottinger, F.: Precipitation estimates for the eastern Saharan palaeomonsoon based on a water balance model of the West Nubian Palaeolake Basin, Global And Planetary Change, 26, 105–120, 2000.

Hoelzmann, P., Keding, B., Berke, H., Kropelin, S., and Kruse, H. J.: Environmental change and archaeology: lake evolution and human occupation in the Eastern Sahara during the Holocene, Palaeogeography Palaeoclimatology Palaeoecology, 169, 193–217, 2001.

Hui, W. J., Cook, B., Ravi, S., Fuentes, J., and D'Odorico, P.: Dust-rainfall feedbacks in the West African Sahel, Water Resour. Res., 44, W05 202, doi: 10.1029/2008WR006885, 2008.

Hurrell, J. W., Hack, J. J., Shea, D., Caron, J. M., and Rosinski, J.: A New Sea Surface Temperature and Sea Ice Boundary Dataset for the Community Atmosphere Model, Journal of Climate, 21, 5145–5153, doi:10.1175/2008JCLI2292.1, 2008.

IPCC: Climate Change 2007: The Physical Science Basis., in: Contribution of Working Group I to the Fourth Assessment Report of the Intergovernmental Panel on Climate Change, edited by Solomon, S., Qin, D., Manning, M., Chen, Z., Marquis, M., Averyt, K., Tignor, M., and Miller, H., p. 996, Cambridge University Press, Cambridge, United Kingdom and New York, NY, USA, 2007a.

IPCC: Climate change 2007: impacts, adaptation and vulnerability., in: Contribution of Working Group II to the Fourth Assessment Report of the Intergovernmental Panel on Climate Change, edited by Parry, M., Canziani, O., Palutikof, J., van der Linden, P., and Hanson, C., p. 976, Cambridge University Press, Cambridge, United Kingdom and New York, NY, USA, 2007b.

Janicot, S., Moron, V., and Fontaine, B.: Sahel droughts and ENSO dynamics, Geophysical Research Letters, 23, 515–518, doi:10.1029/96GL00246, 1996.

Janicot, S., Trzaska, S., and Poccard, I.: Summer Sahel-ENSO teleconnection and decadal time scale SST variations, Climate Dynamics, 18, 303–320, 2001.

Jolly, D., Harrison, S. P., Damnati, B., and Bonnefille, R.: Simulated climate and biomes of Africa during the late quaternary: Comparison with pollen and lake status data, Quaternary Science Reviews, 17, 629–657, 1998a.

Jolly, D., Prentice, I. C., Bonnefille, R., Ballouche, A., Bengo, M., Brenac, P., Buchet, G., Burney, D., Cazet, J. P., Cheddadi, R., Edorh, T., Elenga, H., Elmoutaki, S., Guiot, J., Laarif, F., Lamb, H., Lezine, A. M., Maley, J., Mbenza, M., Peyron, O., Reille, M., Reynaud-Farrera, I., Riollet, G., Ritchie, J. C., Roche, E., Scott, L., Ssemmanda, I., Straka, H., Umer, M., Van Campo, E., Vilimumbalo, S., Vincens, A., and Waller, M.: Biome reconstruction from pollen and plant macrofossil data for Africa and the Arabian peninsula at 0 and 6000 years, Journal Of Biogeography, 25, 1007–1027, 1998b.

Joussaume, S. and Braconnot, P.: Sensitivity of paleoclimate simulation results to season definitions, Journal Of Geophysical Research-Atmospheres, 102, 1943–1956, 1997.

Joussaume, S., Taylor, K. E., Braconnot, P., Mitchell, J. F. B., Kutzbach, J. E., Harrison, S. P., Prentice, I. C., Broccoli, A. J., Abe-Ouchi, A., Bartlein, P. J., Bonfils, C., Dong, B., Guiot, J., Herterich, K., Hewitt, C. D., Jolly, D., Kim, J. W., Kislov, A., Kitoh, A., Loutre, M. F., Masson, V., McAvaney, B., McFarlane, N., de Noblet, N., Peltier, W. R., Peterschmitt, J. Y., Pollard, D., Rind, D., Royer, J. F., Schlesinger, M. E., Syktus, J., Thompson, S., Valdes, P., Vettoretti, G., Webb, R. S., and Wyputta, U.: Monsoon changes for 6000 years ago: Results of 18 simulations from the Paleoclimate Modeling Intercomparison Project (PMIP), Geophysical Research Letters, 26, 859–862, 1999.

Jungclaus, J. H., Haak, H., Latif, M., and Mikolajewicz, U.: Arctic-North Atlantic Interactions and Multidecadal Variability of the Meridional Overturning Circulation, Journal of Climate, 18, 4013–4031, doi:10.1175/JCLI3462.1, 2005.

Knorr, W. and Schnitzler, K. G.: Enhanced albedo feedback in North Africa from possible combined vegetation and soil-formation processes, Climate Dynamics, 26, 55–63, 2006.

Knorr, W., Schnitzler, K. G., and Govaerts, Y.: The role of bright desert regions

in shaping North African climate, Geophysical Research Letters, 28, 3489–3492, 2001.

Körner, C., Morgan, J., and Norby, R.: $C0_2$ Fertilization: When, Where, How Much?, in: Terrestrial ecosystems in a changing world, edited by Canadell, J., D.E., P., and Pitelka, L., pp. 9–21, Springer Berlin Heidelberg, 2007.

Kröpelin, S. and Petit-Maire, N.: Paleomonsoon variations and terrestrial environmental change during the late Quaternary - Foreword, Global And Planetary Change, 26, VII–VIII, 2000.

Kröpelin, S., Verschuren, D., Lezine, A. . M., Eggermont, H., Cocquyt, C., Francus, P., Cazet, J. . P., Fagot, M., Rumes, B., Russell, J. M., Darius, F., Conley, D. J., Schuster, M., von Suchodoletz, H., and Engstrom, D. R.: Climate-driven ecosystem succession in the Sahara: The past 6000 years, Science (Washington D C), 320, 765–768, 2008.

Kutzbach, J. E. and Liu, Z.: Response of the African monsoon to orbital forcing and ocean feedbacks in the middle Holocene, Science, 278, 440–443, 1997.

Ladoni, M., Bahrami, H. A., Alavipanah, S. K., and Norouzi, A. A.: Estimating soil organic carbon from soil reflectance: a review, Precision Agriculture, 11, 82–99, 2010.

Lamb, P. J.: Large-Scale Tropical Atlantic Surface Circulation Patterns Associated With Sub-Saharan Weather Anomalies, Tellus, 30, 240–251, 1978.

Lamb, P. J. and Peppler, R. A.: Further Case-Studies Of Tropical Atlantic Surface Atmospheric And Oceanic Patterns Associated With Sub-Saharan Drought, Journal Of Climate, 5, 476–488, 1992.

Lawrence, P. J. and Chase, T. N.: Representing a new MODIS consistent land surface in the Community Land Model (CLM 3.0), Journal Of Geophysical Research-Biogeosciences, 112, G01 023, 2007.

Levis, S., Bonan, G. B., and Bonfils, C.: Soil feedback drives the mid-Holocene North African monsoon northward in fully coupled CCSM2 simulations with a dynamic vegetation model, Climate Dynamics, 23, 791–802, 2004.

Lezine, A. M.: Late Quaternary Vegetation And Climate Of The Sahel, Quaternary Research, 32, 317–334, 1989.

Lezine, A. M.: Timing of vegetation changes at the end of the Holocene Humid Period in desert areas at the northern edge of the Atlantic and Indian monsoon systems, Comptes Rendus Geoscience, 341, 750–759, 2009.

Liu, Z., Harrison, S. P., Kutzbach, J., and Otto-Bliesner, B.: Global monsoons in the mid-Holocene and oceanic feedback, Climate Dynamics, 22, 157–182, 2004.

Liu, Z., Wang, Y., Gallimore, R., Gasse, F., Johnson, T., deMenocal, P., Adkins, J., Notaro, M., Prenticer, I. C., Kutzbach, J., Jacob, R., Behling, P., Wang, L., and Ong, E.: Simulating the transient evolution and abrupt change of Northern Africa atmosphere-ocean-terrestrial ecosystem in the Holocene, Quaternary Science Reviews, 26, 1818–1837, 2007.

Liu, Z. Y., Kutzbach, J., and Wu, L. X.: Modeling climate shift of El Nino variability in the Holocene, Geophysical Research Letters, 27, 2265–2268, 2000.

Lobell, D. B. and Asner, G. P.: Moisture effects on soil reflectance, Soil Science Society Of America Journal, 66, 722–727, 2002.

Loew, A. and Govaerts, Y.: Towards Multidecadal Consistent Meteosat Surface Albedo Time Series, Remote Sensing, 2, 957–967, doi:10.3390/rs2040957, 2010.

Marsland, S. J., Haak, H., Jungclaus, J. H., Latif, M., and Roske, F.: The Max-Planck-Institute global ocean/sea ice model with orthogonal curvilinear coordinates, Ocean Modelling, 5, 91–127, 2003.

McGregor, H. V. and Gagan, M. K.: Western Pacific coral delta O-18 records of anomalous Holocene variability in the El Nino-Southern Oscillation, Geophysical Research Letters, 31, L11 204, doi:10.1029/2004GL019972, 2004.

Mitchell, T. D. and Jones, P. D.: An improved method of constructing a database of monthly climate observations and associated high-resolution grids, International Journal Of Climatology, 25, 693–712, 2005.

Mohino, E., Janicot, S., and Bader, J.: Sahel rainfall and decadal to multidecadal sea surface temperature variability, Climate Dynamics, pp. 1–22, doi: 10.1007/s00382-010-0867-2, 2010.

Monsi, M. and Saeki, T.: Über den Lichtfaktor in den Pflanzengesellschaften und seine Bedeutung für die Stoffproduktion, Japanese Journal of Botany, 14, 22–52, 1953.

Myhre, G., Govaerts, Y., Haywood, J. M., Berntsen, T. K., and Lattanzio, A.: Radiative effect of surface albedo change from biomass burning, Geophysical Research Letters, 32, L20 812, doi:10.1029/2005GL022897, 2005.

Ni, J., Harrison, S. P., Prentice, I. C., Kutzbach, J. E., and Sitch, S.: Impact of climate variability on present and Holocene vegetation: A model-based study, Ecological Modelling, 191, 469–486, 2006.

Nicholson, S.: The historical climatology of Africa., in: Climate and History, edited by Wigley, T., Ingram, M., and Farmer, G., pp. 249–270, Cambridge University Press, 1981.

Nicholson, S. E.: The Nature Of Rainfall Fluctuations In Sub-Tropical West-Africa, Monthly Weather Review, 108, 473–487, 1980.

Nicholson, S. E.: Long-term changes in African rainfall, Weather, 44, 46–56, 1989.

Nicholson, S. E. and Grist, J. P.: A conceptual model for understanding rainfall variability in the West African Sahel on interannual and interdecadal timescales, International Journal of Climatology, 21, 1733–1757, 2001.

Nicholson, S. E. and Webster, P. J.: A physical basis for the interannual variability of rainfall in the Sahel, Quarterly Journal Of The Royal Meteorological Society, 133, 2065–2084, 2007.

Oleson, K., Dai, Y., Bonan, G. B., Bosilovich, M., Dickinson, R. E., Dirmeyer, P., Hoffman, F., Houser, P. R., Levis, S., Niu, G.-Y., Thornton, P., Vertenstein, M., Yang, Z.-L., and Zeng, X.: Technical Description of the Community Land Model, Tech. rep., NCAR Tech. Note TN-461+STR, National Centre for Atmospheric Research, Boulder, Colorado, 2004.

Otterman, J.: Baring High-Albedo Soils By Overgrazing - Hypothesized Desertification Mechanism, Science, 186, 531–533, 1974.

Otto-Bliesner, B. L., Brady, E. C., Shin, S.-I., Liu, Z., and Shields, C.: Modeling El Nino and its tropical teleconnections during the last glacial-interglacial cycle, Geophysical Research Letters, 30, CLM4–1–4, doi:10.1029/2003GL018553, 2003.

Pachur, H.-J. and Altmann, N.: The Quaternary (Holocene, ca. 8000 a BP), in: Palaeo-geographic-Palaeotectonic atlas of North-Eastern Africa, Arabia, and

adjacent areas Late Neoproterozoic to Holocene., edited by Schandelmeier, H. and Reynolds, P.-O. H., pp. 111–125, A.A. Balkema, Rotterdam, Brookfield, 1997.

Pachur, H. J. and Kröpelin, S.: Wadi Howar - Paleoclimatic Evidence From An Extinct River System In The Southeastern Sahara, Science, 237, 298–300, 1987.

Pachur, H. J. and Rottinger, F.: Evidence for a large extended paleolake in the eastern Sahara as revealed by spaceborne radar lab images, Remote Sensing Of Environment, 61, 437–440, 1997.

Patricola, C. M. and Cook, K. H.: Northern African climate at the end of the twenty-first century: an integrated application of regional and global climate models, Climate Dynamics, 35, 193–212, doi:10.1007/s00382-009-0623-7, 2010.

Peters, M. and Tetzlaff, G.: The Structure Of West-African Squall Lines And Their Environmental Moisture Budget, Meteorology And Atmospheric Physics, 39, 74–84, 1988.

Pinzon, J., Brown, M., and Tucker, C.: Satellite time series correction of orbital drift artifacts using empirical mode decomposition., in: Hilbert-Huang Transform: Introduction and Applications, edited by Huang, N., pp. 167–186, Hackensack, N.J.: World Scientific., 2005.

Prentice, I. C. and Webb, T.: BIOME 6000: reconstructing global mid-Holocene vegetation patterns from palaeoecological records, Journal Of Biogeography, 25, 997–1005, 1998.

Quaife, T., Lewis, P., Kauwe, M. D., Williams, M., Law, B. E., Disney, M., and Bowyer, P.: Assimilating canopy reflectance data into an ecosystem model with an Ensemble Kalman Filter, Remote Sensing of Environment, 112, 1347 – 1364, doi:DOI: 10.1016/j.rse.2007.05.020, remote Sensing Data Assimilation Special Issue, 2008.

Raddatz, T. J., Reick, C. H., Knorr, W., Kattge, J., Roeckner, E., Schnur, R., Schnitzler, K. G., Wetzel, P., and Jungclaus, J.: Will the tropical land biosphere dominate the climate-carbon cycle feedback during the twenty-first century?, Climate Dynamics, 29, 565–574, 2007.

Rechid, D., Raddatz, T., and Jacob, D.: Parameterization of snow-free land surface albedo as a function of vegetation phenology based on MODIS data

and applied in climate modelling, Theoretical And Applied Climatology, 95, 245–255, 2009.

Ritchie, J. C. and Haynes, C. V.: Holocene Vegetation Zonation In The Eastern Sahara, Nature, 330, 645–647, 1987.

Ritchie, J. C., Eyles, C. H., and Haynes, C. V.: Sediment And Pollen Evidence For An Early To Mid-Holocene Humid Period In The Eastern Sahara, Nature, 314, 352–355, 1985.

Roeckner, E., Bäuml, G., Bonaventura, L., Brokopf, R., Esch, M., M., G., Hagemann, S., Kirchner, I., Kornblueh, L., Manzini, E., Rhodin, A., Schlese, U., Schulzweida, U., and Tompkins, A.: The atmospheric general circulation model ECHAM5. Part I: Model description., Tech. Rep. Rep. 349, 127 pp., Max Planck Institute for Meteorology, Available from MPI for Meteorology, Bundesstr. 53, 20146 Hamburg, Germany., 2003.

Samain, O., Kergoat, L., Hiernaux, P., Guichard, F., Mougin, E., Timouk, F., and Lavenu, F.: Analysis of the in situ and MODIS albedo variability at multiple timescales in the Sahel, Journal Of Geophysical Research-Atmospheres, 113, D14 119, doi:10.1029/2007JD009174, 2008.

Schnitzler, K. G., Knorr, W., Latif, M., Bader, J., and Zeng, N.: Vegetation feedback on Sahelian rainfall variability in a coupled climate land - vegetation model, Tech. Rep. Rep. 329, 13 pp., Max Planck Institute for Meteorology, Available from MPI for Meteorology, Bundesstr. 53, 20146 Hamburg, Germany., 2001.

Schurgers, G., Mikolajewicz, U., Groger, M., Maier-Reimer, E., Vizcaino, M., and Winguth, A.: The effect of land surface changes on Eemian climate, Climate Dynamics, 29, 357–373, 2007.

Sellers, P. J., Los, S. O., Tucker, C. J., Justice, C. O., Dazlich, D. A., Collatz, G. J., and Randall, D. A.: A revised land surface parameterization (SiB2) for atmospheric GCMs .2. The generation of global fields of terrestrial biophysical parameters from satellite data, Journal Of Climate, 9, 706–737, 1996.

Stoner, E. R. and Baumgardner, M. F.: Characteristic Variations In Reflectance Of Surface Soils, Soil Science Society Of America Journal, 45, 1161–1165, 1981.

Tjallingii, R., Claussen, M., Stuut, J. B. W., Fohlmeister, J., Jahn, A., Bickert, T., Lamy, F., and Rohl, U.: Coherent high- and low-latitude control of the northwest African hydrological balance, Nature Geoscience, 1, 670–675, 2008.

Tompkins, A. M., Cardinali, C., Morcrette, J., and Rodwell, M.: Influence of aerosol climatology on forecasts of the African Easterly Jet, Geophysical Research Letters, 32, L10 801, doi:10.1029/2004GL022189., 2005.

Tsvetsinskaya, E. A., Schaaf, C. B., Gao, F., Strahler, A. H., Dickinson, R. E., Zeng, X., and Lucht, W.: Relating MODIS-derived surface albedo to soils and rock types over Northern Africa and the Arabian peninsula, Geophysical Research Letters, 29, 1353, doi:10.1029/2001GL014096, 2002.

Tsvetsinskaya, E. A., Schaaf, C. B., Gao, F., Strahler, A. H., and Dickinson, R. E.: Spatial and temporal variability in Moderate Resolution Imaging Spectroradiometer-derived surface albedo over global arid regions, Journal Of Geophysical Research-Atmospheres, 111, D20 106, doi:10.1029/2005JD006772, 2006.

Tucker, C., Pinzon, J., Brown, M., Slayback, D., Pak, E., Mahoney, R., Vermote, E., and Saleous, N.: An Extended AVHRR 8-km NDVI Data Set Compatible with MODIS and SPOT Vegetation NDVI Data, International Journal of Remote Sensing, 26(20), 4485–4498, 2005.

Tucker, C. J. and Nicholson, S. E.: Variations in the size of the Sahara Desert from 1980 to 1997, Ambio, 28, 587–591, 1999.

Tudhope, A. W., Chilcott, C. P., McCulloch, M. T., Cook, E. R., Chappell, J., Ellam, R. M., Lea, D. W., Lough, J. M., and Shimmield, G. B.: Variability in the El Nino - Southern oscillation through a glacial-interglacial cycle, Science, 291, 1511–1517, 2001.

Wang, G., Eltahir, E. A. B., Foley, J. A., Pollard, D., and Levis, S.: Decadal variability of rainfall in the Sahel: results from the coupled GENESIS-IBIS atmosphere-biosphere model, Climate Dynamics, 22, 625–637, 2004.

Wang, G. L. and Eltahir, E. A. B.: Biosphere-atmosphere interactions over West Africa. I: Development and validation of a coupled dynamic model, Quarterly Journal Of The Royal Meteorological Society, 126, 1239–1260, 2000.

Wang, S., Trishchenko, A. P., and Sun, X. M.: Simulation of canopy radiation transfer and surface albedo in the EALCO model, Climate Dynamics, 29, 615–632, 2007.

Wang, S. S.: Dynamics of surface albedo of a boreal forest and its simulation, Ecological Modelling, 183, 477–494, 2005.

Ward, M. N.: Diagnosis and Short-Lead Time Prediction of Summer Rainfall in Tropical North Africa at Interannual and Multidecadal Timescales, Journal of Climate, 11, 3167–3191, doi:10.1175/1520-0442(1998)011¡3167:DASLTP¿2.0.CO;2, 1998.

Werner, M., Tegen, I., Harrison, S., Kohfeld, K., Prentice, I., Balkanski, Y., Rodhe, H., and Roelandt, C.: Seasonal and interannual variability of the mineral dust cycle under present and glacial climate conditions, Journal of Geophysical Research, 107(D24), 4744, doi:10.1029/2002JD002365, 2002.

Wijk, M. T. v. and Williams, M.: Optical Instruments for Measuring Leaf Area Index in Low Vegetation: Application in Arctic Ecosystems, Ecological Applications, 15, 1462–1470, 2005.

Xue, Y. K. and Shukla, J.: The Influence Of Land-Surface Properties On Sahel Climate .1. Desertification, Journal Of Climate, 6, 2232–2245, 1993.

Yoshioka, M., Mahowald, N. M., Conley, A. J., Collins, W. D., Fillmore, D. W., Zender, C. S., and Coleman, D. B.: Impact of Desert Dust Radiative Forcing on Sahel Precipitation: Relative Importance of Dust Compared to Sea Surface Temperature Variations, Vegetation Changes, and Greenhouse Gas Warming, Journal of Climate, 20, 1445–1467, doi:10.1175/JCLI4056.1, 2007.

Zeng, N., Neelin, J. D., Lau, K. M., and Tucker, C. J.: Enhancement of interdecadal climate variability in the Sahel by vegetation interaction, Science, 286, 1537–1540, 1999.

Zhang, R. and Delworth, T. L.: Impact of the Atlantic Multidecadal Oscillation on North Pacific climate variability, Geophysical Research Letters, 34, L23 708, doi:10.1029/2007GL031601, 2007.

Zhao, Y., Braconnot, P., Harrison, S. P., Yiou, P., and Marti, O.: Simulated changes in the relationship between tropical ocean temperatures and the west-

ern African monsoon during the mid-Holocene, Climate Dynamics, 28, 533–551, 2007.

Zheng, W., Braconnot, P., Guilyardi, E., Merkel, U., and Yu, Y.: ENSO at 6ka and 21ka from ocean-atmosphere coupled model simulations, Climate Dynamics, 30, 745–762, 2008.

Acknowledgements

I want to thank Martin Claussen for introducing me to the topic and for great supervision, my supervisor Victor Brovkin for guidance, heaps of patience and interesting conversations and Prof. Klaus Fraedrich, the chair of my Advisory Panel, for helpful comments both during and outside of panel meetings.

Thanks to the IMPRS, especially Antje and Conni, for support and advice, as well as to my fellow PhD-students, the ZMAW people: Nils, Florian, Aiko, Malte, Werner, Peter, Rosi and Steffen, the 17th floor people: Julia, Juliane, Robert, Daniel, Sebastian and Helge, and a special thank you to Fanny.

I also want to thank Veronika, Reiner and Thomas for help related to JSBACH and COSMOS, and my other LAND-colleagues for a great working environment. My thanks also go to Tornado, Eibe and Magnolia. We have had our moments (especially me and the dear Tornado), but all in all I could not have finished my PhD without you.

Many thanks to Thomas Kleinen, Nils Fischer, Jürgen Bader and Tim Brücher, for great comments and suggestions, as well as proof-reading. Further thanks go to Alex Löw, who provided the Meteosat and GIMMS data-sets, and to Nils Fischer for providing the output data of the Holocene transient experiment.

On a more personal level I would like thank my RBL rowing teams; Achter Hamburg and Hansa Sprinter. Thanks for getting me out of the office and out onto the water.

I also want to thank Erik och Göran Ennerfelts fond for their kind and generous support.

Last but not least, thanks to mamma (and the 1210 e-mails I have received from her since the beginning of my PhD), pappa, Tuva, Ylva and Heiner!



ISSN 1614-1199